Time-Resolved Fluorescence-Based Europium-Derived Probes for Peroxidase Bioassays, Citrate Cycle Imaging and Chirality Sensing

Dissertation zur Erlangung des Doktorgrades der Naturwissenschaften
(doktorum rerum naturalis, Dr. rer. nat.)

der Fakultät Chemie und Pharmazie,
Universität Regensburg,
Bundesrepublik Deutschland

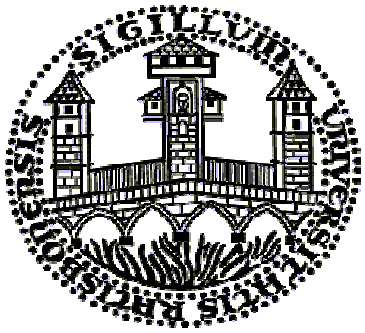

vorgelegt von

Zhihong Lin

aus Wuhan, China

im Januar 2004

Time-Resolved Fluorescence-Based Europium-Derived Probes for Peroxidase Bioassays, Citrate Cycle Imaging and Chirality Sensing

Doctoral Dissertation

by

Zhihong Lin

Faculty of Chemistry and Pharmacy
in University of Regensburg
Federal Republic of Germany

January 2004

This study was performed at the Institute of Analytical Chemistry, Chemo- and Biosensors of the University of Regensburg between August 2001 and January 2004 under the supervision of Prof. Otto S. Wolfbeis.

Date of defense: 20.01. 2004

Committee of defense (Prüfungsausschuss):

Chairperson	(Vorsitzender):	Prof. Dr. Manfred Liefländer
First expert	(Erstgutachter):	Prof. Dr. Otto S. Wolfbeis
Second expert	(Zweitgutachter):	Prof. Dr. Claudia Steinem
Third expert	(Drittprüfer):	Prof. Dr. Jörg Daub

谨以此篇献给我的父亲母亲和儿子

This dissertation is dedicated to my parents and my son

Table of Contents

Acronyms and Symbols

[α]	Optical activity
A	Absorbance
AP	Alkaline-phosphatase
CAT	Catalase
CD	Circular dichroism
Cit	Citrate
CL	Citrate lyase
CLIA	Chemiluminiscent immunoassay
CoA	Coenzyme A
CPL	Circular polarized luminescence
CS	Citrate synthase
DELFIA	Dissociation enhanced lanthanide fluoroimmunoassay
DIFP	Phosphate ester of diflunisal
DLCLLA	Direct lanthanide chelate label-based luminescence assay
Dy	Dysprosium
EALL	Enzyme-amplified lanthanide luminescence
ECIA	Electrochemical immunoassay
EDTA	Ethylenediaminetetraacetic acid
ee	Enantiomeric excess
EHEC	Enterohemorrhagic E. coli
ELISA	Enzyme-linked immunosorbent assay
Eu	Europium
EuTc	Europium tetracycline complex
EuTc-Cit	Europium-tetracycline-citrate (molar ratio of Eu^{3+}:Tc is 1 : 1)
EuTc-HP	Europium tetracycline hydrogen peroxide complex (molar ratio of Eu^{3+}:Tc is 3 : 1)
F	Fluorescence
FIA	Fluorescent immunoassay
FLIM	Fluorescence lifetime imaging microscopy
FM	Fumarase
FRET	Fluorescence resonance energy transfer
FSAP	5-fluoresalicyl phosphate
Fum	Fumarate
GOx	Glucose oxidase
HP	Hydrogen peroxide, H_2O_2
HRP	Horseradish peroxidase
HST	High throughput screening
iCit	Isocitrate

IDL	Interactive data language
KG	α-ketoglutarate
LOD	limit of detection
Mal	Malate
MDH	Malic dehydrogenase
MOPS	3-(N-Morpholino)propanesulfonate
NAD^+	β-Nicotinamide adenine dinucleotide
NADH	β-Nicotinamide adenine dinucleotide reduction
NTA	β-naphthoyltrifluoroacetone
Oxa	Oxaloacatate
pHPA	p-Hydroxyphenylacetate
pHPPA	4-hydroxyphenylpropionic acid
POx	Peroxidase
QY	Quantum yield
RIA	Radioimmunoassay
RLD	Rapid lifetime determination
S/N	Signal-to-noise ratio
SA	Salicylaldehyde
SLT1	Shiga-like toxins
Sm	Samarium
Suc	Succinate
Tb	Terbium
TBDRH	Tris(2,2'-bipyridyl)dichlororuthenium(II) hexahydrate
Tc	Tetracycline
TCSPC	Time-correlated single photon counting
TOPO	Trioctylphosphine oxide
TRFI-ELISA	Time-resolved fluorescence imaging ELISA

Chapter 1. Introduction

1.1. Characteristics of Fluorescence Spectra of Lanthanide

Fluorometry is a very useful tool in a variety of analytical regions since it can provide high sensitivity, good selectivity and multiparameter information, such as fluorescence intensity, lifetime, anisotropy and others. It has been widely applied in biomedical research and clinical diagnosis [1, 2], such as in astrospace living and environmental monitoring, interaction mechanisms of molecules, immunoassay, DNA sequencing, fluorescence in situ hybridization, and in cellular imaging. Developing new fluorescent reagents and analytical methods is one of main research directions for improving sensitivity and selectivity of bioanalysis. Lanthanide complexes have become a particularly attractive focus because of the specific features of their fluorescence.

1.1.1. Fluorescence Emission Mechanism of Lanthanide Complexes

Fluorescence [3, 4] of conventional fluorophores is the result of several processes as shown in the left of Fig. 1.1 (Jablonski diagram). In the excitation stage, the fluorophore absorbs energy supplied by an external radiation and is raised to any one of the vibrational multiplets of the first excited singlet state (S_1) from ground state (S_0). Most of the fluorophores in the S_1 state rapidly relax, through internal conversion (non-radiative decay), to the lowest vibrational level S_1, in which fluorescence emission originates. A photon is emitted on returning to the ground state (S_0). Other processes such as collisional quenching, energy transfer and solvent interactions may also occur. They are non-radiative decay. Conversion from S_1 to the first triplet state T_1 is intersystem crossing and transition from T_1 to ground state is forbidden, so its decay rate is slow, yields phosphorescence.

There are 15 elements in the lanthanide series, but only Sm^{3+}, Eu^{3+}, Tb^{3+} and Dy^{3+} enabling fluorescence. However, the absorption and fluorescence of these ions are very low and difficult to be used in analysis. They usually need to ligate an organic compound as antenna for energy transfer to metal ions.

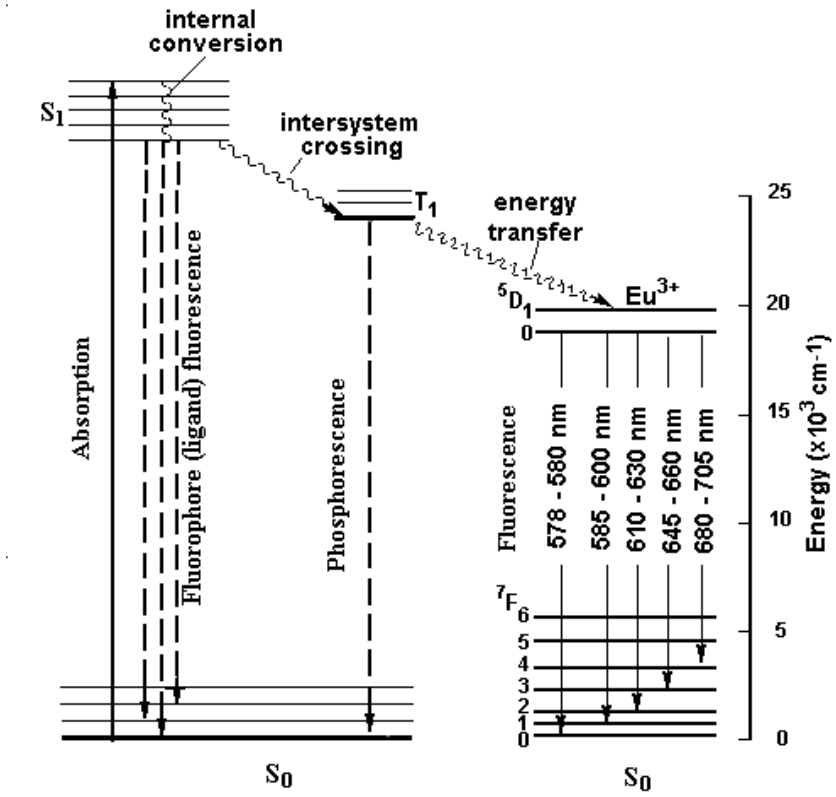

Figure 1.1. Fluorescence emission mechanism of Eu^{3+} complex.
S_0, S_1 and T_1 are singlet ground state, singlet excited state, and triplet state, respectively.

The fluorescence emission process of lanthanide complex [5, 6, 7] (in Fig. 1.1) is of some particularities that is absent in conventional fluorophores: (a) The ligand, not the lanthanide ion itself, absorbs energy from external source into S_1 from its S_0, then proceeds on the internal conversion. b) That intersystem crossing to T_1 from the lowest vibrational level S_1 can further proceed to intramolecular energy transfer from T_1 of the ligand to the localized appropriate 4f energy level of the central lanthanide ion, which in turn can moves up to its

own excited singlet state. It requires that deactivating ligand transition ($S_1 \rightarrow S_0$ and $T_1 \rightarrow S_0$) must be minimal and the energy level of ligand T_1 should be matched, namely close to, but just higher than the resonance level of lanthanide ion. c) The multiple emissions. For example in the europium complex, multiple emissions [8] are observed as several electronic transitions $^5D_0 \rightarrow {}^7F_J$ (J = 0, 1, 2, 3, 4) and $^5D_1 \rightarrow {}^7F_J$ (J = 1, 2, 3, 5, 6), the most intense transitions are $^5D_0 \rightarrow {}^7F_2$, and $^5D_0 \rightarrow {}^7F_1$ with emissions around 610-660 nm and 585-600 nm.

The above mechanism results in the three main advantages of lanthanide complexes in fluorometry. First is the large Stokes´ shift (150 – 300 nm). Owing to energy dissipation during internal conversion, intersystem crossing, and intramolecular energy transfer, energy of photon emitted from lanthanide complexes is significantly different from that of the excitation radiation, and therefore the Stokes´ shift of lanthanide complexes is usually large. This feature can be applied to avoid the overlap between excitation and emission spectra of fluorophore itself (inner filter effect) or emission from biological matrix.

Second is the narrow emission bands (1 – 20 nm), namely line-like bands. It is because of the shielding of the f orbitals by the higher s and p orbitals of lanthanide. It is noted that there are three and five components of the emission splitting patterns [9, 10] from $^5D_0 \rightarrow {}^7F_1$ and $^7F_2$, for example in Eu^{3+} complexes. But the failure to observe such splitting may be due to spectral resolution limitations of instrument rather than to inherent structural properties of the system. In addition, the fluorescence intensity of main band of lanthanide complex is very strong although its quantum yield is usually lower than that of conventional fluorophores. The reason is that the transferred energy is largely emitted by the line-like main band. The narrow emission bands also offer the possibility for the multiplex assays without overlapping spectra.

Third is the long fluorescence decay time (10 – 2000 μs). The f-f electronic transitions of lanthanide are forbidden, leading to long excited state decay time. Decay times of

lanthanide complexes are quite sensitive to the detailed nature of the ligand environment, and especially to the number of water molecules occupying inner coordination sites. The forbidden f-f transitions is also reflected in low extinction coefficients, making direct photoexcitation of lanthanide ions rather difficult, and requiring organic ligands for energy absorption. The relatively long decay times of lanthanide complexes have greatly facilitated the time-resolved fluorometry.

1.1.2. Time-Resolved Fluorescence Assays

The fluorescence decay time [5, 8, 11] is one of the most important characteristics of a fluorophore. There are mainly two kinds of method used for the measurement of the fluorescence decay times, namely time-domain or pulse fluorometry and frequency domain or phase-modulation fluorometry. In this dissertation, only time-domain methods will be discussed.

Compared with the lanthanide complexes, the conventional fluorophores have relative short decay times between 5-100 ns. The decay times of most light source background, such as Tyndall, Raman scatter, Rayleigh scatter, and sample background, such as cuvette, plate, and sample matrix (protein, NADH, etc), are around 0.1-10 ns. So the gated fluorometry based on the lanthanide complexes can be used as shown in Fig. 1.2.

The gated fluorescence experiment starts with the excitation pulse, but does not measure the fluorescence emission until the background has decayed to zero or minimum by a temporal lag. As lanthanide complexes have longer lifetimes, the background should be possible to be eliminated entirely. The sensitivity and selectivity of determination can be therefore improved.

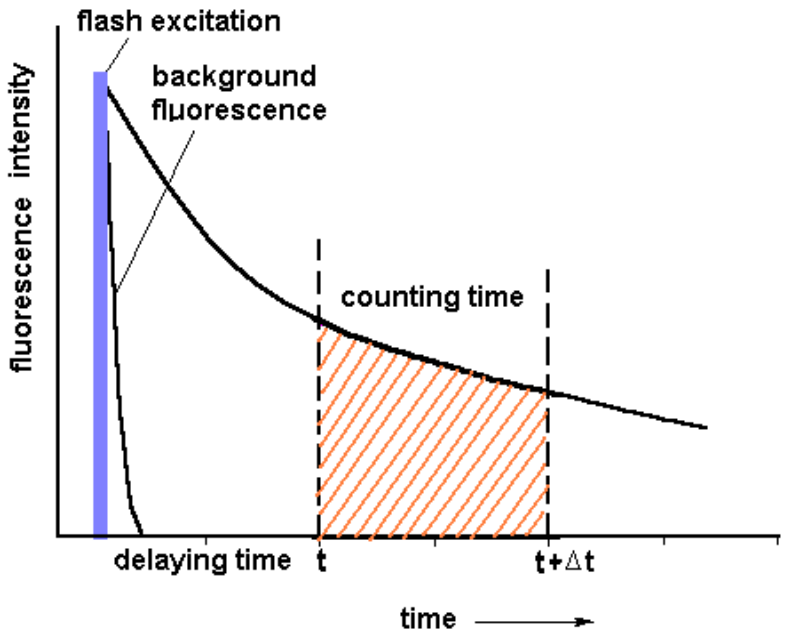

Figure 1.2. Principle of time-resolved (gated) fluorescence assay

The μs scale decay time of lanthanide complexes have also greatly facilitated their decay time determination. The decay time based fluorometry has the following advantages: (1) decay time is the inherent characteristics of fluorophores, not affected by the concentration of fluorophores and photobleaching. (2) decay time is independence of the light source fluctuation. (3) decay time of lanthanide complex is only sensitive to its microenvironment, such as water in inner coordination field. With the development of fluorescence theories and instruments, there have been a lot of applications of lanthanide fluorescence as in different time–resolved determination [5-8] and imaging [12, 13]. There have been several techniques developed, such as lifetime based time-correlated single photon counting (TCSPC) and rapid lifetime determination (RLD) in time-domain fluorometry. Time-resolved fluorometry can also been applied in anisotropy (polarization) detection as time-resolved anisotropy [14].

1.2. Time-Resolved Detection of Lanthanide Fluorescence for Bioassays

Fluorescence lanthanide chelates have been successfully developed as labels and probes for the highly sensitive and selective bioassays in the past two decades. Time-resolved fluorescence detection [15, 16] has been widely applied in fluoroimmunoassay, DNA hybridization assay, enzyme assay, cell activity assay, and fluorescence imaging microscopy. According to the necessity of analyte immobilization, these bioassays can be broadly classified into heterogeneous and homogeneous fluorescence determination. Although the latter, especially utilizing the principle of fluorescence resonance energy transfer (FRET) [17, 18] , has shown powerful potentials, it does not yet surpass the solid phase fluorescence bioassay in sensitivities, selectivities and virtual applications now. In the following, the three main approaches for time-resolved lanthanide fluorescence in heterogeneous phase, direct lanthanide chelate label-based luminescence assay (DLCLLA), dissociation enhanced lanthanide fluoroimmunoassay (DELFIA) and enzyme-amplified lanthanide luminescence (EALL), will be discussed in some details.

1.2.1. Direct Lanthanide Chelate Label-based Luminescence Assay (DLCLLA)

In contrast to other analytical methodologies (DELFIA and EALL), the experimental protocol of DLCLLA is simple. Its measurement principle (in Fig.1.3.) is that recognition molecules are labeled with fluorescent lanthanide chelate, being used to capture an analyte. The fluorescence intensity from label reports the quantity of analyte captured after excess labeled recognition molecules are washed off.

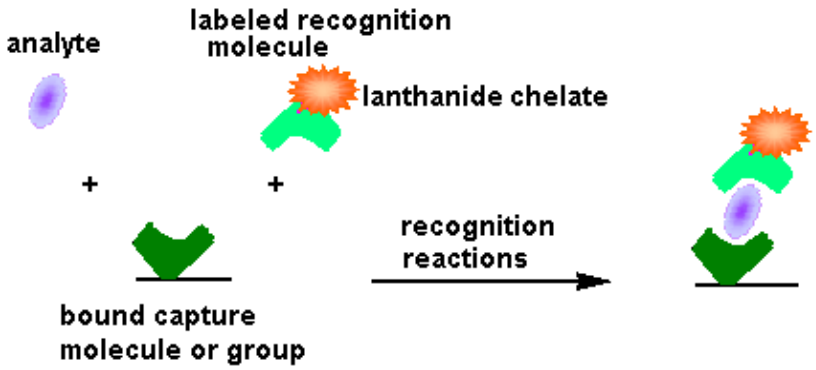

Figure 1.3. Scheme of DLCLLA
Recognitions include immunoaffinity or hybridization.

But an ideal fluorescence lanthanide chelate for DLCLLA is not easily achieved because the lanthanide chelate as label must undergoes the whole experiment processes including labeling reaction, recognition reaction and several rinses. Thus, there are some strict requirements for lanthanide chelate [15]: (a) high luminescence in water, (b) chemically and photochemically stable, (c) high metal-chelate binding constant and the presence of contain reactive groups appropriate for effective labeling reactions.

Many synthetic organic chelators (see Fig. 1.4) have emerged. 4,7-Bis-(chlorosulfophenyl)-1,10-phenanthroline-2,9-dicarboxylic acid (BCPDA) [19, 20] as ligands binding Eu^{3+} was the first commercial reagent for direct time-resolved fluorescence bioassay. It has been other applied in immunoassays [21], Western blots [22] and membrane based nucleic acid hybridization assay [23]. Subsequently, polyamino-polycarboxylate compounds and cage-type ligands have been synthesized, such as trisbipyridine cryptate (TBP), 4'-(3-isothiocyanato-4-methoxyphenyl)-6,6''-bis[N,N-bis(carboxymethyl)aminomethyl)-2,2';6',2''-terpyridine (TMT), and others. [Eu^{3+}-TBP] can be used the detection of specific amplified

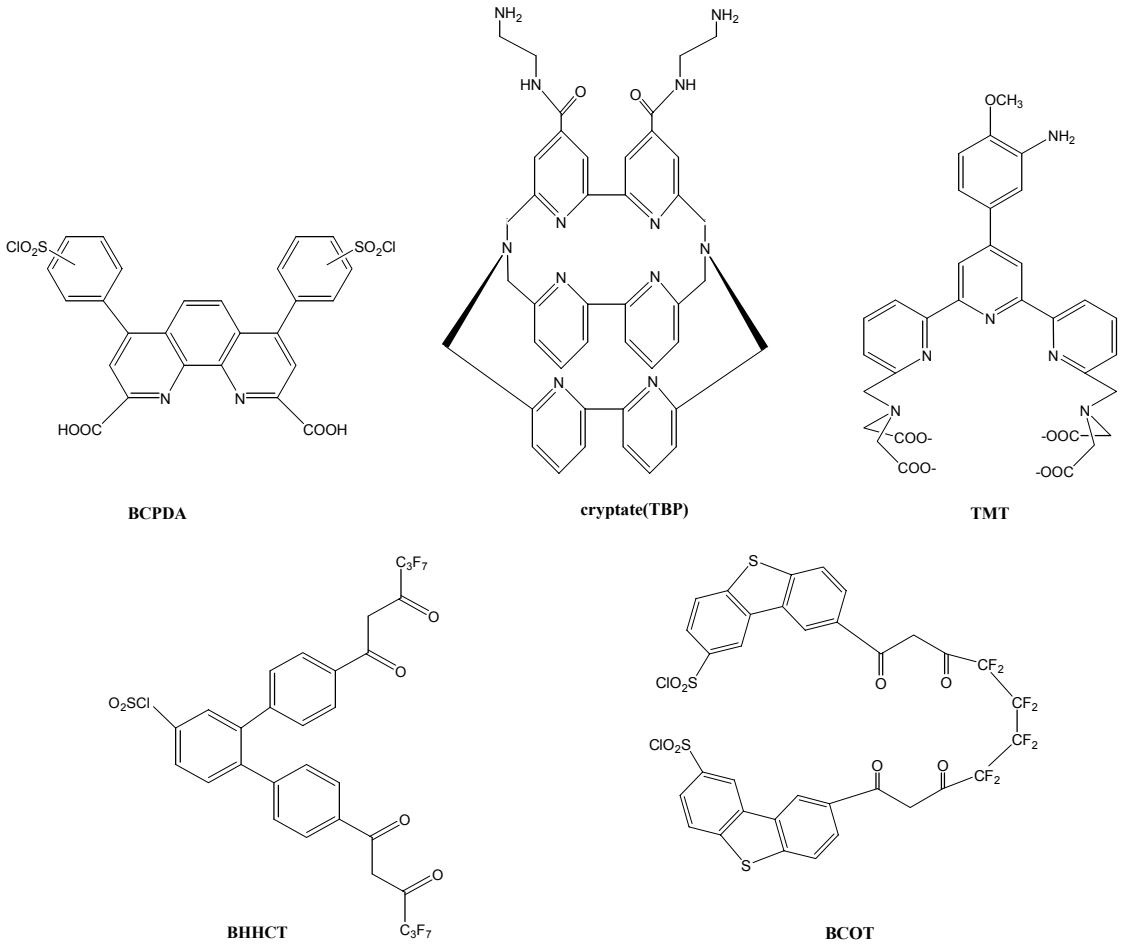

Figure 1.4. Chelators for lunimescent lanthanide labels.

target DNA [24, 25], but it is more often used in homogeneous detection for biomolecular interaction via FRET [16]. [Eu^{3+}-TMT] was employed for the determination of protein and DNA samples [26] and its limit of detection is approx. 10^{-16} mol. Many lanthanide *β*-diketonate chelates also display intensive fluorescence, but a few are suitable for the requirement of DLCLLA, for example, BHHCT [27] and BTOT [28] (Fig. 1.4.). They have been used in albumin and IgE assays [29]. Other *β*-diketonate compounds, e g. 1,10-bis(thiophene-2′-yl)-4,4,5,5,6,6,7,7–octafluorodecane-1,3,8,10-tetraone (BTOT) [30] and 4,4′-bis(1’,1’,1’-trifluoro-2’,4’-butanedione-6’-yl)-chlorosulfo-*o*-terphenyl) (BTBCT) [31] have also been reported.

1.2.2. Dissociation Enhanced Lanthanide Fluoroimmunoassay (DELFIA)

In lanthanide chelate based fluorescence detection systems, DELFIA [32, 33] is the most widely utilized approach. Its principle (Fig. 1.5) is that recognition molecule is labeled by the lanthanide chelate, which has a strong binding ability, but no or much weak fluorescence itself in the assay medium. After specific binding reaction for the analyte has been performed and the non-bound fraction of the label molecule has been efficiently washed away, lanthanide ion must be dissociated and released from the lanthanide chelate label, then enter an enhancement solution and micelle environment in which it coordinates new ligand and is measured via fluorescence.

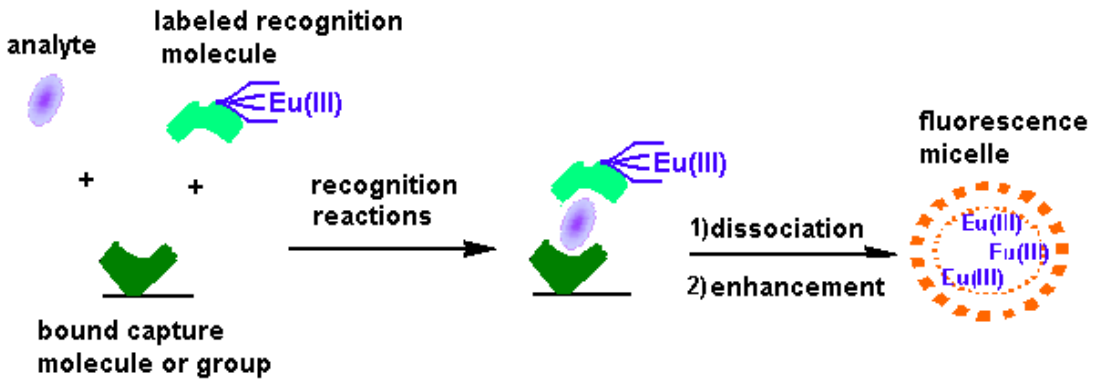

Figure 1.5. Scheme of DELFIA
Recognitions include immunoaffinity or hybridization.

In DELFIA [32-36] diethylene-triaminetetraacetic acid or the derivative of ethylenediaminetetraacetic acid (EDTA) as chelating agent coordinates with europium ion to form lanthanide chelate label, such as, isothiocyanatophenyl–EDTA-Eu^{3+}. Dissociative enhancement solution usually includes β-naphthoyltrifluoroacetone (NTA) as the energy transfer chelator, trioctylphosphine oxide (TOPO) as synergistic ligand, and Triton X-100 as detergent. In phthalate buffer at low pH 3.4, the stability of lanthanide chelate label is strongly

decreased in comparison to NTA present in the solution in large excess. Under these conditions the ligand exchange reaction is completed very fast. A new chelate is formed with NTA and the remaining empty coordination sites are occupied with TOPO, which prevents aqueous quenching. The hydrophobic chelate formed is dissolved in a micellar detergent solution (Triton X-100), in which the high fluorescence intensity can be determined.

This method has been employed in many areas, such as PCR [37], nucleic acid hybridization [38, 39], immunoassays [40] for hormones [41], steroid [42] and inhibitor [43], proteins in cells [44-45] , and drug discovery [46].

In addition, multiplexing DELFIA has been also developed. Its protocol is (a) the same chelators are used to ligate several of lanthanide ions and to form differently colored fluorescent lanthanide chelates; (b) these lanthanide chelates are labeled on different recognition molecules (or groups) in same system; (c) "co-fluorescence enhancement" solution is employed for fluorescence measurement [47, 48]. Due to the narrow emission peaks of lanthanides at different wavelengths and their different fluorescence lifetime, the combination of spectral windows and temporal windows can be employed for the optimization of the measurement parameters. Thus, maximal sensitivity and minimal signal loss are obtained. All labels can be determined simultaneously, even if one is present in a significant excess, which is based on co-fluorescence enhancement. Multiplexing DELFIA assays, such as Eu^{3+} and Sm^{3+} [49, 50], Eu^{3+} and Y^{3+} [51], or Eu^{3+}, Sm^{3+}, Tb^{3+} and Dy^{3+} [52, 53], have been reported.

1.2.3. Enzyme Amplified Lanthanide Luminescence (EALL)

The concept and experiment of EALL [54] were first reported by Evangelista and co-workers in 1991. It is a bridge to connect the two sectors of enzyme assay and lanthanide

fluorescence assay. The basic principles of EALL is shown in Fig. 1.6. The label of recognition molecule is enzyme, not lanthanide chelate. After the analyte is recognized, substrate for enzyme is added. Its reaction product can associate with lanthanide ion to form fluorescence chelate to be detected.

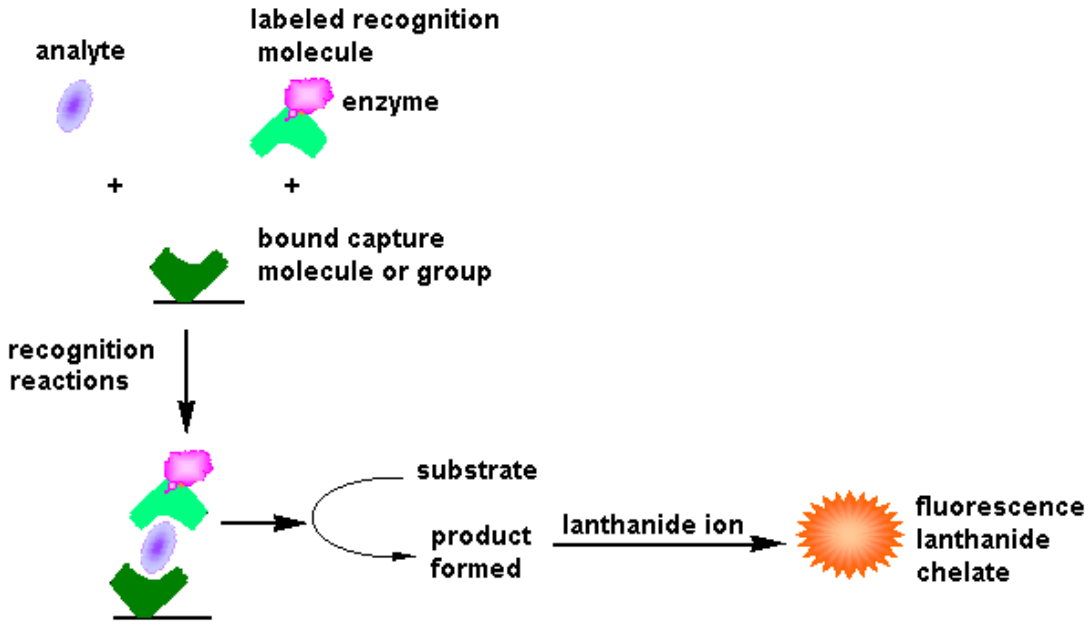

Figure 1.6. Scheme of EALL
Recognitions include immunoaffinity or hybridization.

As many enzymes can catalyze different substrates to form a lot of different products, the wide application area of EALL can be predicted. Up to now, Eu^{3+} and Tb^{3+} as main lanthanide element are employed in EALL. Some enzymes, such as alkaline-phosphatase (AP), glucose oxidase (GOx), peroxidase (POx), galactosidase, esterase and catalase, have been employed in EALL as summarized in Table 1.1. As these enzymes are of high stability and sensitivity, they have been usually used as label in many biological recognition molecules and have been commercialized.

On the other hand, since the property of substrate as media will influence the fluorescence of the final lanthanide chelate, There are some stipulations [54]: a) the substrate does not absorb the excitation light efficiently in the absorption spectrum of lanthanide chelate; b) the substrate does not efficiently transfer the excitation energy to the chelated lanthanide; c) the substrate does not efficiently chelate the lanthanide. Now some substrates have been used in different enzymes, for example, salicylaldehyde (SA), 5-fluorosalicyl phosphate (FSAP), phosphate ester of diflunisal (DIFP) and other salicyl phosphate-derived compounds for AP; 4-hydroxyphenylpropionic acid (pHPPA) for POx.

Since enzyme amplification cycling reactions, EALL has a very low limit of detection (Table 5.1). It is conceivable that, in the scheme of EALL, substrate may be also a strong fluorescent lanthanide chelate to yield no or weak fluorescence product by enzyme catalytically. So the determinations of GOx [67] and of catalase [68] can be considered as this scheme.

In addition, some improved schemes from enzyme and lanthanide chelates have been presented. For example, Ioannou and co-workers [55] reported the two-round enzymatic amplification, first combined with tyramide signal amplification [56], then with EALL, so that the selectivity and sensitivity have been increased.

TABLE 1.1. MAIN APPLICATIONS OF ENZYME-AMPLIFIED LANTHANIDE LUMINESCENCE (EALL)

	Target	**Enzyme**	**Substrate**	**Detection Chelates**	**LOD**	**Ref.**
1	Alkaline-phosphatase (AP)	AP	5-fluorosalicyl phosphate (FSAP)	FSA-Tb^{3+}-EDTA	0.2 amol	54
2	IgG	AP	5-fluorosalicyl phosphate (FSAP)	FSA-Tb^{3+}-EDTA	5 pg	54
3	Xanthine oxidase(XOD)	XOD	salicylaldehyde	SA-Tb^{3+}-EDTA	1 µUnits	54
4	β-Galactosidase (Gas)	GAs	salicyl- β-D-galactoside	SA-Tb^{3+}-EDTA	90 amol	54
5	Glucose oxidase (GOx)	GOx	1,10-phenanthroline-2,9-dicarboxylic acid dihydrazide (PDAdh)	PDA-Tb^{3+}-EDTA	2 fmol	54
6	DNA fragment	AP	salicylaldehyde	SA-Tb^{3+}-EDTA	4 pg	57
7	α-Fetoprotein (AFP)	AP	5-fluoresalicyl phosphate (FSAP)	FSA-Tb^{3+}-EDTA	0.15 pg/mL	58
8	α-Fetoprotein (AFP)	AP	phosphate ester of diflunisal (DIFP)	DIF-Tb^{3+}-EDTA	5 pg/mL	59
9	Horseradish peroxidase (HRP)	HRP	4-hydroxyphenylpropionic acid (pHPPA)	pHPPA (dimer)-Tb^{3+}-EDTA +	2 x 10^{-12} mol / L	60
10	IgG	POx	4-hydroxyphenylpropionic acid (pHPPA)	pHPPA (dimer)-Tb^{3+}-EDTA +	3 µg/L	61
11	Porcine liver esterase	esterase	acetic acid eater of bis(2-pyridylmethyl)-(2-hydroxyrbenzyl)amine	bis(2-pyridylmethyl)-(2-hydroxyrbenzyl)amine-Tb^{3+}	3 x10^{-9} M	62
12	DNA fragment (PCR)	AP	FSAP	FSA-Tb^{3+}-EDTA	1x10^{3}-2x10^{5} molecules	63
13	pBR322 plasmid DNA (dot-blot DNA hybridization)	AP	alkyl and aryl-substituted salicyl phosphates	xSA-Tb^{3+}-EDTA	125 pg	64
14	Interleukin 6	AP	DIFP	DIF-Tb^{3+}-EDTA	0.15 ng/L	65
15	Tumor necrosis factor- α (TNF- α)	AP	DIFP	DIF-Tb^{3+}-EDTA	0.2 ng/L	66
16	Glucose oxidase (GOx)	GOx	glucose	Tc-Eu^{3+}-HP	0.32 mUnits/mL	67
17	Catalase	catalase	tetracycline-Eu(III)-hydrogen peroxide	Tc-Eu $^{3+}$-HP→ Tc-Eu(III)	0.046 Units /mL	68

From these discussions, some characterizations of these approaches can be concluded: (a) lanthanide chelate as labels are used in DLCLLA and in DELFIA, but requirements are different. Label in DLCLLA must have intense fluorescence, while that in DELFIA must have no (or weak) fluorescence. However, the lanthanide chelate in EALL is a probe, in which the label is an enzyme. (b) DLCLLA in principle and protocol is simple, some cases have even higher sensitivity than DELFIA. But its labeling chelates need much stronger fluorescence intensity and stability, thereby its applications are restricted. (c) DELFIA is a highly sensitive scheme as its processes of molecule recognition and enhance fluorescence are separated. However, this feature also prevents its application in cytofluorometry, in-situ immunostaining, etc although it has enough widely application area. (d) The good perspective of EALL may be conceivable as enzymes correspond to numerous substrates and products, and it can be connected to other technologies to improve its applications, but now the available substrates and lanthanide chelates are rather limited and need to further explored.

1.3. Aim of Research

The goal of this dissertation is to develop ternary europium-derived (different stoichiometry) fluorescent probe for bioassays in aqueous solution. There are three main aspects: the first is based on the europium-tetracycline-hydrogen peroxide (EuTc-HP) probe, which can be converted into europium-tetracycline (EuTc) by peroxidase (POx), so that the activity of POx and POx labeled biomolecules will be possible determined; The second is based on the changes of fluorescence of EuTc probe when ligated to hydroxy acid (or oxyanions). Citrate and the main intermediates in the Krebs cycle can be determined and imaged without enzymes or multi-enzyme systems. The third relates to fluorescent discrimination of enantiomeric malates in aqueous solution.

Different fluorescence technologies, namely conventional steady-state and time-resolved (gated) fluorescence detection, conventional and time-resolved (gated and rapid lifetime detection) imaging, are being applied.

1.4. References

[1] Kraayenhof, R.; Visser, A. J. W. G. and Gerritsen, H. C. (Eds), **Fluorescence Spectroscepy, Imaging and Probes: New Tools in Chemical, Physical and Life Sciences** (Springer series on fluorescence methods and applications 2), Springer, 2002

[2] Mason, W. T. (Ed) **Fluorescent and Luminescent Probes for Biological Activity**, Second Edition, Academic Press, 1999.

[3] Lakowicz, J. R. **Principles of Fluorescence Spectroscopy**, Second Edition, Kluwer Academic / Plenum Plublishers, 1999.

[4] Valeur, B. **Molecular Fluorescence: Principles and Applications**, Wiley-VCH, 2002

[5] Richardson, F. S. **Terbium(III) and europium(III) ions as luminescent probes and stains for biomolecular systems**. Chemical Reviews 1982, 82(5), 541-52.

[6] Diamandis, E. P.; Christopoulos, T. K. **Europium chelate labels in time-resolved fluorescence immunoassays and DNA hybridization assays.** Analytical Chemistry 1990, 62(22), 1149A-1157A.

[7] Georges, J. **Lanthanide-sensitized luminescence and applications to the determination of organic analytes. A review**. Analyst 1993, 118(12), 1481-6.

[8] Arnaud, N.; Georges, J. **Comprehensive study of the luminescent properties and lifetimes of Eu^{3+} and Tb^{3+} chelated with various ligands in aqueous solutions: influence of the synergic agent, the surfactant and the energy level of the ligand triplet.** Spectrochimica Acta, Part A: Molecular and Biomolecular Spectroscopy 2003, 59A(8), 1829-1840.

[9] Yatsimirskii, K. B.; Davidenko, N. K. **Absorption spectra and structure of lanthanide coordination compounds in solution.** Coordination Chemistry Reviews 1979, 27(3), 223-73.

[10] Richardson, F. S.; Gupta, A. D. **Spectroscopic studies on the interaction of the antibiotic lasalocid A (X537A) with lanthanide(III) ions in methanol.** Journal of the American Chemical Society 1981, 103(19), 5716-25.

[11] Hemmila, I.; Webb, S. **Time-resolved fluorometry: an overview of the labels and core technologies for drug screening applications.** Drug Discovery Today 1997, 2(9), 373-381.

[12] Gerritsen, H. C.; De Grauw, K. **One- and two-photon confocal fluorescence lifetime imaging and its applications.** Methods in Cellular Imaging 2001, 309-323.

[13] Clegg, R. M.; Holub, O.; Gohlke, C. **Fluorescence lifetime-resolved imaging: Measuring lifetimes in an image.** Methods in Enzymology 2003, 360 (Biophotonics, Part A), 509-542.

[14] Bain, A. J. **Time-resolved polarised fluorescence studies of ordered molecular systems.** Introduction to Laser Spectroscopy 2002, 171-210.

[15] Gudgin Dickson, E. F.; Pollak, A.; Diamandis, E. P. **Time-resolved detection of lanthanide luminescence for ultrasensitive bioanalytical assays.** Journal of Photochemistry and Photobiology, B: Biology 1995, 27(1), 3-19.

[16] Elbanowski, M.; Makowska, B. **The lanthanides as luminescent probes in investigations of biochemical systems** J. Photochem. Photobiol. A. 1996, 99, 85-92.

[17] Bazin, H.; Trinquet, E.; Mathis, G. **Time resolved amplification of cryptate emission: a versatile technology to trace biomolecular interactions.** Reviews in Molecular Biotechnology 2002, 82(3), 233-250.

[18] Tsourkas, A.; Behlke, M. A.; Xu, Y.; Bao, G. **Spectroscopic features of dual fluorescence/luminescence resonance energy-transfer molecular beacons.** Analytical Chemistry 2003, 75(15), 3697-3703.

[19] Diamandis, E. P.; Morton, R. C. **Time-resolved fluorescence using a europium chelate of 4,7-bis-(chlorosulfophenyl)-1,10-phenanthroline-2,9-dicarboxylic acid (BCPDA). Labeling procedures and applications in immunoassays.** Journal of Immunological Methods 1988, 112(1), 43-52.

[20] Evangelista, R. A.; Pollak, A.; Allore, B.; Templeton, E. F.; Morton, R. C.; Diamandis, E. P. **A new europium chelate for protein labelling and time-resolved fluorometric applications**. Clinical Biochemistry 1988, 21(3), 173-8.

[21] Reichstein, E.; Shami, Y.; Ramjeesingh, M.; Diamandis, E. P. **Laser-excited time-resolved solid-phase fluoroimmunoassays with the new europium chelate 4,7-bis(chlorosulfophenyl)-1,10-phenanthroline-2,9-dicarboxylic acid as label.** Analytical Chemistry 1988, 60(10), 1069-74.

[22] Diamandis, E. P.; Christopoulos, T. K.; Bean, C. C. **Quantitative western blot analysis and spot immunodetection using time-resolved fluorometry**. Journal of Immunological Methods 1992, 147(2), 251-9.

[23] Christopoulos, T. K.; Diamandis, E. P.; Wilson, G. **Quantification of nucleic acids on nitrocellulose membranes with time-resolved fluorometry**. Nucleic Acids Research 1991, 19(21), 6015-9.

[24] Prat, O.; Lopez, E.; Mathis, G. **Europium(III) cryptate: a fluorescent label for the detection of DNA hybrids on solid support.** Analytical Biochemistry 1991, 195(2), 283-9.

[25] Lopez, E.; Chypre, C.; Alpha, B.; Mathis, G . **Europium(III) trisbipyridine cryptate label for time-resolved fluorescence detection of polymerase chain reaction products fixed on a solid support**. Clinical Chemistry 1993, 39(2), 196-201.

[26] Saha, A. K.; Kross, K.; Kloszewski, E. D.; Upson, D. A.; Toner, J. L.; Snow, R. A.; Black, C. D. V.; Desai, V. C. **Time-resolved fluorescence of a new europium-chelate complex: demonstration of highly sensitive detection of protein and DNA samples** Journal of the American Chemical Society 1993, 115(23), 11032-3.

[27] Yuan, J.; Matsumoto, K. **A new tetradentate -diketonate-europium chelate that can be covalently bound to proteins for time-resolved fluoroimmunoassay**. Analytical Chemistry. 1998, 7, 596–601.

[28] Yuan, J.; Matsumoto, K. **Synthesis of a new tetradentate β-diketonate-europium chelate and its application for time-resolved fluorimetry of albumin.** Journal of Pharmaceutical and Biomedical Analysis 1997, 15(9,10), 1397-1403.

[29] Yuan, J.; Wang, G.; Kimura, H.; Matsumoto, K. **Highly sensitive time-resolved fluoroimmunoassay of human immunoglobulin E by using a new europium fluorescent chelate as a label.** Analytical Biochemistry 1997, 254(2), 283-287.

[30] Wu, F.; Han, S.; Zhang, C.; He, Y. **Synthesis of a highly fluorescent β-diketone-europium chelate and its utility in time-resolved fluoroimmunoassay of serum total thyroxine**. Analytical Chemistry 2002, 74(22), 5882-5889.

[31] Wu, F.; Zhang, C. **A new europium β-diketone chelate for ultrasensitive time-resolved fluorescence immunoassays.** Analytical Biochemistry 2002, 311(1), 57-67.

[32] Hemmila, I. A. **Photoluminescence immunoassays.** Immunochemistry 1997, 1,193-214.

[33] http://las.perkinelmer.com/content/ApplicationNotes/12349847-MultiplexingDELFIA.pdf

[34] Degan, P.; Abbondandolo, A.; Montagnoli, G. **A new fluorescence enhancement solution for europium-based time-resolved fluoroimmunoassays.** Journal of Bioluminescence and Chemiluminescence 1990, 5(3), 207-12.

[35] Keelan, J. A.; France, J. T.; Barling,P. M. **An alternative fluorescence enhancement solution for use in lanthanide-based time-resolved fluoroimmunoassays**. Clinical Chemistry 1987, 33(12), 2292-5.

[36] Mukkala, V. M.; Mikola, H.; Hemmila, I. **The synthesis and use of activated N-benzyl derivatives of diethylenetriaminetetraacetic acids: alternative reagents for labeling of antibodies with metal ions.** Analytical Biochemistry 1989, 176(2), 319-25.

[37] Seddon, H. R.; Gray, G.; Pollitt, R. J.; Iitia, A.; Green, A. **Population screening for the common G985 mutation causing medium-chain acyl-CoA dehydrogenase deficiency with Eu-labeled oligonucleotides and the DELFIA system.** Clinical Chemistry 1997, 43(3), 436-442.

[38] Diamandis, E. P. **Time-resolved fluorometry in nucleic acid hybridization and western blotting techniques.** Electrophoresis 1993, 14(9), 866-75.

[39] Dahlen, P.; Carlson, J.; Liukkonen, L.; Lilja, H.; Siitari, H.; Hurskainen, P.; Iita, A.; Jeppsson, J. O.; Lovgren, T. **Europium-labeled oligonucleotides to detect point mutations: application to PIZ alpha 1-antitrypsin deficiency**. Clinical Chemistry 1993, 39(8), 1626-31.

[40] Qin, Q.; Christiansen, M.; Pettersson, K. **Point-of-care time-resolved immunofluorometric assay for human pregnancy-associated plasma protein A: use in first-trimester screening for down syndrome**. Clinical Chemistry 2002, 48(3), 473-483.

[41] Daijo, J. E.; Sportsman, J. R. **A time-resolved fluorescence immunoassay for insulin in rodent plasma.** Journal of Pharmaceutical and Biomedical Analysis 1999, 19(3-4), 335-342.

[42] Fiet, J.; Giton, F.; Boudi, A.; Boudou, P.; Soliman, H.; Villette, J.-M.; Galons, H. **Development of a sensitive and specific new plasma 4-androstene-3,17- dione time-resolved fluoroimmunoassay (TR-FIA).** Steroids 2001, 66(8), 609-614.

[43] Logianzo, F.; Hardy, C. **A sensitive, time-resolved fluorometric assay for detection of inhibitors of phosphotyrosine kinases**. American Biotechnology Laboratory 1998, 16(13), 26, 28.

[44] Waddleton, D.; Ramachandran, C.; Wang, Q. **Development of a time-resolved fluorescent assay for measuring tyrosine-phosphorylated proteins in cells**. Analytical Biochemistry 2002, 309(1), 150-157.

[45] Knipping, G.; Gogg-Fassolter, G.; Frohnwieser, B.; Krempler, F.; Kostner, G. M.; Malle, E. **Quantification of apolipoprotein D by an immunoassay with time-resolved fluorescence spectroscopy.** Journal of Immunological Methods 1997, 202(1), 85-95.

[46] Willson, V. J. C.; Lockley, W. J. S.; Mather, A.; Singh, J.; Gilbert, C. M.; Bayliss, M. A.; Wilkinson, D. **A time-resolved fluorescence immunoassay for the determination of a novel respiratory therapeutic agent, AR-C68397XX (Viozan) in human plasma.** Journal of Pharmaceutical and Biomedical Analysis 2000, 23(6), 947-954.

[47] Selvin, P. R. **Lanthanide-labeled DNA.** Topics in Fluorescence Spectroscopy 2003, 7 (DNA Technology), 177-212.

[48] Heinonen, P.; Iitia, A.; Torresani, T.; Lovgren, T. **Simple triple-label detection of seven cystic fibrosis mutations by time-resolved fluorometry**. Clinical Chemistry 1997, 43(7), 1142-50.

[49] Kimura, H.; Mukaida, M.; Wang, G.; Yuan, J.; Matsumoto, K. **Dual-label time-resolved fluoroimmunoassay of psychopharmaceuticals and stimulants in serum.** Forensic Science International 2000, 113(1-3), 345-351.

[50] Qin, Q.; Christiansen, M.; Loevgren, T.; Norgaard-Pedersen, B.; Pettersson, K**. Dual-label time-resolved immunofluorometric assay for simultaneous determination of pregnancy-associated plasma protein A and free β-subunit of human chorionic gonadotropin.** Journal of Immunological Methods 1997, 205(2), 169-175.

[51] Latva, M.; Takalo, H.; Simberg, K.; Kankare, J. **Enhanced EuIII ion luminescence and efficient energy transfer between lanthanide chelates within the polymeric structure in aqueous solutions**. Journal of the Chemical Society, Perkin Transactions 2: Physical Organic Chemistry 1995, (5), 995-9.

[52] Siitari, H.; Hemmila, I.; Soini, E.; Lovgren, T.; Koistinen, V. **Detection of hepatitis B surface antigen using time-resolved fluoroimmunoassay**. Nature 1983, 301(5897), 258-60.

[53] Xu, Y. Y.; Pettersson, K.; Blomberg, K.; Hemmila, I.; Mikola, H.; Lovgren, T. **Simultaneous quadruple-label fluorometric immunoassay of thyroid-stimulating hormone, 17 alpha-hydroxyprogesterone, immunoreactive trypsin, and creatine kinase MM isoenzyme in dried blood spots.** Clinical Chemistry 1992, 38(10), 2038-43.

[54] Evangelista, R. A.; Pollak, A.; Templeton, E. F. G. **Enzyme-amplified lanthanide luminescence for enzyme detection in bioanalytical assays.** Analytical Biochemistry 1991, 197(1), 213-24.

[55] Ioannou, P. C.; Christopoulos, T. K. **Two-round enzymic amplification combined with time-resolved fluorometry of Tb3+ chelates for enhanced sensitivity in DNA hybridization assays.** Analytical Chemistry 1998, 70(4), 698-702.

[56] http://www.probes.com/handbook/sections/0602.html

[57] Templeton, E. F. G., W.; Hector, E.; Evangelista, R. A.; Granger, T.; Pollak, A. **Time-resolved fluorescence detection of enzyme-amplified lanthanide luminescence for nucleic acid hybridization assays.** Clinical Chemistry 1991, 37(9), 1506-12.

[58] Christopoulos, T. K.; Diamandis, E. P. **Enzymically amplified time-resolved fluorescence immunoassay with terbium chelates.** Analytical Chemistry 1992, 64(4), 342-6.

[59] Veiopoulou, C. J.; Lianidou, E. S.; Ioannou, P. C.; Efstathiou, C. E. **Comparative study of fluorescent ternary terbium complexes. Application in enzyme amplified fluorimetric immunoassay for α-fetoprotein.** Analytica Chimica Acta 1996, 335(1-2), 177-184.

[60] Meyer, J.; Karst, U. **Peroxidase enhanced lanthanide luminescence-a new technique for the evaluation of bioassays.** Analyst 2000, 125(9), 1537-1538.

[61] Meyer, J.; Karst, U. **Enzyme-linked immunosorbent assays based on peroxidase labels and enzyme-amplified lanthanide luminescence detection**. Analyst 2001, 126(2), 175-178.

[62] Steinkamp, T.; Schweppe, F.; Krebs, B.; Karst, U. **A tripod ligand as new sensitiser for the enzyme amplified lanthanide luminescence determination of esterase**. Analyst 2003, 128(1), 29-31.

[63] Bortolin, S.; Christopoulos, T. K.; Verhaegen, M. **Quantitative polymerase chain reaction using a recombinant DNA internal standard and time-resolved fluorometry.** Analytical Chemistry 1996, 68(5), 834-40.

[64] Evangelista, R. A.; Wong, H. E.; Templeton, E. F. G.; Granger, T.; Allore, B.; Pollak, A. **Alkyl- and aryl-substituted salicyl phosphates as detection reagents in enzyme-amplified fluorescence DNA hybridization assays on solid support.** Analytical Biochemistry 1992, 203(2), 218-26

[65] Bathrellos, L. M.; Lianidou, E. S.; Ioannou, P. C. **A highly sensitive enzyme-amplified lanthanide luminescence immunoassay for interleukin 6.** Clinical Chemistry 1998, 44(6), 1351-1353.

[66] Petrovas, C.; Daskas, S. M.; Lianidou, E. S. **Determination of tumor necrosis factor-α (TNF-α) in serum by a highly sensitive enzyme amplified lanthanide luminescence immunoassay**. Clinical Biochemistry 1999, 32(4), 241-247.

[67] Wolfbeis, O. S.; Duerkop, A.; Wu, M.; Lin, Z. **A Europium-ion-based luminescent sensing probe for hydrogen peroxide.** Angewandte Chemie, International Edition 2002, 41(23), 4495-4498.

[68] Wu, M.; Lin, Z.; Wolfbeis, O. S. **Determination of the activity of catalase using a europium(III)-tetracycline-derived fluorescent substrate**. Analytical Biochemistry 2003, 320(1), 129-135.

Chapter 2. Determination of the Activity of Peroxidase via the EuTc-HP Probe

2.1. Introduction

Peroxidases are widely studied [1-3] across a range of scientific disciplines, and applied [4-6] in bioanalytical protocols, in chemical and biomedical research, and in the food and pharmaceutical industries in general. They are known for being sensitive to ultra-low concentrations of substrates and tolerant to relatively harsh conditions, and therefore probably among the most preferred enzyme labels in enzyme-linked immunosorbent assay (ELISA) [7], nucleic acid assay [8], high-throughput screening (HTS) [9], and histochemical staining imaging [10].

Quite a variety of methods is known for the determination of the activity of peroxidase (POx). Practically all are based on the fact that POx reacts with hydrogen peroxide and a second substrate. Numerous such second substrates [11, 12] (often referred to as hydrogen donors) are suitable for chromogenic, fluorogenic or other signal-generating purposes. As a result, kinetic assays have been developed based on spectrophotometry / reflectometry [13, 14], fluorometry [15, 16], chemiluminescence [17-19], electrochemiluminescence [20] and electroanalysis [21-23]. Among the fluorometric methods, those based on time-resolution [24] are the most sensitive tools in biological assays. Surprisingly, there is only one report [25] on the application of time-resolved lanthanide luminescence (using Tb^{3+} ion) now, although it is a particularly attractive scheme for the determination of the activity of POx.

A new and easily accessible fluorescent probe, the europium-tetracycline-hydrogen peroxide (EuTc-HP) complex, is presented here for the time-resolved detection of the activity of peroxidase. It is based on the findings that (a) H_2O_2 forms a strongly fluorescent system

with the europium-tetracycline complex (EuTc) [26, 27], (b) this system (EuTc-HP) is decomposed by POx and reversed to the weakly fluorescent EuTc, and (c) the average lifetime of EuTc-HP (~60 μs) is about two times that of EuTc (~30 μs), which offers the possibility for a time-resolved assay of POx. The results presented here demonstrate that EuTc-HP can be used for a new type of fluorometric assay for the activity of POx.

2.2. Results and Discussion

2.2.1. Principle of POx Assay

2.2.1.1. Structure and Reaction Mechanism of POx

Among of POx, horseradish peroxidase (HRP) [1, 2] is the most comprehensively studied. Its structure [1, 2, 28] is shown in Fig. 2.1. HRP is specifically discussed in this dissertation.

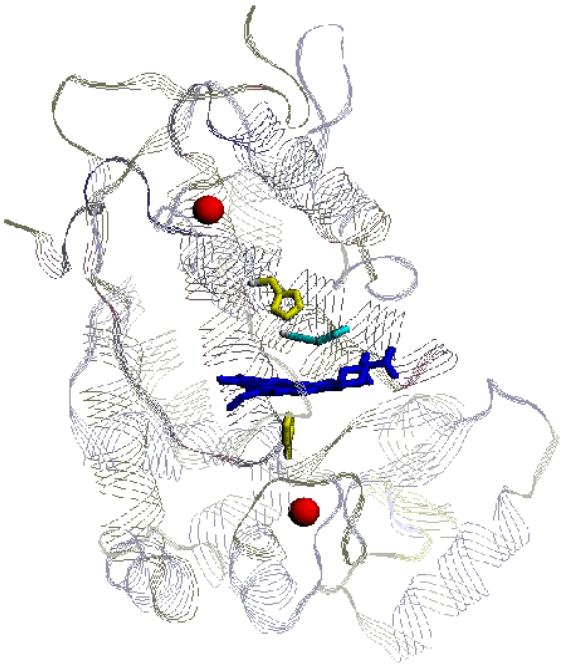

Fig.2.1. HRP structure. The main components are the heme (blue), the essential calcium ions (red), and the three key aminoacid residues: the proximal (below the heme) and distal (above the heme) histidines (yellow) and the distal pocket arginine (cyan). (From: Radu L. Silaghi-Dumitrescu, ref.[12])

The processes [1, 29, 30] through which hydrogen peroxide oxidizes the second substrate catalytically by HPR, compose of multi-step reactions in Fig. 2.2. In the figure, compound-I and compound-II are enzyme intermediates, and AH_2 is the second substrate (hydrogen donor). •AH is a radical product which has several possible fates, depending upon its

chemistry and environment of the reaction, to become a dimer, to react with another substrate molecule, or to attack another species causing cooxidation.

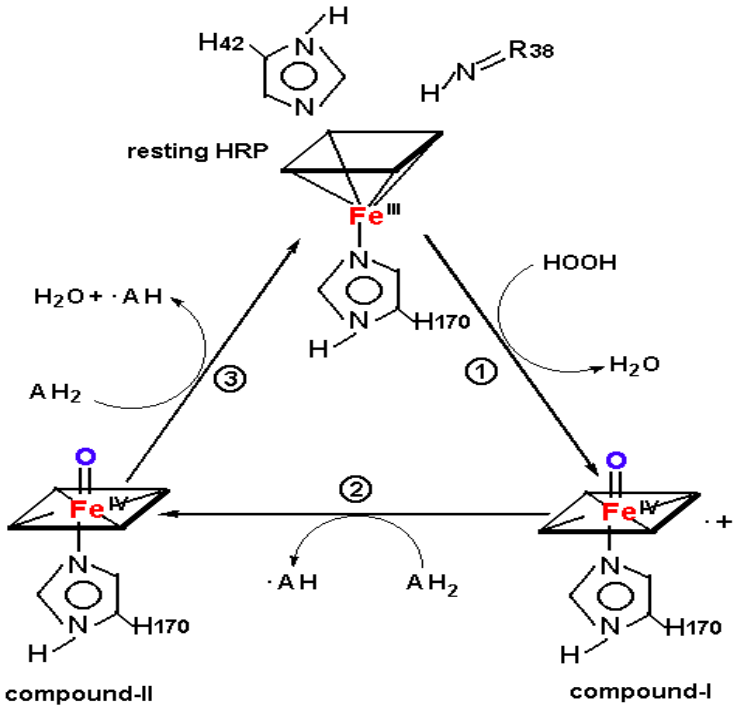

Figure 2.2. Proposed mechanism of HRP

Besides the Fe^{3+} in the centre of heme, the functional role of the key residues in the active site of HRP are very important in the processes of catalysis [1, 2, 31, 32]. The three amino acids, histidine 170 (H170), histidine 42 (H42) and arginine 38 (R38), synergistic act for the decomposition of H_2O_2.

The kinetic mechanism scheme in Fig. 2.2 is generally considered as the following: (1) From HRP to compound-I is a complicated process [33, 34]. H_2O_2 forms the iron-peroxide bond via H170, then H42, R38 and H170 together promote heterolytic cleavage of the O-O bond leading to formation of the ferryl group, Fe=O, and formation of water which is a leaving group. (2) Second substrate joins the process of transferring compound-I to

compound-II. Electron transfer occurs to the porphyrin ring and the π-cation radical disappears [35, 36]. Proton transfer occurs to H42. (3) In the process of compound-II reaction to native HRP [37, 38], both proton and electron transfer occur to the ferryl group with second substrate, simultaneously reducing Fe(IV) to Fe(III) and forming water.

The step of reduction of compound-II to native HRP is often rate-limiting in the POx catalytic cycle [39]. Sometimes the compound-I formation can possibly become the rate-controlling step by limiting concentration of H_2O_2 and a large excess of second substrate, but the production of compound-II is never the rate-limiting step. Obviously, the different concentration and kind of substrates can be reflected in the change of velocity of catalytic reaction, which usually governs the activity of enzyme.

2.2.1.2. Detection Scheme for POx

EuTc is a fluorescent probe for hydrogen peroxide (H_2O_2) [26]. It is based on the finding that the complex formed between Eu^{3+} and tetracycline undergoes a large increase in fluorescent intensity on exposure to H_2O_2. The fluorescent complex formed between EuTc and H_2O_2 (referred to as EuTc-HP) can be reversibly decomposed by peroxidases to EuTc.

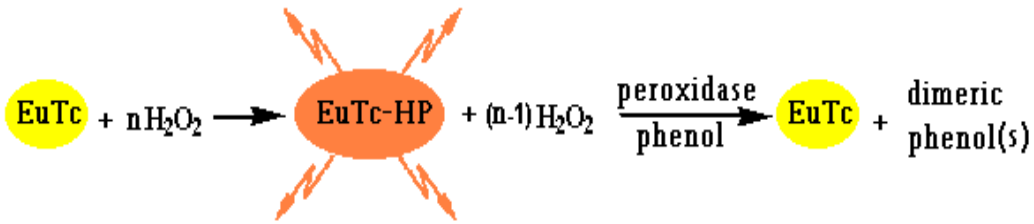

Figure 2.3. Schematic diagram of the principle underlying the POx activity assay. EuTc and hydrogen peroxide form a strongly fluorescent complex that is decomposed by POx on addition of the second substrate phenol.

Hence, the EuTc-HP reagent, which is easy to prepare, is highly promising for the kinetic assay of peroxidases, their substrates, activators, and inhibitors. The principle of the assay is shown in Fig. 2.3.

Phenol was used as the second substrate in this assay of POx because it is easily available, stable, does not absorb at the excitation wavelength for EuTc-HP (~400 nm), and does not give fluorescent products. In a system composed of EuTc-HP, POx, and phenol, the activity of peroxidase is proportional to the reaction rate, i.e. $\Delta F/min$, where ΔF is the difference between the initial fluorescence intensity (F_0) and the final fluorescence intensity (F), ideally both corrected for a (conceivable) blank. Unless excited with light (of λ 350 – 440 nm), no light is emitted, thus excluding the possibility of chemiluminescence.

2.2.2. Spectral Characterizations

The excitation and emission spectra of EuTc-HP and EuTc are given in Fig. 2.4. Like in other lanthanide complexes, the photonic energy absorbed by the ligand (Tc) in the EuTc complex is transferred to the central Eu^{3+} ion with its typical emission [40-42] in the form of main line ($^5D_0 \rightarrow {}^7F_2$) peaking at 613 and 618 nm (two peaks) and several side bands (Fig. 2.4). The appearance of two main peaks is a clear indication of the change of the crystal field [41] around Eu^{3+}. From the findings presented so far the proposal is that H_2O_2, on addition to EuTc, replaces at least one water molecule ligated to Eu^{3+}. However, no significant redox reactions are involved. Rather, water ligand (acting as a strong quencher) is replaced by H_2O_2 ligands. On addition of H_2O_2 and subsequent formation of the EuTc-HP complex, the intensity of the emission increases by a factor of about 15. On the other hand, the spectra of EuTc-HP do not significantly change on addition of phenol alone. In order to obtain the optimum fluorescence intensity of H_2O_2 in EuTc, the molar ratio of Eu^{3+}:Tc is kept at 3:1.

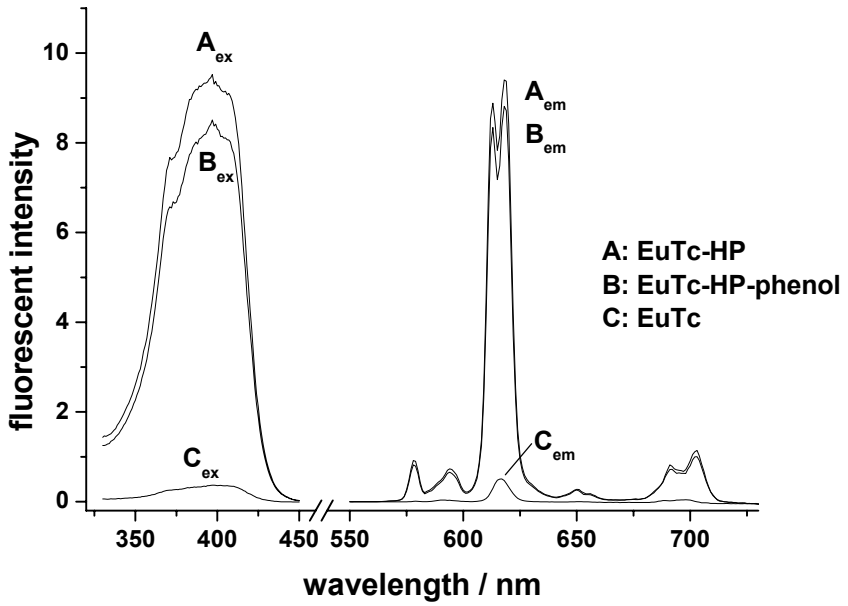

Figure 2.4. Fluorescence excitation (left) and emission spectra (right) of EuTc and the EuTc-HP complex in MOPS buffer of pH 6.9. 400 µL of EuTc stock solution, 160 µL of 5 mM H_2O_2 and 136 µL of 49 mM phenol, with MOPS to total volume 2 mL. (A), EuTc plus excesss HP; (B), EuTc-HP plus phenol; (C), EuTc.

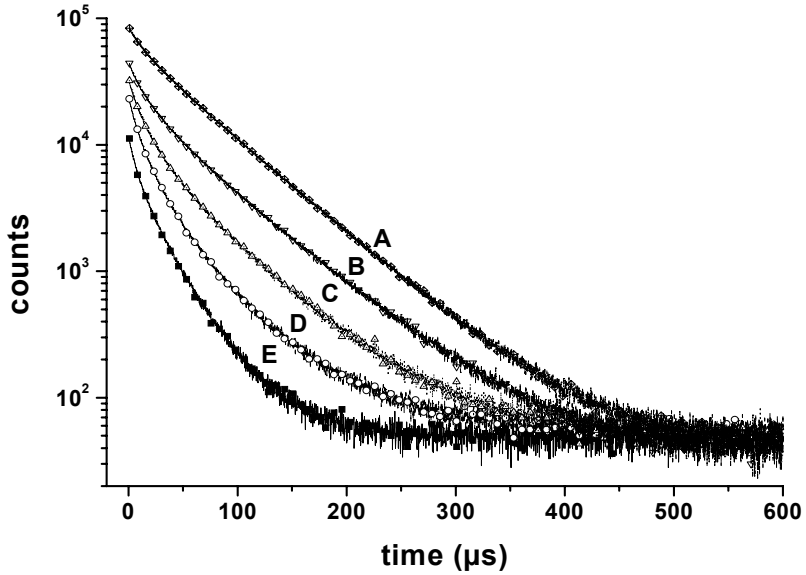

Figure 2.5. Effect of the concentration of H_2O_2 on the fluorescence decay profile of EuTc-HP. From (A) to (E), the concentrations of H_2O_2 decrease from 300 to 60, 30, 12 and 0 µM, respectively. All samples contain 500 µL of EuTc stock solution in a total volume of 2 mL.

Fig. 2.5. shows the fluorescence decay profiles of EuTc on addition of increasing concentrations of H_2O_2 from curve (E) to curve (A). EuTc and EuTc-HP have rather different decay patterns and decay times. An analysis of the data in Fig. 2.5 has indicated [26] that the decay profile of EuTc-HP can be fitted to a three-component model. The respective decay times are 10 μs (relative amplitude 17%), 34 μs (18%) and 61 μs (65%). The average decay time is ~60 μs. EuTc also has three components as 7 μs (40%), 24 μs (54%) and 53 μs (6%), with its average decay time ~30 μs only. From these results it is obvious that time-resolved measurements are best performed with a lag time of ~ 60 μs in order to selectively detect the EuTc-HP complex and minimize interference from EuTc, proteins and plates.

2.2.3. Kinetic Studies

The activity of POx is directly related to the change in the fluorescence intensity of the EuTc-HP system as shown in Fig. 2.6. In the absence of POx (curve A) only small changes

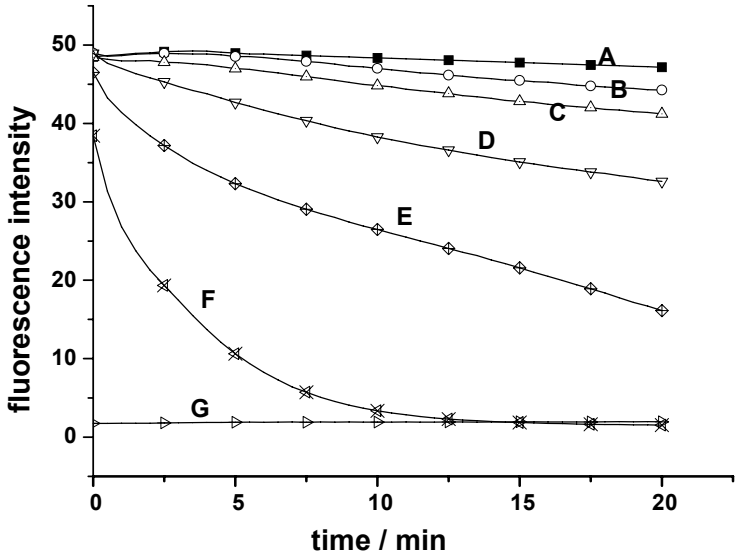

Figure 2.6. Time trace of the decomposition of the EuTc-HP complex by POx and phenol (A), phenol added to the EuTc-HP system, in which including 50 μL of stock solution of EuTc, 20 μL of 4 mM H_2O_2 and 1 7μL of 49 mM phenol,with MOPS to 250 μL total volume, but no POx; (B) to (F), kinetic trace in presence of 7.6, 22, 76, 220 and 760 mUnits/mL of POx , respectively; (G), no H_2O_2 and POx at all (EuTc alone).

are observed; these are ascribed to effects of temperature. As the activities of POx increase from (B) to (F), the slope increases, and this can be used to determine its activity. Curve (G) is a time trace of the system to which no H_2O_2 and no POx have been added (i. e. that of plain EuTc). It is worth noting that in the assay described here, fluorescence does not drop to zero but only from the level of the fluorescence of EuTc-HP to that of EuTc. Once formed, EuTc is not affected by POx. Incubation at elevated temperature accelerates the reaction, so that fluorescence intensity changes more rapidly and strongly. Therefore, lower activities of POx can be detected. The dynamic range of the determination can also be adjusted by the incubation time.

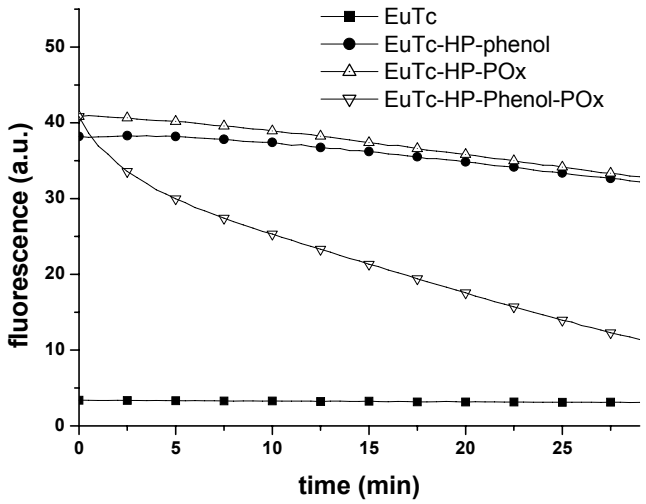

Figure 2.7. The influence of substrate-phenol to the catalytic cycle of POx. 50 µL of EuTc stock solution in each well (total volum 250 µL). Concentrations of H_2O_2 and phenol are 0.5 and 4 mM, the activity of POx is 0.012 U/mL.

It needs to be emphasized that POx as a protein itself does not induce the decrease of fluorescence intensity, and that there is no change of the fluorescence of EuTc-HP if only POx is added, without phenol as indicated in Fig. 2.7. Additionally, if POx is denatured by

heating, none of the kinetic effects were observed that are associated with the presence of active POx.

2.2.4. Effect of Substrates

H_2O_2 is not only a substrate of peroxidase, but also an enhancer of the fluorescence of EuTc. Fluorescence reaches a maximum on increasing the concentration of H_2O_2 from zero to 1.5 mM. The increase in fluorescence also depends on the concentration of EuTc. The optimal condition is obtained when a solution containing 20 μL of 5 mM H_2O_2 and 50 μL of the EuTc stock solution in a total of 250 μL is applied for POx activity assay.

As a result of the reaction mechanism of POx discussed in section 2.2.1.1, H_2O_2 is catalytically decomposed by POx, and the two phenoxy radicals formed undergo dimerization (and possibly other reactions). From a mechanistic point of view it is important to keep in mind that such assays work best if the concentration of the substrate (phenol) is much higher than that of hydrogen peroxide, since only in this case the activity of POx can be determined via the consumption of H_2O_2. No significant change in fluorescence was observed provided the concentration of phenol was ≤ 3.5 mM for the EuTc-HP system (0.4 mM H_2O_2).

2.2.5. Optimization of the POx Assay

Any changes in pH will produce two effects on the system. The first is on tetracycline which has several dissociable groups that also may bind europium ion [44]. Both the absorption and emission spectra of tetracycline are highly sensitive to pH. The maximum enhancement in the fluorescence intensity on addition of H_2O_2 occurs at pH 6.9 (6.7 – 7.2 are acceptable). The second effect is that on the enzyme, even though POx is rather robust and maintains its activity over the pH 5 – 10 range, albeit with varying activity [45]. A pH of 6.9

was chosen for further experiments since it results in a fairly strong fluorescence of EuTc-HP at acceptable enzyme activity.

The buffers MOPS, HEPES, Tris, and phosphate were tested in the assay. It shows that MOPS buffer is the best, while HEPES has a slight quenching effect. Phosphate interferes most strongly since 12 μM of phosphate cause a quenching by 21% of the fluorescence intensity of EuTc-HP. Tris buffer does not significantly affect. However, its best buffer capacity is between pH 7.5 and 9.0, which is outside our preferred pH range. Therefore, a 10 mM MOPS buffer of pH 6.9 was used throughout the experiments.

Even though the temperature optimum for POx is reported [45] to lie between 40 and 50 °C, the experiment was performed at 30 °C since this already gave adequate kinetics. Conceivably, higher temperatures may be applied in certain cases or if shorter reaction times are desired.

The interferences by common cations and anions were studied and no significant effects were found [26] except for phosphate and citrate. Known interferants [42, 45] for the EuTc-HP system, such as ascorbic acid, uric acid, and bilirubin if present in concentrations of > 6, 40, 7, and 16 μM, respectively.

2.2.6. Steady-state Fluorescence Intensity Assay

For the conventional fluorescent intensity assay, 50 μL of EuTc stock solution in each well (total volume 250 μL), the dynamic range is between 8.5×10^{-5} and 4.5×10^{-2} Units/mL, with the limit of detection 7.0×10^{-5} Units/mL after incubating for 10 min. Such a low LOD suggests that this probe be used for enzyme-linked immunosorbent assays using POx as a label.

2.2.7. Time-resolved Fluorescence Assay

The principle of time-resolved fluorescence has been demonstrated in Fig. 1.2. Due to the long decay times of europium complexes, they are often used in time-resolved fluorescent assays which can effectively eliminate background fluorescence, such as the intrinsic short-lived fluorescence of proteins and microtiter plates. In the assay presented here, it also can largely reduce the fluorescence of EuTc. From the decay profile and the experimental optimization, a lag time of 60 μs and an integration time of 40 μs were found to be the most appropriate for the POx assay. No significant improvement is found when the integration time is increased from 40 to 100 μs. For the determination of high activities of POx, a short incubation time is adequate as can be seen from Fig. 2.8. For the gated assay, the dynamic range is from 4.0×10^{-5} to 5.9×10^{-3} Units/mL, with a limit of detection (S/N = 3) of 1.0×10^{-5} Units/mL.

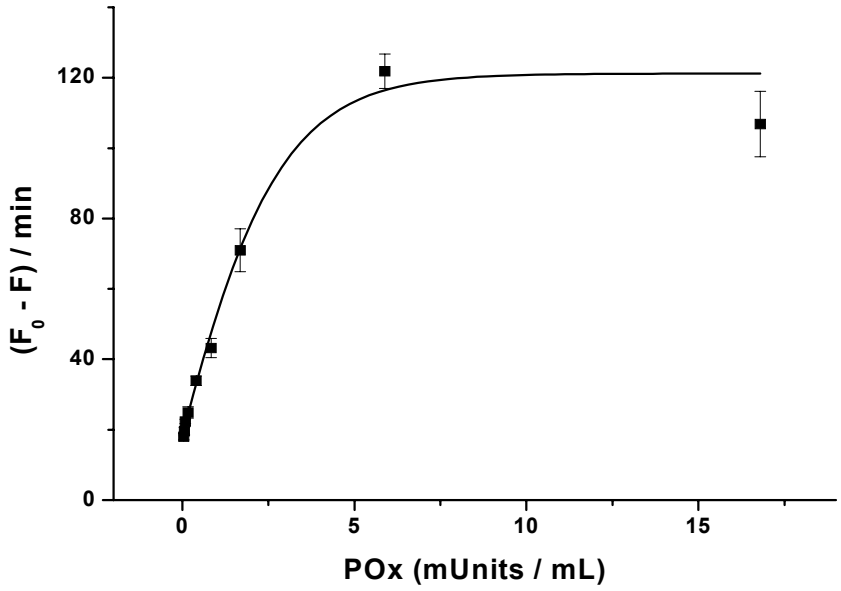

Figure 2.8. Calibration curve of the activity of POx by time-resolved fluorescence determination. 50 μL of EuTc stock solution in each well (total volum 250 μL)

2.2.8. Inhibitors of POx

Cyanide is a strong but reversible inhibitor of POx [1]. It binds to the sixth coordination site of the ferric ion heme complex of POx which also binds H_2O_2. Thus, it retards or prevents the catalytic cycle [46, 47]. In order to demonstrate inhibition, the kinetics due to inhibition of POx as monitored by the EuTc-HP system is shown in Fig. 2.9. Curve (A) shows a time trace where cyanide was added to the EuTc-HP/phenol system, but in absence of POx. Fluorescence remains unaffected, and this is also true for cyanide concentrations of less than 0.44 mM. Curve (E) shows an uninhibited kinetics, while curves (B), (C), and (D) demonstrate that POx is inhibited if cyanide is present in concentrations of 2.2 µM or higher. This indicates that (a) the rate of the decomposition of H_2O_2 by POx decreases with increasing concentrations of cyanide; and (b) the probe may also be used to determination the concentration of inhibitors cyanide and to monitor the change of activity of POx.

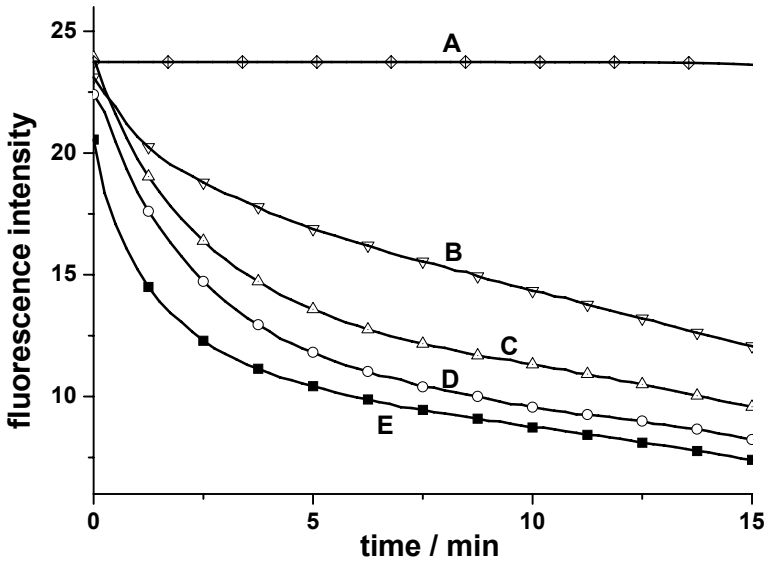

Figure 2.9. Effect of cyanide on the activity of POx. Each well (250 µL total volum) includes 22 µl of EuTc, 20 µl of 5 mM HP and 17 µl of 49 mM phenol. (A), cyanide added to the system, but no POx; (B) – (D), in presence of 0.2 Units/mL of POx plus cyanide in final concentrations of 440, 67, or 2.2 µM, respectively; (E), plus 0.2 Units/mL of POx added, but no cyanide.

Other known inhibitors of POx include sodium azide, whose effect on the EuTc-HP system (both in presence and absence of POx) is the same as that of cyanide. Hydroxylamine, in contrast, exerts a quenching effect on fluorescence of the EuTc-HP even in the absence of POx. Consequently, azide (but not hydroxylamine) can be also assayed via its inhibitory effect on POx.

2.2.9. Comparison with Known Fluorescent Methods for POx

The main fluorescence detections for the activity of POx are summarized in Table 2.1. Since H_2O_2 is not directly detectable by optical signals (which is contrast to electrochemical detection), substantial efforts have been made to identify chromogenic, fluorogenic and chemiluminogenic second substrates. They express the relationship between the second substrate and the activity of POx. Among the fluorogenic substrates in Table. 2.1, homovanillic acid [11], p-hydroxyphenylacetic acid [15], p-hydroxyphenyl-propionic acid [16], Amplex Red [48] are widely used. Recently, new substrates such as 4-(N-methylhydrazino)-7-nitro-1,2,3-benzooxadiazole [49] and 10-methylacridan-9-carboxy-hydrazide [50] have also been developed. None of them have been explored for the time-resolved determination of POx. However, Meyer and Karst [25] have presented an enzyme amplified lanthanide luminescence (EALL) method. It utilizes the ternary complex formed between Tb^{3+}, EDTA and the oxidation product of ρ-hydroxyphenylpropionic acid which has a decay time of about 100 μs, thus enabling the gated determination and working best in presence of an enhancer such as CsCl.

On the other hand, the direct determination of H_2O_2, rather than the optimization of the second substrate for POx, has been not fully explored yet. Theoretically, direct H_2O_2 detection, which is independent of possible effects of the sometimes complicated second

substrate on POx, offers more advantages than the above-mentioned methods if sensitivity is comparable. Certain metal ion complexes also have been used for the determination of H_2O_2 [51, 52] for example titanium complexes. While these methods enable the assay of H_2O_2 by photometry, they do not enable fluorescent or gated assays since the probes are not fluorescent. Conceivably, they also may be used for POx assay, but this has not been demonstrated yet.

Compared to the above methods, the POx assay presented here is first direct H_2O_2 – based time-resolved fluorometric assay with comparable sensitivity. It does not require the addition of other enhancers, works best at neutral pH and can be applied to both intensity-based and time-resolved determination of the enzyme.

2.3. Conclusion

The EuTc-HP probe presented here represents the first lanthanide probe suitable for POx determination via H_2O_2 at neutral pH. It enables a convenient and sensitive assay for POx, is easily accessible, and has the typical virtues of a europium probe including large Stokes shifts (thereby reducing background luminescence) and µs decay times. It demonstrates, as well as in follow works, the suitability of EuTc-HP as a probe for POx-associated ELISAs, nucleic acid hybridization assays, and in other bioassays.

TABLE 2.1. COMPARISON OF KNOWN FLUORESCENT METHODS FOR DETERMINATION OF POX ACTIVITY

	Name	Structure	ex/em (nm)	LOD (reported)	range (reported)	ref.
1	Homovanillic acid (HVA)	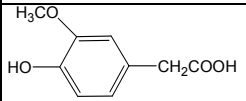	315/425	1 mU	1-10 mU	11,15, 16
2	Tyramine	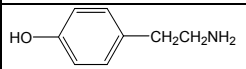	326/410	500 µU	500 µU-10 mU	11,15, 16
3	3-(*p*-hydroxyphenyl) propionic acid (HPPA)	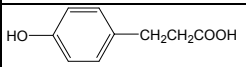	320/404	7.8 µU	7.8 µU-1 mU	16
4	*p*-hydroxyphenethyl alcohol (*p*-tyrosol)	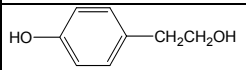	320/404	15.6 µU	15.6 µU-1 mU	16
5	*N,N′*-Dicyamomethyl-*o*-phenylenediamine (DCM-OPA)	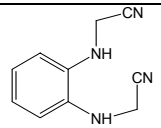	255,334, 353/455		21-150 pM	53
6	10-methylacridan-9-carboxylatehydrazide	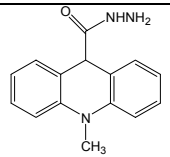	357/510	4.6 x 10^{-14} M	5 orders of magnitude	50
7	*o*-phenylenediamine	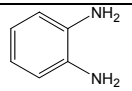	428/560	0.56 µU/mL (2mL)		54

8	10-acetyl-3,7-dihydroxyphenoxazine (Amplex Red)	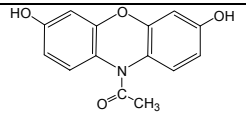	563/587	10 µU/mL	0.0-2 mU/mL	48
9	4-(*N*-methylhydrazino)-7-nitro-2,1,3-benzooxadiazole (MNBDH)	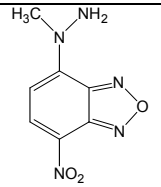	470/547		determination glucose with POx	49
10	tetra-substituted amino aluminium phthalocyanine (TAAlPc)	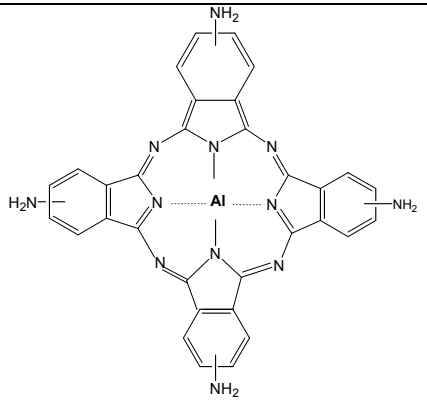	610/678	5.9 x 10^{-13} mol·L^{-1}	0.0-3.94 x 10^{-11} mol·L^{-1}	55
11	oxidation of *p*HPPA-Tb(III)-EDTA, CsCl	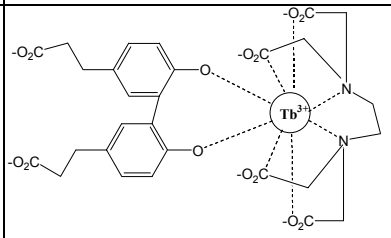	320/545	2 x 10^{-12} M	$2 \cdot 10^{-12}$ – 1.0 x 10^{-8} M	25
12	EuTc-HP		390-410/618	10 µU/mL	14µU/mL -·2 mU/mL	

2.4. Experimental Section

2.4.1. Reagents

Peroxidase (EC 1.11.1.7., type I, from horseradish, 148 U/mg solid) was purchased from Sigma (Deisenhofen, Germany; www.sigmaaldrich.com). The activity unit used in this article is based on the one defined by Sigma: one unit will form 1.0 mg purpurogallin from pyrogallol in 20 s at pH 6.0 at 20 °C. All inorganic salts were obtained in analytical purity from Merck (Darmstadt, Germany; www.vwr.com) unless otherwise stated. All solutions were prepared in 10 mM 3-(N-morpholino)- propanesulfonic acid (MOPS) buffer of pH 6.9 (Roth, Karlsruhe, Germany, www.carl-roth.de) unless otherwise specified. High-purity hydrogen peroxide (H_2O_2) as a 30% solution was from Merck. Europium(III) trichloride hexahydrate was from Alfa Products (Danvers, USA; www.alfa.com), tetracycline hydrochloride from Serva (Heidelberg, Germany; www.serva.de). Tris- (hydroxymethyl) aminomethane (TRIS) and 4-(2-hydroxyethyl) piperazine-1-ethanesulfonic acid (HEPES) were from Sigma-Aldrich.

The stock EuTc solution was prepared by mixing of 10 mL of 6.3 mM Eu^{3+} solution with 10 mL of a 2.1 mM tetracycline solution, then diluting to 100 mL with MOPS buffer. This reagent is also available from Chromeon GmbH (Regensburg, Germany; www.chromeon.com) and may be diluted to the concentration required. A 5 mM solution of hydrogen peroxide was prepared fresh daily. The 0.49 M phenol solution was stored at 4 °C and diluted as required.

2.4.2. Apparatus

Absorption spectra were acquired on a Cary WinUV photometer (Varian, Australia, www.varian.com). Fluorescence studies of the effect of H_2O_2 and phenol on spectra the EuTc and EuTc-HP were performed on an SLM AB2 luminescence spectrometer (Spectronic Unicam; Rochester, New York, USA; www.thermospectronic.com). Fluorescence intensity and kinetics were acquired on either a Fluoroskan Ascent micro titer plate reader (from Thermo Labsystems, Helsinki, Finland; www. labsystems.com) or on a Tecan GENios+ micro plate reader (Tecan, Groedig, Austria, www.tecan. com). The excitation/emission filters were set to 405/620 nm, or 405/612 nm respectively. The 96-well micro titer plates were obtained from Greiner Bio-One GmbH (Frickenhausen, Germany; www.greiner- lab.com). The luminescence lifetimes of different concentration of H_2O_2 in EuTc were detected with a pulsed 392-nm laser (LDH-C-400, PicoQuant GmbH, Berlin, Germany; www.picoquant.de), and an H5783-P04 PMT detector (Hamamatsu) with multiphoton-counting board in a multipass cuvette. Data were processed wither by FluoFit (PicoQuant GmbH)

2.4.3. Recommended POx Assay Protocol

Place, in each well of a thermostatted (30 °C) 96-well micro titer plate, 50 µL of EuTc stock solution, 20 µL of 5 mM H_2O_2 solution, 17 µL of 49 mM phenol solution, and with MOPS buffer to make up to a final volume of 250 µL. After 10 min, POx solutions of activities ranging from 4.0×10^{-5} to 4.5×10^{-2} Units/mL are added, and the decrease in the time-resolved fluorescence intensity is recorded on the Tecan GENios + reader over typically 5 to 60 min, depending on activity of POx, with a lag time of 60 µs and the integration time of 40 µs. Conventional steady-state fluorescence was detected with the same samples and micro plates as described above.

2.5. References

[1] Dunford, H. B. **Horseradish peroxidase: structure and kinetic properties, In: Peroxidases in Chemistry and Biology.** Everse, J.; Everse, K. E.; Grisham, M. B. (eds.), CRC Press, 1991; vol. II, chap. 1, pp. 1-24

[2] Veitch, N. C.; Smith, A. T. **Horseradish peroxidase**. Advances in Inorganic Chemistry 2001, 51, 107-162.

[3] Dunford, H. B.; Stillman, J. S. **On the function and mechanism of action of peroxidases.** Coordination Chemistry Reviews 1976, 19(3), 187-251.

[4] Bhandari, A.; Xu, F. **Impact of Peroxidase Addition on the Sorption-Desorption Behavior of Phenolic Contaminants in Surface Soils.** Environmental Science and Technology 2001, 35(15), 3163-3168.

[5] Darwish, I. A.; Blake, D. A. **One-Step Competitive Immunoassay for Cadmium Ions: Development and Validation for Environmental Water Samples**. Analytical Chemistry 2001, 73(8), 1889-1895.

[6] Piletsky, S. A.; Piletska, E. V.; Chen, B.; Karim, K.; Weston, D.; Barrett, G.; Lowe, P.; Turner, A. P. F. **Chemical Grafting of Molecularly Imprinted Homopolymers to the Surface of Microplates. Application of Artificial Adrenergic Receptor in Enzyme-Linked Assay for b-Agonists Determination**. Analytical Chemistry 2000, 72(18), 4381-4385.

[7] Little, J. **Enzyme Labeled Immunoassay;** in**: Immunoassay**. Edwards R. (Ed). Wiley, Chichester, 1996, p 47-62

[8] Durrant, I. **Direct peroxidase labelling of hybridisation probes and chemiluminescence detection In: Nonradioactive Analysis of Biomolecules**, Kessler, C. (Ed) 2nd ed., Springer (Heidelberg), 2000, chap. 12, p. 206-213.

[9] Nakayama, G. R. **Microplate assays for high-throughput screening.** Current Opinion in Drug Discovery & Development, 1998, 1(1), 85-91.

[10] Speel, E. J. M.; Hopman, A. H. N.; Komminoth, P. **Amplification methods to increase the sensitivity of in situ hybridization: play CARD(s).** Journal of Histochemistry and Cytochemistry, 1999, 47(3), 281-288.

[11] Guilbault, G. G.; Brignac, P. J. Jr.; Zimmer, M. **Homovanillic acid as a fluorometric substrate for oxidative enzymes. Analytical applications of the peroxidase, glucose oxidase, and xanthine oxidase systems.** Analytical Chemistry, 1968, 40(1), 190-6

[12] http://www.unige.ch/LABPV/perox.html

[13] Rodriguez-Lopez, J. N.; Smith, A. T.; Thorneley, R. N. F. **Role of arginine 38 in horseradish peroxidase. A critical residue for substrate binding and catalysis.** Journal of Biological Chemistry, 1996, 271(8), 4023-30.

[14] Josephy, P. D.; Eling, T.; Mason, R. P. **The horseradish peroxidase-catalyzed oxidation of 3,5,3',5'-tetramethylbenzidine. Free radical and charge-transfer complex intermediates**. Journal of Biological Chemistry, 1982, 257(7), 3669-75.

[15] Guilbault, G. G.; Brignac, P. J. Jr., Juneau, M. **New ubstrates for the fluorometric determination of oxidative enzymes,** Analytical Chemistry, 1968 , 40(8)1256 - 1263.

[16] Zaitsu, K.; Ohkura, Y. **New fluorogenic substrates for horseradish peroxidase: rapid and sensitive assays for hydrogen peroxide and the peroxidase**. Analytical Biochemistry, 1980 , 109(1), 109-13.

[17] Diaz, A. N.; Sanchez, F. G.; Garcia, J. A. G. **Hydrogen peroxide assay by using enhanced chemiluminescence of the luminol-H2O2-horseradish peroxidase system**: Comparative studies. Analytica Chimica Acta, 1996, 327(2), 161-165.

[18] Kricka, L. J.; Ji, X. **Enhanced chemiluminescence assay for peroxidase: application in immunoassay, protein blotting and DNA hybridization**. Analytical Sciences 1991, 2, 1501-6.

[19] Vladimirov, Y. A.; Sharov, V. S.; Suslova, T. B. **Europium(+3)-tetracycline complex activates chemiluminescence accompanying lipid peroxidation in liposomes**. Photobiochemistry and Photobiophysics, 1981, 2(4-5), 279-84.

[20] Marquette, C. A.; Blum, L. J. **Electrochemiluminescence of luminol for 2,4-D optical immunosensing in a flow injection analysis system.** Sensors and Actuators, B: Chemical, 1998, B51(1-3), 100-106.

[21] Darder, M.; Takada, K.; Pariente, F.; Lorenzo, E.; Abruna, H. D. **Dithiobissuccinimidyl Propionate as an Anchor for Assembling Peroxidases at Electrodes Surfaces and Its Application in a H2O2 Biosensor.** Analytical Chemistry, 1999, 71(24), 5530-5537.

[22] Collins, A.; Mikeladze, E.; Bengtsson, M.; Kokaia, M.; Laurell, T.; Csoregi, E. **Interference elimination in glutamate monitoring with chip integrated enzyme microreactors.** Electroanalysis, 2001, 13(6), 425-431.

[23] Morrin, A.; Guzman, A.; Killard, A. J.; Pingarron, J. M.; Smyth, M. R. **Characterisation of horseradish peroxidase immobilisation on an electrochemical biosensor by colorimetric and amperometric techniques.** Biosensors & Bioelectronics 2003, 18(5-6), 715-720.

[24] Gudgin Dickson, E. F.; Pollak, A.; Diamandis, E. P. **Time-resolved detection of lanthanide luminescence for ultrasensitive bioanalytical assays.** Journal of Photochemistry and Photobiology, B: Biology 1995, 27(1), 3-19.

[25] Meyer, J.; Karst, U. **Peroxidase enhanced lanthanide luminescence-a new technique for the evaluation of bioassays.** Analyst , 2000, 125(9), 1537-1538.

[26] Wolfbeis, O. S.; Duerkop, A.; Wu, M.; Lin, Z. **A Europium-ion-based luminescent sensing probe for hydrogen peroxide.** Angewandte Chemie, International Edition 2002, 41(23), 4495-4498.

[27] Rakicioglu, Y.; Perrin, J. H.; Schulman, S. G. **Increased luminescence of the tetracycline-europium(III) system following oxidation by hydrogen peroxide.** Journal of Pharmaceutical and Biomedical Analysis, 1999, 20(1-2), 397-399.

[28] Banci, L. **Structural properties of peroxidases**. Journal of Biotechnology 1997, 53(2,3), 253-263.

[29] Veitch, N. C.; Smith, A. T. **Horseradish peroxidase**. Advances in Inorganic Chemistry 2001, 51 107-162.

[30] Everse, J. **The structure of heme proteins compounds I and II: some misconceptions**. Free Radical Biology & Medicine 1998, 24(7/8), 1338-1346.

[31] Smulevich, G. **The functional role of the key residues in the active site of peroxidases.** Biochemical Society Transactions 1995, 23(2), 240-4.

[32] Schejter, A.; Lanir, A.; Epstein, N. **Binding of hydrogen donors to horseradish peroxidase: a spectroscopic study.** Archives of Biochemistry and Biophysics 1976, 174(1), 36-44.

[33] Poulos, T. L. **Heme enzyme crystal structures.** Advances in Inorganic Biochemistry 1988, 7, 1-36.

[34] Dawson, J. H. **Probing structure-function relations in heme-containing oxygenases and peroxidases.** Science 1988 , 240(4851), 433-9.

[35] Ator, M. A.; Ortiz de Montellano, P. R. **Protein control of prosthetic heme reactivity. Reaction of substrates with the heme edge of horseradish peroxidase**. Journal of Biological Chemistry 1987, 262(4), 1542-51.

[36] Ortiz de Montellano, P. R. **Control of the catalytic activity of prosthetic heme by the structure of hemoproteins.** Accounts of Chemical Research 1987, 20(8), 289-94.

[37] Sitter, A. J.; Reczek, C. M.; Terner, J. **Heme-linked ionization of horseradish peroxidase compound II monitored by the resonance Raman Fe(IV)=O stretching vibration**. Journal of Biological Chemistry 1985, 260(12), 7515-22.

[38] Makino, R.; Uno, T.; Nishimura, Y.; Iizuka, T.; Tsuboi, M.; Ishimura, Y. **Coordination structures and reactivities of compound II in iron and manganese horseradish peroxidases. A resonance Raman study**. Journal of Biological Chemistry 1986, 261(18), 8376-82.

[39] Rodriguez-Lopez, J. N.; Smith, A. T.; Thorneley, R. N. F. **Role of arginine 38 in horseradish peroxidase. A critical residue for substrate binding and catalysis.** Journal of Biological Chemistry 1996, 271(8), 4023-30.

[40] Hirschy, L. M.; Van Geel, T. F.; Winefordner, J. D.; Kelly, R. N.; Schulman, S. G. **Characteristics of the binding of europium(III) to tetracycline**. Analytica Chimica Acta 1984, 166 207-19.

[41] Richardson, F. S. **Terbium(III) and europium(III) ions as luminescent probes and stains for biomolecular systems,** Chemistry Review 1982, 82, 541-552.

[42] Wu, M; Lin, Z; Wolfbeis, O.S; **Determination of the activity of catalase using a europium(III)–tetracycline-derived fluorescent substrate.** Analytical Biochemistry, 2003, 320,129-135.

[43] Parker, D.; Dickins, R. S.; Puschmann, H.; Crossland, C.; Howard, J. A. K. **Being Excited by Lanthanide Coordination Complexes: Aqua Species, Chirality, Excited-State Chemistry, and Exchange Dynamics**, Chemistry Review, 2002, 102, 1977-2010.

[44] Duarte, H. L. A.; Carvalho, S.; Paniago, E. B.; Simas, A. M. **Importance of tautomers in the chemical behavior of tetracyclines** Journal of Pharmaceutical Sciences 1999, *88*, 111-120.

[45] Schomburg, D.; Stephan, D. (Eds), **Enzyme Handbook**, Springer, Berlin - Heidelberg, 1994

[46] de Ropp, J. S.; Mandal, P. K.; La Mar, G. N. **Solution 1H NMR Investigation of the Heme Cavity and Substrate Binding Site in Cyanide-Inhibited Horseradish Peroxidase**. Biochemtry. 1999, *38*, 1077-1086.

[47] Henriksen, A.; Smith, A. T.; Gajhede, M. **The structures of the horseradish peroxidase C-ferulic acid complex and the ternary complex with cyanide suggest how peroxidases oxidize small phenolic substrates.** Journal of Biological Chemistry , 1999, 274(49), 35005-11.

[48] http://www.probes.com/media/pis/mp22188.pdf

[49] Meyer, J.; Buldt, A.; Vogel, M.; Karst, U. **4-(N-methylhydrazino)-7-nitro-1,2,3-benzooxadiazole (MNBDH): A novel fluorogenic peroxidase substrate**. Angewandte Chemie, International Edition, 2000, 39(8), 1453-1455.

[50] Akhavan-Tafti, H.; deSilva, R.; Eickholt, R.; Handley, R.; Mazelis, M.; Sandison, M. **Characterization of new fluorescent peroxidase substrates**. Talanta 2003, 60(2-3), 345-354.

[51] Inamo, M.; Funahashi, S.; Tanaka, M.. **Kinetics of the reaction of hydrogen peroxide with some oxotitanium (IV) complexes as studied by a high-pressure stopped-flow technique**. Inorganic Chemistry, 1983, 22(25), 3734-7.

[52] Matsubara, C.; Kawamoto, N.; Takamura, K. **Oxo[5,10,15,20-tetra(4-pyridyl) porphyrinato] titanium(IV): an ultrahigh-sensitive spectrophotometric reagent for hydrogen peroxide**. Analyst, 1992, 117(11), 1781-4.

[53] Li, Y.; Liu, H.; Dong, Z.; Chang, W.; Ci, Y. **Synthesis and characteristics of a new fluorogenic substrate for horseradish peroxidase.** Microchemical Journal 1996, 53(4), 428-436.

[54] Akhavan-Tafti, H.; deSilva, R.; Eickholt, R.; Handley, R.; Mazelis, M.; Sandison, M. **Characterization of new fluorescent peroxidase substrates.** Talanta 2003, 60(2-3), 345-354.

[55] Chen, X.; Yang, H.; Zhu, Q.; Zheng, H.; Xu, J.; Li, D. **A new red-region substrate, tetra-substituted amino aluminum phthalocyanine, for the fluorimetric determination of H2O2 catalyzed by mimetic peroxidases**. Analyst, 2001, 126(4), 523-527.

Chapter 3. Peroxidase as a Label for ELISA and Oligonucleotide Hybridization Assay

3.1. Introduction

Immunoassays and DNA hybridization assays as two main members of broad category of bioassays have been widely utilized in biochemical research [1-5], clinical diagnosis [6-8] and pharmaceutical industries [9,10]. With the development of the electronic and analytical technologies, immunoassays and DNA hybridization assays have been combined to improve *de novo* chip technologies [11-13], including the protein chip [14, 15] arrays.

There are different analytical schemes in immunoassays, such as radioimmunoassay (RIA) [16], spectrophotometric immunoassay, fluorescence immunoassay (FIA) [17], chemiluminescence immunoassay (CLIA) [18] and electrochemical immunoassay (ECIA) [19]. RIA is the most sensitive method in all biological and medical assays, but its isotopic hazard potential have recently limited its wide application. The photoluminescence approaches are main stream for bioassays because they are more sensitive than ECIA. These technologies are also used in DNA hybridization assays [20-22].

Fluorescence imaging is a powerful means for presenting the distribution of species, but is possible only (a) if the species of interest has a fluorescence by its own (such as NADH, many flavins and porphyrins) [23, 24], (b) if the species of interest can be rendered fluorescent by attaching a label (for instance, in immunofluorescence and DNA fluorescence studies) [25, 26] or (c) if appropriate fluorescent probes are available for the species of interest (e.g. probes for pH, oxygen, ions, as in this case hydrogen peroxide) [27-29].

In this chapter, POx as a label has been further explored in IgG and oligonucleotide detection, based on the measurement of the activity of POx studied in chapter 2. The fluorescence of EuTc-HP decreases if POx catalyzes the consumption of H_2O_2. The time-resolved fluorescent assay for biological specimen has more advantages than the conventional steady-state fluorescence assay because of its ability to eliminate the background fluorescence of proteins and biological matrix. On the other hand, this probe can be used as a reversible molecular sensor for the imaging of POx-ELISA.

3.2. Results and Discussion

3.2.1. Principle of Fluorescence Detection of POx-ELISA

IgG, as a model, is employed for POx-ELISA with EuTc-HP. Scheme of principle of POx as a label for sandwich ELISA has been shown in Fig. 3.1. Anti-IgG is first coated onto

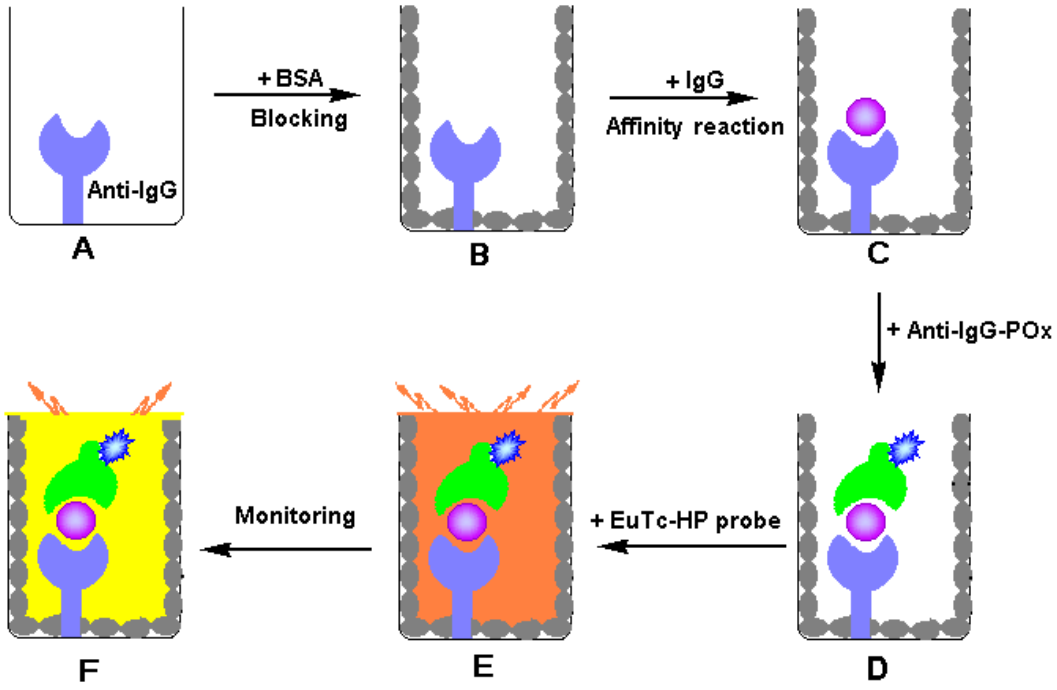

Figure 3.1. Scheme of the principle of POx- ELISA using EuTc-HP

the polystyrene surface of microtiter plate, different concentrations of analyte IgG react with it after BSA has blocked the extraneous binding sites. EuTc-HP is added when the secondary POx labeled anti-IgG has recognized IgG, then after incubating, IgG can be determined via the fluorescence decrease of EuTc-HP because H_2O_2 is catalytically decomposed by POx.

POx as a label for direct ELISA is shown in Fig. 3. 2. Instead of anti-IgG, analyte IgG is directly coated on the microtiter plate. Other processes are the same as Fig. 3.1.

Detail protocols of sandwich POx-ELISA and direct POx-ELISA are in experimental Section 3.4.3.

Figure 3.2. Scheme of direct ELISA

3.2.2. Kinetic Studies of Sandwich POx-ELISA

Fig. 3.3. presents the fluorescence change of the decomposition of EuTc-HP probe by IgG versus POx labeled anti-IgG. Curve(A) is a time trace for blank, which coated anti-IgG same as other wells without target molecular IgG. (B) to (D) are curves of kinetic process of the concentrations of IgG versus the activity of POx-labeled anti-IgG. With the increasing amount of POx-anti-IgG, from (B) to (D), the slope of curve is increasing, which can be used to indicate the activity of POx. Therefore, the concentration of IgG can be determined by this method. The kinetic curve of the direct POx-ELISA is similar as this case.

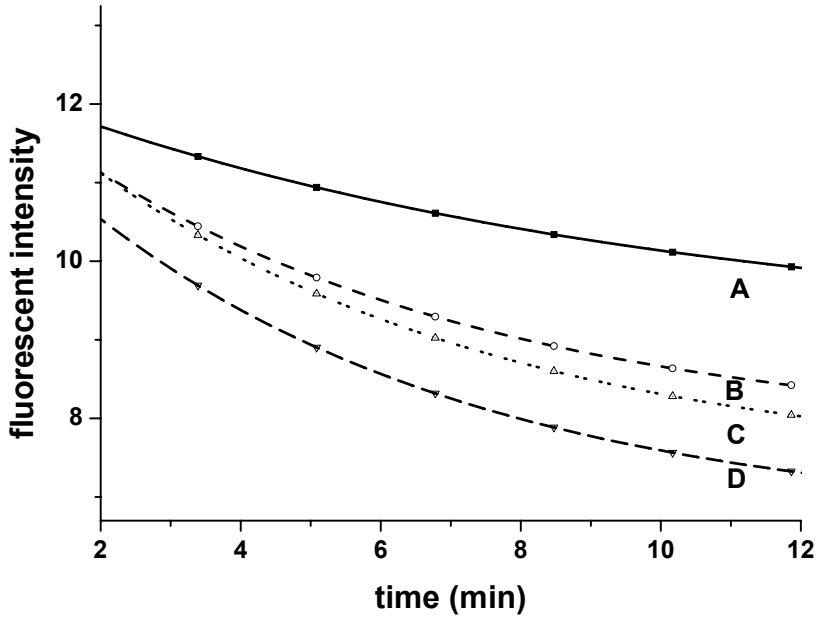

Figure 3.3. Time trace of the decomposition of the EuTc-HP complex by IgG versus POx- anti-IgG as monitored via fluorescence. (A) blank; (B) - (D) time trace after addition

3.2.3. POx – ELISA for IgG via the EuTc-HP Probe

3.2.3.1. Steady-state fluorescence POx –ELISA

The activity of peroxidase labeled on anti-IgG can be measured with the EuTc-HP fluorescence probe. The calibration curves (after incubating for 20 min, expressed as $\Delta F = (F_0 - F)$ of fluorescence) are shown in Fig. 3.4. It indicates that (a) for the sandwich POx-ELISA, its limit of detection is 0.1 ng/mL, and the linear range is between 0.3 - 6 ng/ml, r = 0.98; (b) for the direct POx-ELISA, its limit of detection is 2 ng/mL, and the linear range is between 10 - 2000 ng/ml, r = 0.99; (c) the sandwich POx-ELISA with EuTc-HP fluorescent probe is more sensitive than the direct one.

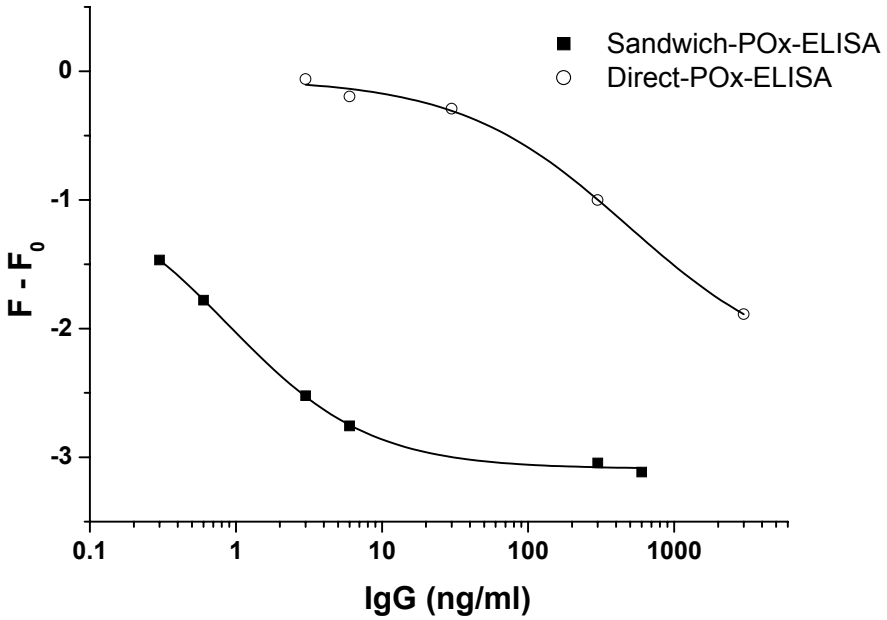

Figure 3.4. Calibration plot of steady-state fluorescence detection for IgG by POx-Anti-IgG versus the decrease in fluorescence intensity (F-F_0) over 20 min.F_0 and F are fluorescence intensities of blank and sample.

3.2.3.2. Time-resolved fluorescence detection of POx-ELISA

One of the advantages of time-resolved fluorescence of ELISA is suppression of the background fluorescence, especially that from biological samples. This experiment is performed and recorded with a time lag of 60 μs after the pulsed excitation light source is switched off. The best integration time was found to be 40 μs. Fig. 3.5. shows the resulting normalized calibration plot for this linear range, which was obtained by plotting the normalized fluorescence [(F_0 – F) / F_0] versus the concentration of IgG. The limit of detection of this time-resolved fluorometric sandwich POx-ELISA is calculated to be 0.1 ng/ml of IgG. The linear range is from 0.1 to 8.0 ng/ml. For direct POx-ELISA, the linear range is from1.0 to 88.0 ng/mL, with 1.0 ng/mL of limit of detection. Obviously, the sandwich POx-ELISA is more sensitive than direct POx ELISA whether in conventional steady-state or in time-

resolved fluorescence detection. Both methods have enough good sensitivity and is suitable for the requirements of regular clinical assay.

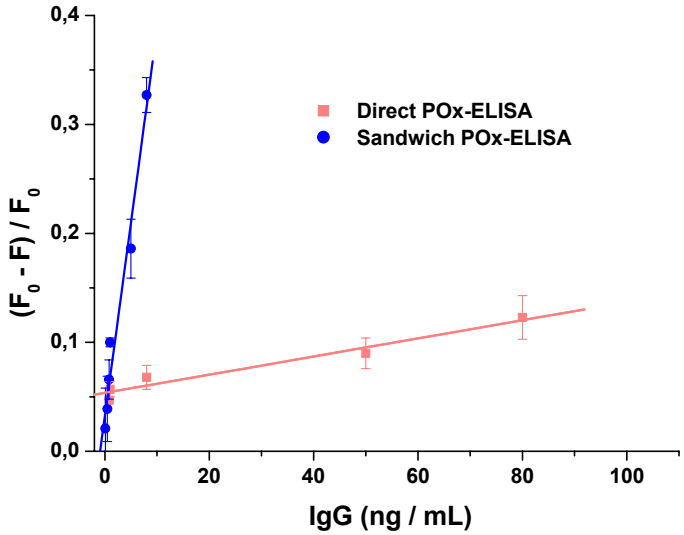

Figure 3.5. Calibration plot of time-resolved detection for IgG by POx-Anti-IgG versus the decrease in fluorescence intensity ($F-F_0$) over 20 min, with 60 µs lag time and 40 µs integration time. F are fluorescence intensities of blank and sample.

3.2.3.3. Time-resolved fluorescence imaging ELISA (TRFI-ELISA)

The pathway of light of imaging [29] is indicated in Fig. 3.6. As in conventional fluorescence reader, all spots of the microtiter plate can be excited simultaneously with a pulsed 96-LED array (λ_{max} = 405 nm). The light from the pulsable LED array passes an excitation filter and hits the wells of the microtiter plate. The emission from the fluorescent sample is filtered by an excitation filter and is detected

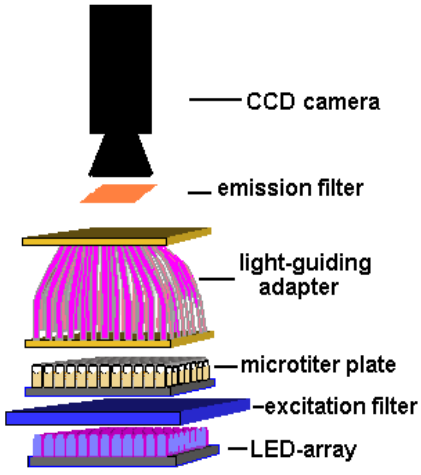

Figure 3.6 Scheme of imaging

by the CCD camera.

The camera is gated during the total exposure by an external trigger signal. The lag time and integration time are 60 and 40 µs after the LEDs were switched off (Fig. 3.7). The detailed protocol is described as in section 3.4.7.

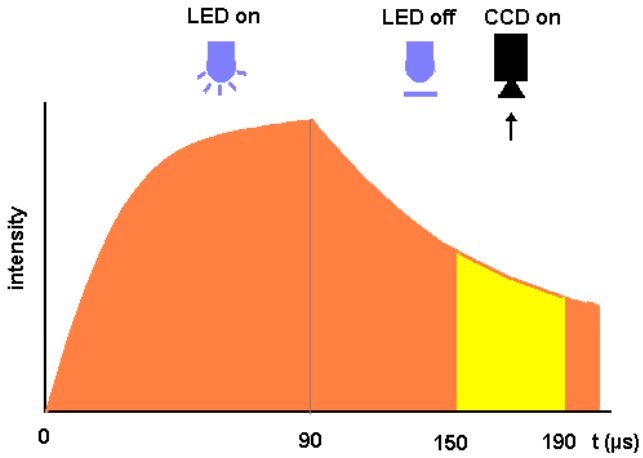

Figure 3.7. Scheme of time-resolved imaging

	1	2	3	4	5	6	7	8	9	10	11
c_{IgG} [ng ml^{-1}]			0	0.1	0.5	1	5	10	40	80	100
F	169	577	402	396	386	423	383	355	311	251	208
SD	20	22	4	28	52	58	29	8	37	13	6

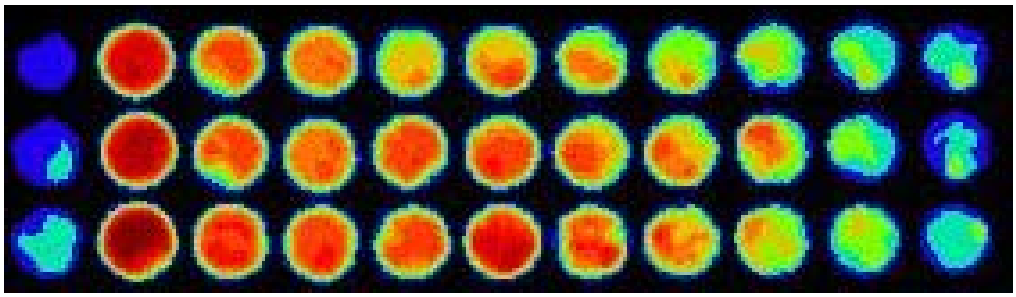

Figure 3.8. TRFI-ELISA for IgG.
F is the intensity value calculated from an area in the centers of the spots and averaged over three spots of equal concentrations. SD is the standard deviation in the spot regions.

Time-resolve fluorescence imaging-ELISA (TRFI-ELISA) for IgG was performed on a microtiter plate (protocol of sandwich POx-ELISA) after 45 min incubation of EuTc-HP probe at room temperature. The result is shown in Fig. 3.8 (false-color, value as arbitrary intensity). The dynamic range of this TRFI-ELISA is from 5 to 100 ng/mL for IgG. At high concentration of IgG, the complete decomposition of the EuTc-HP complex is readily observable. The time-gated fluorescence intensities from imaging decreased nearly to the values of the EuTc reference samples in spot column 1. The fluorescence intensities from imaging were calculated and averaged from the regions in the centers of the spots. The standard deviations between three different spots with the same IgG concentration are in the same magnitude (between 5-10 %).

The advantage of imaging ELISA is the fast data acquisition and the clear and concise data visualization, which makes this method suitable for high-throughput screening applications.

3.2.4. Principle of Competitive POx-Oligonucleotide Hybridization Assay

Competitive oligonucleotide hybridization is a very popular method in nucleic acid assays [30-31], which can improve the selectivity of detection. The scheme of competitive oligonucleotide hybridization is shown in Fig. 3.9. Anti-biotin is coated on the surface of microtiter plate, then affinitively reacts with oligonucleotide conjugated biotin after BSA has blocked the extraneous binding sites. Complementary oligonucleotides with or without POx are added to undergo competitive reaction, after adding EuTc-HP, incubating, the fluorescence changes can be recorded for calculating the concentration of oligonucleotide.

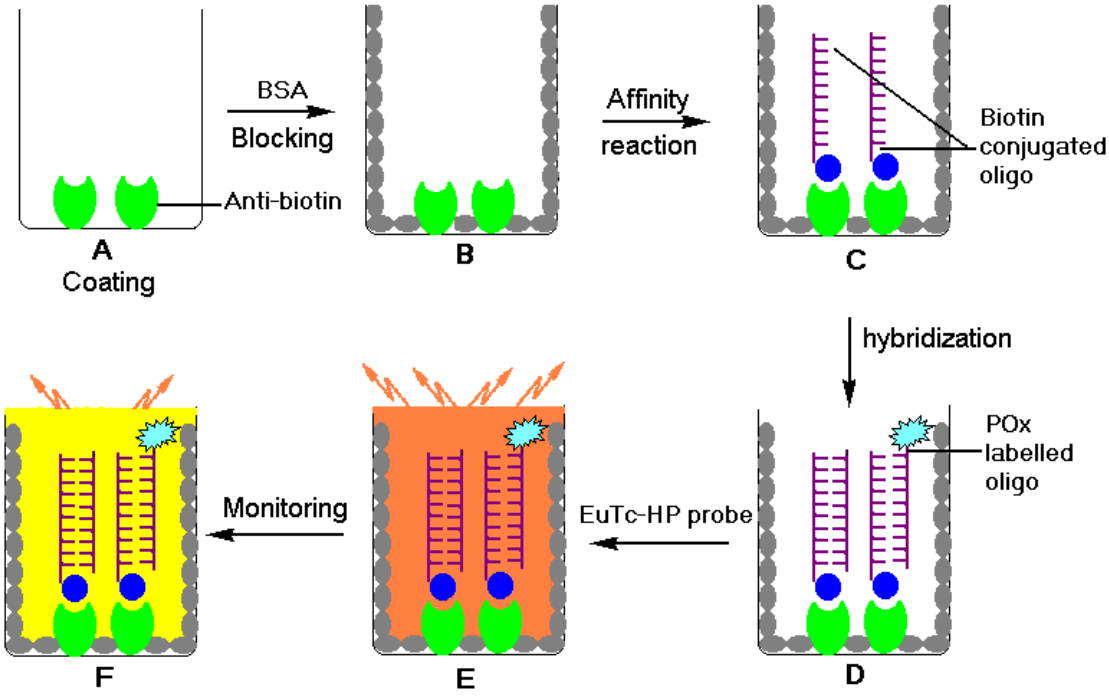

Figure 3. 9. Scheme of the principle of competitive POx-oligonucleic acid hybridization assay using EuTc-HP

3.2.5. Fluorescence Detection of POx-Oligonucleotide Hybridization

In this experiment, the 20 base sequence (TA) from a fragment of SLT1 (Shiga-like toxins), as a model, is employed. The sequence of TA is 5′-AAG TAG TCA ACG AAT GGC GA-3′. Horseradish peroxidase labeled TA is denoted as POx-TA. The complementary oligonucleotide for TA is cTA, which is biotinylated to form BcTA. (see section 3.4.1.)

TA and POx-TA compete to hybridize with immobilized BcTA. The fluorescence change of the decomposition of EuTc-HP probe by POx-TA is used to evaluate the concentration of TA. In the low concentration of TA from 0-2.8 nM, a linear relationship with fluorescence change is obtained, but in high concentration of TA, the results are not so good. The possible reason is that TA is only a 20 base pairs nucleotide, while POx-TA has a

macromolecular protein label, thus competition of POx-TA at low concentration is weaker than that of TA.

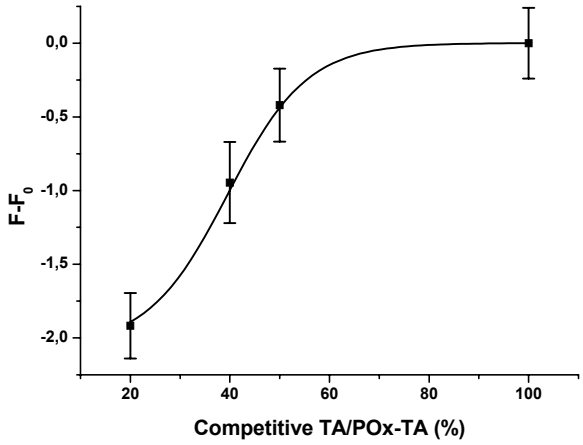

Figure 3.10. Calibration curve of competitive hybridization of TA and PTA, total concentration[TA]+[PTA]= 5 nM

3.3. Conclusion

EuTc-HP as a typical europium probe for bioassay, it need not label or conjugate on protein or DNA. So it is easily prepare and procedure besides it has the merits of lanthanide complex fluorescence. The rate of consumption of the EuTc-HP system as monitored via the decrease in fluorescence intensity is a direct parameter for (a) the activity of the POx, (b) IgG versus POx-labeled-anti-IgG, and (c) oligonucleotide versus POx-oligonucleotide (competitive reaction). From above experiments, it is a evidence that the EuTc-HP can be utilized in bioassays via fluorescence intensity and imaging technologies.

3.4. Experimental Section

3.4.1. Reagents

Rabbit anti-bovine IgG, bovine IgG, rabbit anti-bovine IgG / peroxidase conjugate, BSA were purchased from Sigma (Deisenhofen, Germany; www.sigmaaldrich.com) and used without further purification. Sequence of TA from a fragment of SLT1 (Shiga-like toxins) in EHEC (Enterohemorrhagic E. coli) is 5′-AAG TAG TCA ACG AAT GGC GA-3′. There are no self-complementarity and no hairpin-loop in TA. POx labeled TA (POx-TA) is HRP-5′-AAG TAG TCA ACG AAT GGC GA-3′ and biotinylated complementary oligonucleotide for TA (BcTA) is Bio-5′-TCG CCA TTC GTT GAC TAC TT-3′. They were purchased from Thermo Hybaid (www.thermohybaid.com)

All inorganic salts were obtained in analytical purity from Merck unless otherwise stated. Europium(III) trichloride hexahydrate was from Alfa Products, tetracycline hydrochloride from Serva.

The stock EuTc solution was prepared by mixing of 10 mL of a 6.3 mM Eu^{3+} solution with 10 mL of a 2.1 mM tetracycline solution, then diluting to 100 mL with MOPS buffer. High-purity hydrogen peroxide (H_2O_2) as a 30% solution was from Merck. A 5 mM solution of hydrogen peroxide was prepared fresh daily. The 0.49 M phenol solution was stored at 4 °C and diluted as required.

PBS buffer (0.26 g KH_2PO_4, 2.17 g $Na_2HPO_4 \cdot 7H_2O$ and 8.71 g of NaCl in 800 mL distilled water, adjusted to pH 7.4 with 1.0 M HCl or NaOH) to the corresponding working concentrations, then dilute to 1000 mL. 20 x SSC buffer: dissolve 175.3 g of NaCl and 88.2 g of sodium citrate in 800 mL, adjusted to pH 7.0 with HCl or NaOH, then dilute to 1000 mL.

According to requirements, diluted to 1 x SSC (saline sodium citrate), 1 x SSC + 1% SDS (sodium dodecyl sulfate), 1 x SSC+1% triton-X-100.

3.4.2. Apparatus

Fluorescence intensity and kinetics were acquired on either a Fluoroskan Ascent micro titer plate reader (from Thermo Labsystems, Helsinki, Finland; www. labsystems.com) or on a Tecan GENios+ micro plate reader The excitation/emission filters were set to 405/620 nm, or 405/612 nm respectively.

3.4.3. Protocol of POx-ELISA

The scheme of sandwich POx-ELISA is shown in Fig. 3.1.

*1).*Coating antibody on the microtiter plate: Use 200 µl of Rabbit anti-Bovine-IgG at a concentration of 5 µg/mL in 10mM of PBS at pH 7.4, add to each well of a polystyrene microtiter plate, incubate at 37 °C for 1 hour. Alternatively, incubate at 4 °C overnight.

*2).*Blocking extraneous binding sites: Block remaining binding sites in each well by incubating with 200 µl of 1% BSA in 10mM of PBS at pH 7.4, incubate at 37 °C for 30 min.

*3).*Reacting with analyte: Add 200 µl of different concentrations Bovine IgG to each well, incubate at 37 °C for 1 hour.

*4).*Reacting with POx labeled secondary antibody: Add 200µl of rabbit anti-bovine IgG peroxidase conjugate at 1:1500 in each well, incubated at 37°C for 1 hour.

Between above two times coating, rinse 3 times by 10 mM PBS at pH 7.4.

Last rinse before fluorescence assay, MOPS buffer was used to avoid residual PBS contaminating the EuTc-HP, and ready for detection (section 3.4.5)

For direct POx-ELISA, analyte IgG was coated onto the microtiter plate, other processes are same as sandwich POx-ELISA.

3.4.4. POx-Oligonucleotide Hybridization Assay

The scheme of POx-oligonucleotide hybridization assay is shown in Fig.3.9.

*1).*Coating antibody on the microtiter plate: Use 200 µl of Rabbit anti-biotin-IgG at a concentration of 5 µg/mL in 10 mM pH 7.4 of PBS, add to each well of a polystyrene microtiter plate, incubate at 37 °C for 1 hour. Alternatively, incubate at 4°C overnight.

*2).*Blocking extraneous binding sites: Block remaining binding sites in each well by incubating with 200 µl of 1% BSA in 10mM pH 7.4 of PBS, incubate at 37 °C for 30 min.

*3).*Affinity reaction with biotin-oligonucleotide: Add 200 µl of 5 nM BcTA in 10 mM pH 7.4 of PBS in each well, incubate at 37 °C for 1 hour.

Between above two times coating, need rinse 3 times by 10 mM pH 7.4 PBS.

*4).*Competitive hybridization: Mix different concentration of oligonucleotides of TA and POx-TA in hybridization solution (5 x SSC and 1% SDS) in each well. Incubate for 10 min at 50 °C or 30 min at 45 °C with agitation.

5). Post-hybridization washes

(a) add 200 µl of preheated wash solution 1 (1 x SSC, 1 % SDS) in each well, at 40 °C for 10 min, with shaking

(b) add 200 µl of wash solution 2 (1 x SSC, 1 % Triton X-100) in each well, at 40 °C for 10 min, with shaking

(c) add 200 µl of preheated wash solution 3 (1 x SSC) in each well, at 40 °C for 10 min, with shaking.

Last rinse before fluorescence assay, MOPS buffer was used to avoid residual SSC contaminating the EuTc-HP, and ready for detection (section 3.4.5)

3.4.5. Fluorescent Intensity Detection

Time-resolved fluorescence detection: 250 µL of EuTc-HP- phenol analytical solution, which including 50 µL of EuTc standard solution, 20 µL of 5 mM H_2O_2, 17 µL of 49 mM phenol and other 10 mM of MOPS in 6.9 pH, was added to each well of samples (immunoassay and oligonucleotide hybridization assay). The kinetic curve and the end – point of fluorescence intensity of EuTc-HP system after incubating 20-60 min was record, depending on POx-anti-IgG or POx-TA. Time-gated fluorescence was with a lag time of 60 µs and the integration time of 40 µs. Steady-state fluorescence was detected with the same samples and micro plates as described above without lag time.

3.4.6. Imaging Set-up

The set-up of the self-developed imaging system was used for time-resolved imaging of the emission intensity as described by Liebsch et al [29] and Schaeferling et al [32] in Fig. 3.11. Imaging detection system consists of a fast gatable CCD-camera, a pulsable LED array with 96 UV light emitting diodes (λ_{max} = 405 nm), a 96 fiber light-guiding adapter, a pulse generator, optical excitation and emission filters, and a personal computer for controlling and visualization of the experiments. The pulsed data were acquired process with the

corresponding software modules. The images were processed, visualized and evaluated with the IDL software module (*Research Systems, Inc*., Boulder, CO).

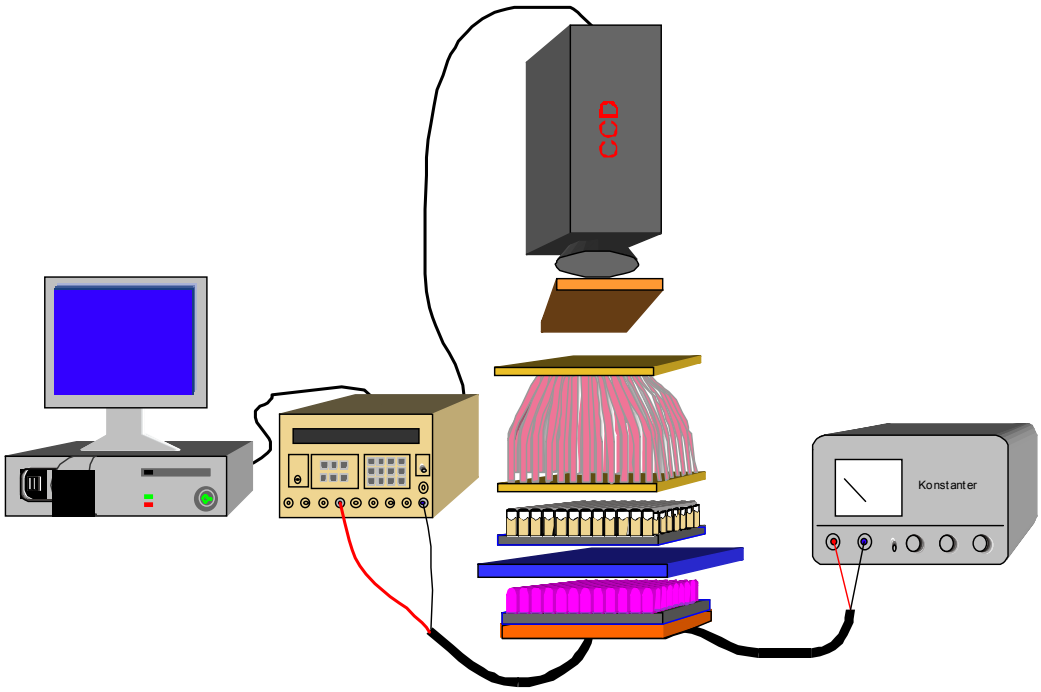

Figure 3.11. Scheme of the imaging setup

Optical system in imaging set-up:

1) CCD camera: The camera had a black/white CCD chip with 640x480 pixels (307200 pixels, VGA resolution) and a 12-bit resolution, equivalent to 4096 gray-scale values. The CCD chip can be gated directly with a minimal trigger time of 100 ns, additional image intensification is not required. and camera is triggered by a pulse generator.

2) LED array: The LEDs (λ_{max} = 405 nm) were arrayed fitting exactly to wells of a 96-well microtiter plate for single illumination of each well by one LED, and LED array was pined to the electronic board, which enables a quick exchange by LED emitting of different wavelengths.

3) Light-guiding adapter: There are 96 optical fibers in light-guiding adapter for reduces the imaged area to fit the standard optics of the imaging set-up. This enables the simultaneous evaluation of 96-well at the same time.

3.4.7. Imaging

The camera is gated during the total exposure by an external trigger signal. The excitation pulse had a width of 90 μs, the lag time was fixed to 60 μs, with a time window from 150-190 μs after the LEDs were switched off. The resulting image is an added superimposition of this single pictures. The corresponding background images were recorded in a second acquisition cycle within the same time gates without prior excitation and finally subtracted from the emission signals. The whole imaging process for the read-out of a microtiter plate is accomplished, using three consecutive acquisition cycles for data evaluation and quantification.

3.5. References

[1] Van Dyke, K. (ed) **Luminescence immunoassay and molecular applications**, CRC press, Boca Raton (Fla), 1990, p35.

[2] Sokoll, L. J.; Chan, D. W. **Clinical Analyzers. Immunoassays**. Analytical Chemistry. 1999, 71(12), 356R-362R.

[3] Hopkins, J. **Molecular immunology-gene regulation and signal transduction**. Veterinary Immunology and Immunopathology 2002 87(3-4), 245-249.

[4] Pines, J. **Localization of cell cycle regulators by immunofluorescence**. Methods in Enzymology , 1997 283, 99-113.

[5] Grabarek, J.; Darzynkiewicz, Z. **Versatility of analytical capabilities of laser scanning cytometry (LSC).** Clinical and Applied Immunology Reviews 2002, 2(2), 75-92.

[6] Hage, D. S. **Immunoassays**. Analytical Chemistry. 1999 71(12), 294R-304R.

[7] Mansfield, E. S.; Worley, J. M.; McKenzie, S. E.; Surrey, S.; Rappaport, E.; Fortina, P. **Nucleic acid detection using non-radioactive labeling methods.** Molecular and Cellular Probes 1995, 9(3), 145-56.

[8] Diamandis, E. P. **Analytical methodology for immunoassays and DNA hybridization assays. Current status and selected systems.** Critical review. Clinica Chimica Acta 1990, 194(1), 19-50.

[9] Nakayama, G. R. **Microplate assays for high-throughput screening**. Curruent. Opinion. in Drug Discov. & Develop. 1998, 1(1), 85-91.

[10] Self, C. H.; Cook, D. B. **Advances in immunoassay technology**. Curruent. Opinion. in Biotechnology 1996,. 7(1), 60-5.

[11] Turner, A. P. F. **Techview: Biochemistry: Biosensors-sense and sensitivity.** Science 2000, 290(5495), 1315-1317.

[12] Tang, K.; Fu, D.; Julien, D.; Braun, A.; Cantor, C. R.; Koster, H. **Chip-based genotyping by mass spectrometry.** Proceedings of the National Academy of Sciences of the United States of America 1999, 96(18), 10016-10020.

[13] Kourkine, I. V.; Hestekin, C. N.; Barron, A. E. **Technical challenges in applying capillary electrophoresis-single strand conformation polymorphism for routine genetic analysis**. Electrophoresis 2002, 23(10), 1375-1385.

[14] Borrebaeck, C. A. K. **Antibodies in diagnostics: From immunoassays to protein chips.** Immunology Today 2000 21(8), 379-382.

[15] Templin, M. F.; Stoll, D.; Schrenk, M.; Traub, P. C.; Vohringer, C. F.; Joos, T. O. **Protein microarray technology.** Drug Discovery Today 2002, 7(15), 815-822.

[16] Parker, C. W. **Radioimmunoassay.** Annual. Review. Pharmacology. Toxicology. 1981, 21 113-32.

[17] Diamandis, E. P. **Immunoassays with time-resolved fluorescence spectroscopy: principles and applications** Clinical. Biochemistry . 1988, 21(3), 139-50.

[18] Puget, K.; Michelson, A. M.; Avrameas, S. **Light emission techniques for the microestimation of femtogram levels of peroxidase. Application to peroxidase (and other enzymes)-coupled antibody-cell antigen interactions.** Analytical Biochemistry 1977, 79(1), 447-56.

[19] Stoellner, D.; Stoecklein, W.; Scheller, F.; Warsinke, A. **Membrane-immobilized haptoglobin as affinity matrix for a hemoglobin-A1c immunosensor.** Analytical. Chime. Acta 2002, 470(2), 111-119.

[20] Epstein, J. R.; Biran, I.; Walt, D. R. **Fluorescence-based nucleic acid detection and microarrays.** Analytica Chimica Acta 2002, 469(1), 3-36.

[21] Brennan, M. D. **High throughput genotyping technologies for pharmacogenomics.** American Journal of PharmacoGenomics 2001, 1(4), 295-302.

[22] Kricka, L. J. **Stains, labels and detection strategies for nucleic acids assays.** Annals of Clinical Biochemistry 2002, 39(2), 114-129.

[23] Konig, K. **Multiphoton microscopy in life sciences.** Journal of Microscopy 2000, 200(2), 83-104.

[24] Herman, P.; Lin, H.; Lakowicz, J. R. **Lifetime-based imaging.** Biomedical Photonics Handbook 2003, 9/1-9/30.

[25] Gerritsen, H. C.; De Grauw, K. **One- and two-photon confocal fluorescence lifetime imaging and its applications.** Methods in Cellular Imaging 2001, 309-323.

[26] Szollosi, J.; Damjanovich, S.; Matyus, L. **Application of fluorescence resonance energy transfer in the clinical laboratory: routine and research.** Cytometry 1998 , 34(4), 159-79.

[27] Grabarek, J.; Darzynkiewicz, Z. **Versatility of analytical capabilities of laser scanning cytometry (LSC).** Clinical and Applied Immunology Reviews 2002, 2(2), 75-92.

[28] Cubeddu, R.; Comelli, D.; D'Andrea, C.; Taroni, P.; Valentini, G. **Time-resolved fluorescence imaging in biology and medicine.** Journal of Physics D: Applied Physics 2002, 35(9), R61-R76.

[29] Liebsch, G.; Klimant, I.; Frank, B.; Holst, G.; Wolfbeis, O. S. **Luminescence lifetime imaging of oxygen, pH, and carbon dioxide distribution using optical sensors.** Applied Spectroscopy 2000, 54(4), 548-559.

[30] Nurmi, J.; Lilja, H.; Ylikoski, A. **Time-resolved fluorometry in end-point and real-time PCR quantification of nucleic acids.** Luminescence 2000, 15(6), 381-8.

[31] Rong, H.; Ji, H.; Pernow, Y.; Sjostedt, U.; Bucht, E. **Quantification of parathyroid hormone-related protein mRNA by competitive PCR and time-resolved lanthanide fluorometry.** Clinical Chemistry (Washington, D. C.) (1997), 43(12), 2268-2273.

[32] Schaeferling, M.; Wu, M.; Enderlein, J.; Bauer, H.; Wolfbeis, O. S. **Time-resolved luminescence imaging of hydrogen peroxide using sensor membranes in a microwell format.** Applied Spectroscopy 2003, 57(11), 1386-1392.

Chapter 4. Fluorescence Determination and Imaging of Citrate

4.1. Introduction

Citrate (Fig. 4.1) is an ubiquitous natural compound that occurs in all living cells since it is an important intermediate in the Krebs cycle (also referred to as the citrate cycle or the tricarboxylic acid cycle) [1, 2], which is the central metabolic hub of the cell. Besides its function in cell metabolism, citrate is also widely studied for other fields. In environmental sciences, as a popular chelating agent that assists in the elimination of heavy metal ions through being uptaken and biotransformed by bacteria [3-6]. In medicine, citrate is used as an anticoagulant [7-9] to prevent blood clotting, and for the evaluation of urinary citrate excretion which in turn is related to kidney stones, renal tubular acidosis and certain bone diseases [10-12]. It is also widely utilized as an additive in the food and pharmaceutical industry [13, 14].

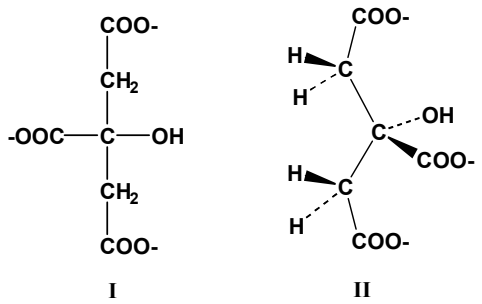

Figure 4.1 Structure of citrate
I: Fischer projection ; II: Wedge projection

Citrate does not have significant physical and chemical properties suitable for direct determination in complex systems, and therefore is difficult to detect and visualize. There are many indirect methods have been exploited, such as by separation technique (such as. high performance liquid chromatography [15-18] and capillary electrophoresis [19-21]), or by enzymes for transformation and synthetic receptors for recognition (Table 4.4).

In most of enzyme-based assays [22], two enzymes, citrate lyase (CL) and malic dehydrogenase (MDH), are usually employed and the decomposition of NADH is detected by absorbance at 355 nm or fluorescence at 445 nm. However, this method would have serious limitations including (a) the need for UV excitation at 355 nm (where almost all materials display fluorescence and background therefore would be strong); (b) the short decay time of NADH (3-5 ns) which hinders the application of time-resolved fluorescence assay and imaging with its unique advantages in terms of background suppression; and (c) the method needs reactions by enzyme catalytically and has rather complicated protocols. So far, however, no direct, intensity based or time-resolved fluorescence assays and imaging for citrate has been reported.

The fluorescence enhancement of citrate on EuTc has been unexpected observed during the studies of interference on EuTc-HP system. This offers a direct method for the fluorescent time-resolved detection of citrate without the involvement of enzymes. So here a europium derived fluorescent probe for the detection and visualization of citrate will be presented. The method is based on the finding that the weak fluorescent europium-tetracycline (EuTc), associates with citrate to form a strongly fluorescent europium-tetracycline-citrate (EuTc-Cit) complex in neutral pH. The features of lanthanide fluorescence of EuTc-Cit are suitable for the time-resolved determination and rapid life detection imaging.

4.2. Results and Discussion

4.2.1. Characterization of EuTc-Cit

4.2.1.1. Spectra of EuTc-Cit

The fluorescence properties of EuTc have been presented before [23, 24] including its application for detection and visualization of hydrogen peroxide [25, 26]. The absorption and fluorescence spectra of the EuTc-Cit system are shown in Fig. 4.2 and their characteristics in Table. 4.1.

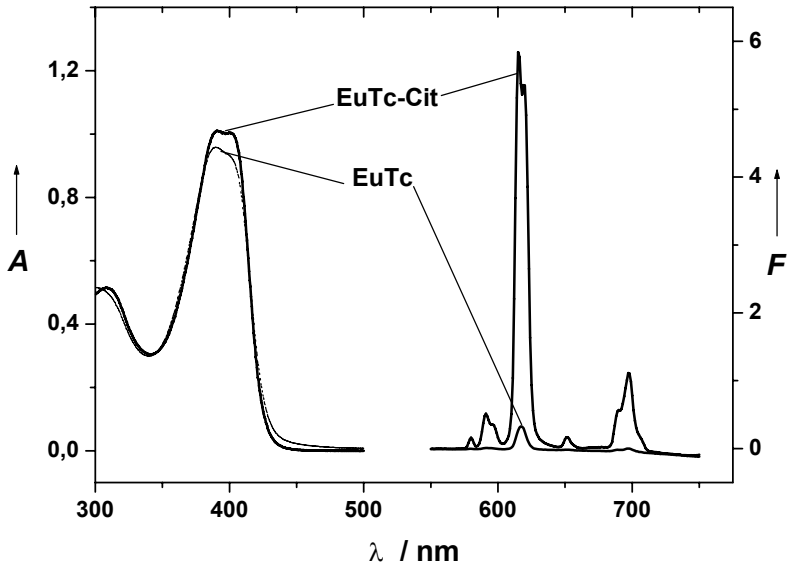

Figure 4.2. Spectra of citrate (150 μM) in EuTc(50 μM of Eu^{3+} and Tc)

TABLE 4.1. THE CHARACTERISTIC PARAMETERS OF IN EUTC-CIT
(citrate: 150 μM, Eu^{3+}: 50 μM, Tc: 50 μM)

	EuTc	EuTc-Cit
absorption peak (nm)	390	389 and 401
molar absorptivity ε ($L\ mol^{-1}\ cm^{-1}$)	1.76×10^4	2.05×10^4
emission (nm)	616	615
average lifetime (μs)	44	83
QY (%)	0.4	3.2

The maximal absorbance of EuTc-Cit are from 381 to 408 nm, similar to that of EuTc. In contrast, the intensity of the emission of EuTc-Cit at 615 nm is much stronger than that of

EuTc. This line-like emission is due to the $^5D_0 \rightarrow {}^7F_2$ electronic transition which is typical for Eu^{3+} fluorescence, with other side bands at 580, 590, 651, and 697 nm, respectively. The quantum yield (QY) of EuTc-Cit increases to 3.2 % from 0.4 % in case of EuTc, (as referring to tris (2,2'-bipyridyl) dichlororuthenium(II) hexahydrate) [27]. In EuTc-Cit complex system, citrate, in being a polydentate ligand, can chelate with Eu^{3+} to form poly-ring via the oxygen atoms of carboxyl and hydroxyl groups [28-30]. It is assumed that citrate displaces water molecules, which ligate to the inner coordination field of Eu^{3+} and quenching its fluorescence. Obviously, the energy transfer in EuTc-Cit is much more effective than that in EuTc.

4.2.1.2. Decay time of EuTc-Cit

The decay profile of EuTc-Cit can be fitted to a three-component model, with decay time components of 15 μs (relative amplitude 12 %), 58 μs (33 %) and 95 μs (55 %), respectively, with an average lifetime (important with respect to imaging) being 83 μs. For EuTc, the three-component model is composed of 8 μs (41 %), 24 μs (55 %) and 123 μs (4 %), respectively, with a average lifetime of 44 μs. The time-resolved fluorescence detection of citrate will benefit from these features of the decay times.

4.2.1.3. Composition of EuTc-Cit

The continuous-variations (or Job´s) method (Fig. 4.3) has been employed for the detection of molar ratio of Eu : Tc : Cit. In Fig. 4.3(a), while the concentration of citrate is excess, the mole fraction of Eu^{3+} : Tc are continuously changed while keeping the total concentration at 25 μM. The peak of curve is at 0.5 of mole fraction of $[Eu^{3+}] / ([Eu^{3+}] + [Tc]$, namely molar ratio of Eu:Tc is 1:1. Changing total concentration to 37.5 and 50 μM, the same result is obtained. Similar case is shown in Fig. 4.3(b) with mole fraction of [Tc] / ([Tc] + [Cit]) being 0.33. Other total concentration of Tc and citrate, 37.5 and 50 μM, are also

employed in this experiment. The result indicates that the molar ratio of Tc: Citrate is 1:2. In combination of Fig. 4.3(a) and (b), the mole ratio of Eu:Tc:Cit is 1:1:2, namely $EuTc(Cit)_2$.

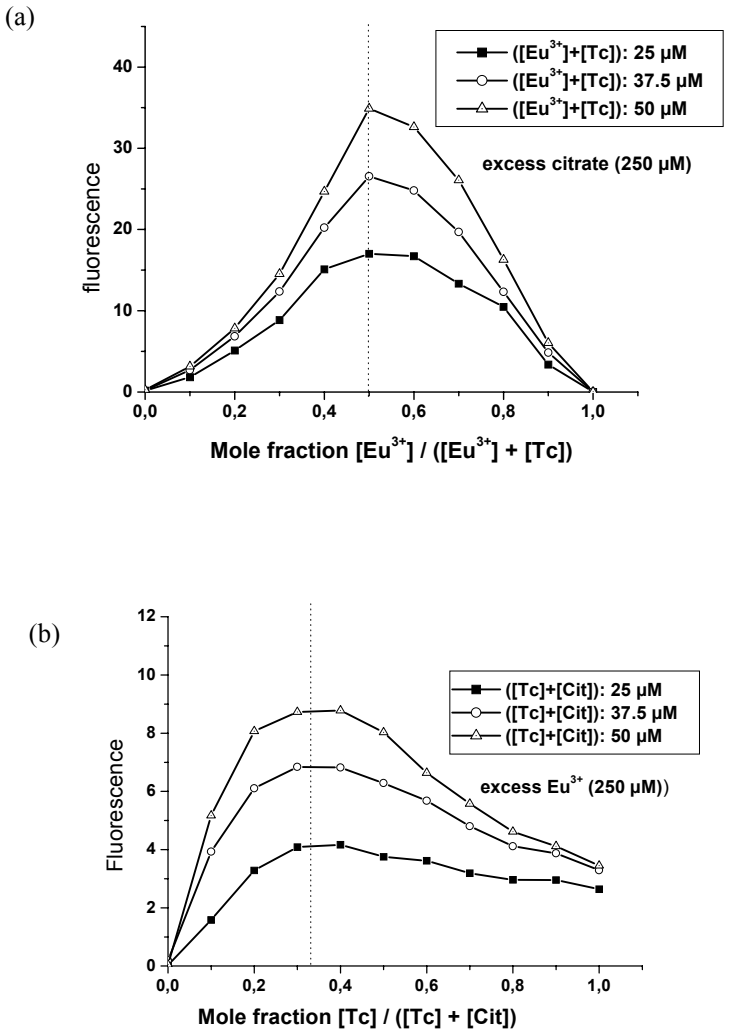

Figure 4.3. Continuous-variations method (Job´s plot)

It is noted that the molar ratio of Eu^{3+} : Tc in EuTc-HP system (chapter 2 and 3) is 3:1. The 1:1 of molar ration of Eu^{3+} : Tc will be used in EuTc - hydroxy acid system (chapter 4, 5, and 6).

Since the molar ratio of (EuTc):citrate is 1:2, there are two dissociation constants K_{d1} and K_{d2} for EuTc-Cit. The disassociation constants are roughly estimated by the Benesi-Hildebrand type equation for a two binding site saturation [31-33]: the pK_{d1} and pK_{d2} are in the range of 4.0 – 5.0.

4.2.1.4. Spectra Circular Dichroism

The circular dichroism (CD) spectra are mainly used for the characterization of chiral compounds and secondary structure of proteins or other biologically important molecules. Tetracycline [34] as chiral molecule, $[\alpha]_D^{25}$ - 257.9° (0.1 N HCl), $[\alpha]_D^{25}$ - 239° (methanol), has five chiral carbons. The spectral change in CD from tetracycline binding Eu^{3+} is shown as in Fig. 4.4. The CD spectrum of tetracycline consisted of two intense exciton couplets

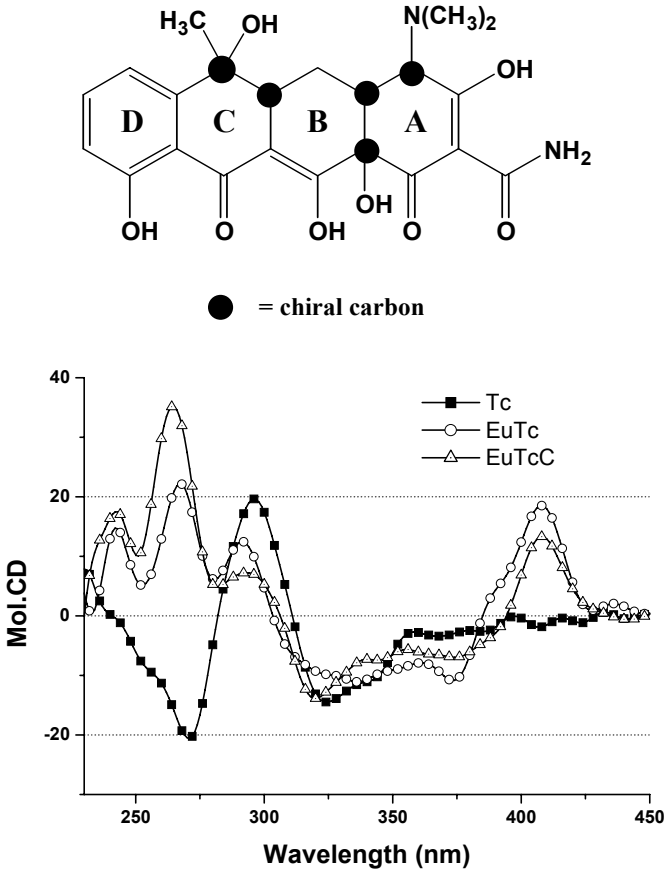

Figure 4.4. CD spectra of EuTc-Cit, EuTc and Tc
Concentrations of Eu^{3+}, Tc and citrate are 50, 50 and 150 μM, respectively.

(maximum at 296 nm, minimum at 271 nm and at 324 nm) with two crossover at 282 nm and at 311 nm. The CD spectra of Tc in ligand of Eu^{3+} or in free state have significant differences. The spectral changes from EuTc are expressed that three bands at 242, 267, and 290 nm instead of one crossover at 282 nm from Tc; a new crossover at 385 nm is occurred (maximum at 408 nm and minimum at 373 nm) which is assumed from the absorption of EuTc around 400 nm (Fig. 4.2). But spectra of EuTc in absence and in present citrate is similar, with only have a little changes. In this case, EuTc is an asymmetric probe, citrate ligating EuTc form ternary complex which is also asymmetric. It indicates that citrate does not significant influence the structure of EuTc at least at ground state.

4.2.1.5. Solid form of EuTc-Cit

The EuTc-Cit shows strong fluorescence not only in solution, but also in solid. Fig. 4.5 (left) is a microscopic photo for the solid EuTc-Cit under UV light. Significant red emission from Eu^{3+} is evident. Under white light, the common solid form of EuTc-Cit can be observed in Fig. 4.5 (right).

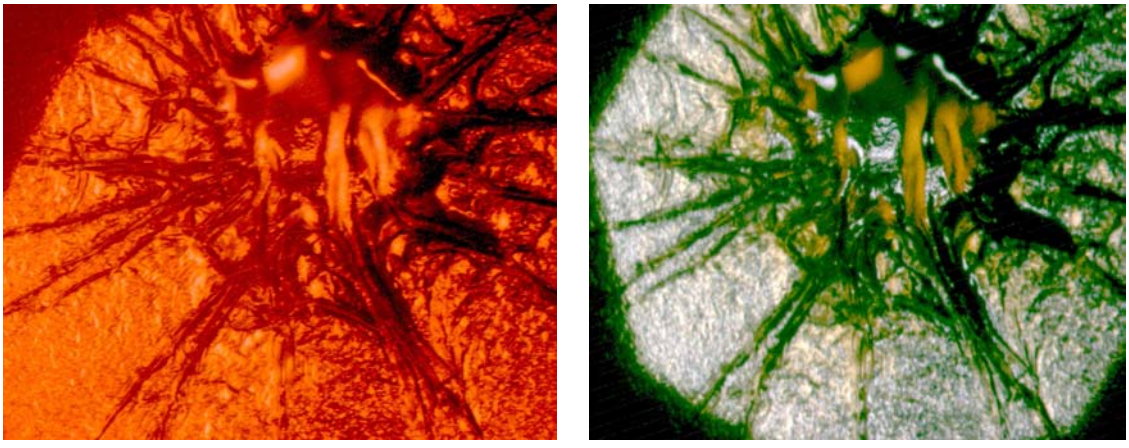

Figure 4.5. Solid form of EuTc-Cit in UV light (left) with 470 nm cut-off objective lens; same EuTc-Cit in white light (right) with common objective lens. Two photos were obtained on Leica DMR fluorescence microscope.

4.2.2. Optimal Experimental Conditions

In EuTc-Cit, tetracycline and citrate as ligands have been deprotonated and are sensitive to pH. The acid dissociation constants of tetracycline [35-38] are pKa_1 ~ 3-4, pKa_2 ~ 7.3-8.1, and pKa_3 ~ 8.8-9.8, that of citric acid [39] are pKa_1 = 3.1, pKa_2 = 4.7, and pKa_3 = 6.4. But once the EuTc -Cit system is formed, it is stable in wide pH range from 7.4 to 9.2 in Fig. 4.6. In this pH range, Tc and citrate, can lose two and three protons, respectively, to become anions with multi-negative charges, and this facilitates binding to europium ion.

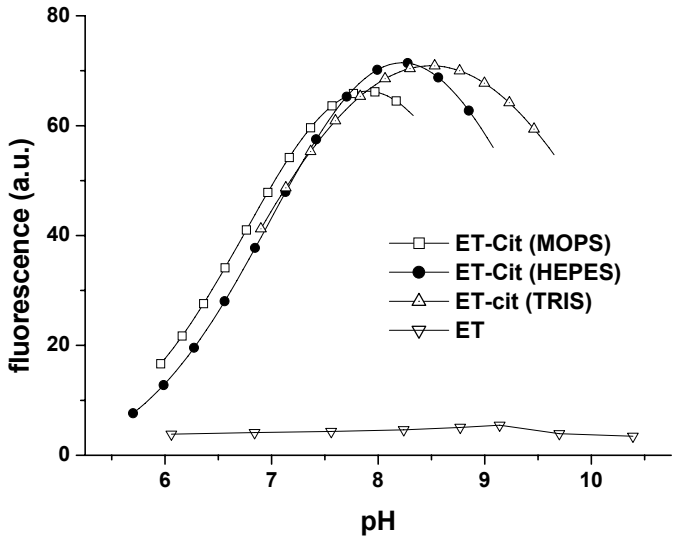

Figure 4.6. The influence of pH for EuTc-Cit. Concentration of Eu^{3+}, Tc and citrate are 50, 50 and 150 μM, respectively.

Three different buffers (HEPES, MOPS and TRIS) were exploited (Fig. 4.6). All of them are suitable for the system. Since the optimal buffer range of MOPS is not coincidental with EuTc-Cit, and TRIS buffer is largely temperature dependent, a 10 mM of HEPES buffer solution of pH 8.0 is used in these experiment.

The time trace (Fig. 4.7) of EuTc binding citrate shows that the increasing of fluorescent intensity depends on time and the concentration of citrate. The higher concentration of citrate, the longer the time to form stable fluorescence.

The fluorescence of EuTc-Cit is inversely proportional to the temperature, as most of the fluorophores. The temperature curve can be describe as y = 14.4 - 0.3 x, (x and y are temperature (°C) and fluorescence intensity).

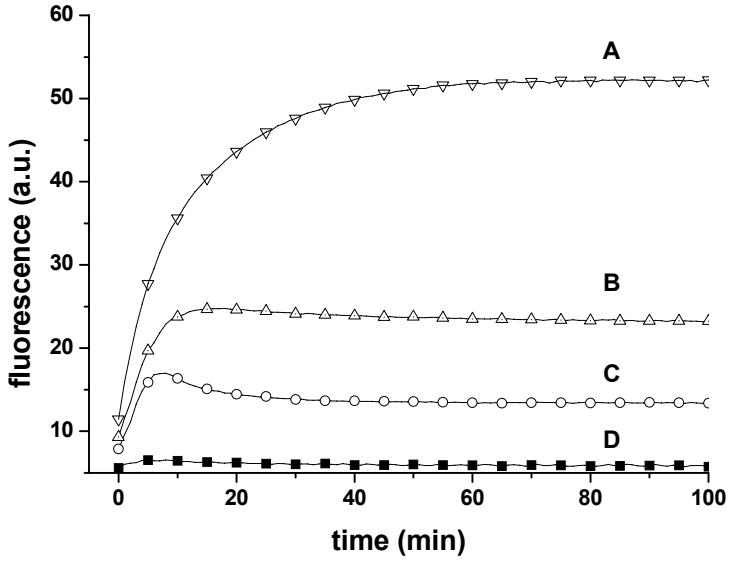

Figure 4.7. Time trace of citrate in EuTc-Cit. Concentration of Eu^{3+} and Tc are all 50 μM, D: blank (EuTc), A, B and C are 50, 15, and 10 μM of citrate.

4.2.3. Interferences

The interferences for EuTc-Cit systems, about 40 common cations in Table 4.2, anions, gases and small biomolecules, were studied. Oxygen has a small effect as its fluorescence in saturated air is 90% of the maximum intensity of that in nitrogen. Alkali, halide, sulfate, nitrate, ammonium, small organic molecules in serum, and human serum albumin (HAS) do not interfere. For heavy metals ions, at pH 8.0, since some of them are precipitated by OH^-, only Ni^{2+}, Co^{2+} and Cu^{2+} , which can complex citrate and tetracycline [40-44], have a constant

affect if their concentration are larger than 16, 16 and 2 μM, respectively, at 40 μM of citrate in EuTc-Cit. Moreover, for phosphate compounds and ions, just 280 μM of phosphate and 8 μM of ATP interfere. It is noted that hydrogen peroxide (which can be probed by EuTc) does not affect the fluorescence of EuTc-Cit, probably because of the much weaker coordinating ability of H_2O_2 to Eu^{3+}, and of different stoichiometry (molar ratio of Eu:Tc is 1:1 here, but the optimal molar ratio of EuTc is 3:1 when probing H_2O_2).

TABLE 4.2. INTERFERENCES OF COMMONS SUBSTANCES FOR EUTC-CIT
(interference is maximally -10 % of initial fluorescence intensity)

EuTc-Cit	**Maximum tolerable concentration ratio (compare with 40 μM of citrate)**
NO^{3-}, F^-, Br^-, I^-, SO_4^{2-}, HCO_3^-, NH_4^+, Na^+, K^+	1000
L-glutamic acid, glucose, glycerol, succinate, acetate	500
Cd^{2+}, L-malate, lactate	200
ascorbate	120
tartrate, fumarate, ketoglutarate, pyruvate	50
AMP	40
Mg^{2+}	32
Ca^{2+}, uric acid, malonate	20
D-malate,	16
NADH	10
phosphate	7
isocitrate	4
Fe^{3+}, Zn^{2+}, oxaloacetate	3
ADP	1
Co^{2+}, Ni^{2+}	0,4
ATP	0,2
Cu^{2+}	0,05
HSA	(1.56 mg/mL)

4.2.4. Quantitative Assay of Citrate

4.2.4.1. Lifetime based assay

Decay time can be used as a parameter for citrate assay, e.g. by time-correlated single photon counting (TCSPC) as shown in Fig. 4.8.

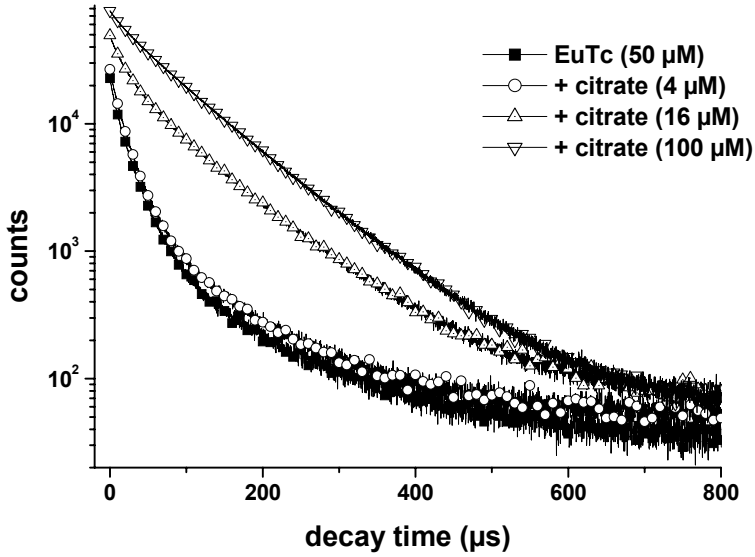

Figure 4.8. Lifetime assay of citrate.

The decay time is increasing with the increase of citrate concentration in EuTc. The decay times of three components from different concentrations of citrate in EuTc are compiled in Table 4.3. The relative amplitudes of third component from each samples at ~ 100 µs increase from 4 % on going to ~ 50 % with concentration of citrate increasing, at last it becomes stable in 100 µM of citrate in EuTc. In contrast to τ_3, the relative amplitudes of first component is decreasing with the increase of citrate concentration.

TABLE 4.3. THE DECAY TIME ASSAY OF EUTC-CIT

(Fitting function: 3-exponentail)

Samples	No.	Decay (μs)	Rel. Amplitude (%)	Av./μs
EuTc(50 μM:50 μM)	τ_1	8.3	40.7	44.3
	τ_2	24.6	55.4	
	τ_3	123.4	4.0	
EuTc-Cit (4 μM)	τ_1	13.8	59.1	48.7
	τ_2	29.9	34.7	
	τ_3	115.9	6.2	
EuTc-Cit (16 μM)	τ_1	17.0	38.0	78.2
	τ_2	58.7	35.3	
	τ_3	106.3	26.8	
EuTc-Cit (100 μM)	τ_1	15.9	13.4	83.6
	τ_2	61.2	35.5	
	τ_3	96.3	51.2	
EuTc-Cit (150 μM)	τ_1	15.1	12.5	83.4
	τ_2	58.5	32.7	
	τ_3	95.0	54.8	

4.2.4.2. Conventional steady-state fluorescence assay

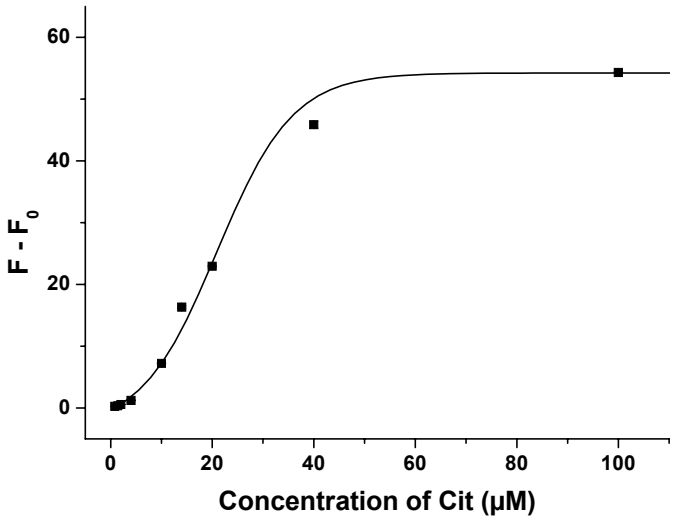

Figure 4.9 .Calibration curve citrate via steady-state fluorescence intensity. Concentration of EuTc is 50 μM. F and F_0 are fluorescence intensities of EuTc in presence and absence citrate.

In contrast to TCSPC, which is usually tedious and requires expensive instrumentation, conventional steady-state fluorescent spectroscopy is widely used. For citrate assay, the dynamic range is from $8x10^{-7}$ to 4×10^{-5} M, with 4×10^{-7} M of the limit of detection (defined as 3σ /slope) and the relatively small error bar (for n=3) in Fig. 4.9.

4.2.4.3. Time-resolved fluorescence assay

The time-resolved fluorometry has also been studied for citrate assay. This method records the fluorescence intensity after a lag time, so it can eliminate the background fluorescence. The effect of different lag times on F/F_0 of the EuTc system in absence and in presence of citrate is shown in Fig 4.10(a). F/F_0 increases on going from 0 μs to a 100 μs lag time. The F / F_0 value reaches a maximum at a lag time from 100 to 150 μs and decreases after 150 μs lag time. This is in accordance with the decay profile of EuTc-Cit because the main component in the decay profile of EuTc-Cit has a 95 μs decay time. Therefore, most of the increase in fluorescence is detected if the integration time window is opened after a lag time of 100 μs.

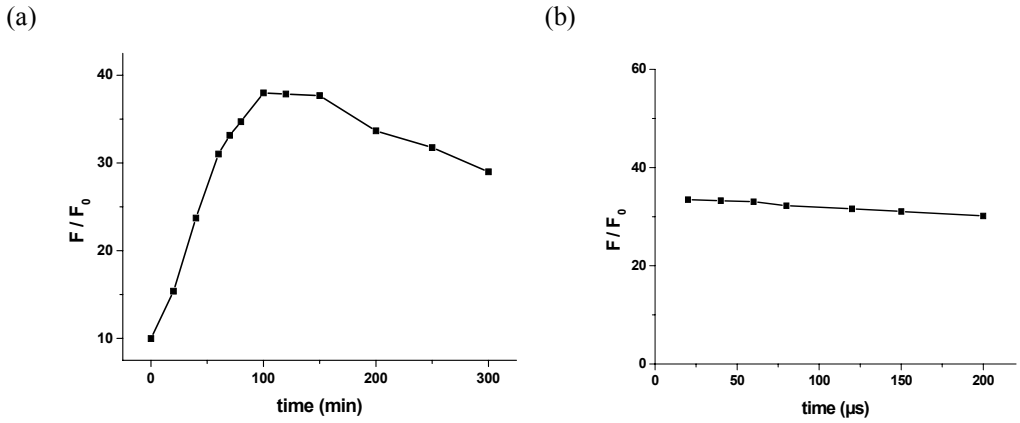

figure 4.10. (a) Fluorescence of F /F_0 in EuTc-Cit at different lag time, with a 40 μs integration time (b) Fluorescence (F /F_0) in EuTc-Cit at different integration time, with 100 μs. F and F_0 are fluorescence intensity of EuTc(50 μM) in presence and absence citrate (150 μM).

The integration time is defined as the length of the time period, the detector is exposed to the emission light. Fig. 4.10(b) shows the effect of the integration time on F / F_0, while 100 μs lag time was employed. If the integration time is increased from 20 μs to 200 μs, F / F_0 decreases slowly. Considering that the major component of the luminescence decay of EuTc-Cit, a 40 μs integration time was regarded to be appropriate. Obviously, the integration time is not really critical.

The time-resolved assay of citrate with a lag time of 100 μs and integration time of 40 μs has a dynamic response between 1.6×10^{-7} and 5.6×10^{-5} M, with a detection limit (defined as 3σ /slope) of 6.0×10^{-8} M of citrate.

4.2.4.4. Imaging

Two imaging schemes were employed for the determination of citrate, the first is conventional steady-state imaging in Fig. 4.11. It shows significant fluorescence changes while EuTc probe was added in the different concentrations of citrate. But the images are greatly affected by fluctuations of the light source and light scatter and leaded to the pictures of substantial heterogeneity.

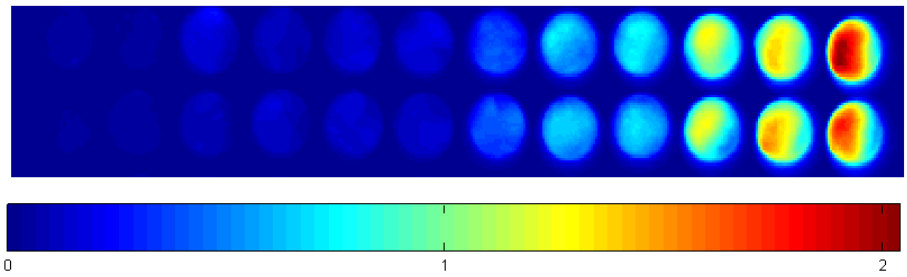

Figure.4.11. Imaging of citrate in EuTc (50 μM) probe. Steady-state imaging, one window for 0-50 μs;. citrate concentrations (from left to right) are 0, 0.16, 0.4, 1.0, 1.6, 4.0, 10.0, 16.0, 20., 40.0, 60.0 and 80.0 μM, respectively

The second is rapid lifetime determination (RLD) imaging [45-47] as shown in Fig. 4.12. The principle of RLD is shown in Fig. 4.12(a), two imaging windows are used in the

decay period of the fluorophore. The LED pulses lasted from 0-50 µs. Image 1 was recorded after a time lag of 50 µs (gating time t_1: 100-180 µs) and image 2 after a time lag of 150 µs (gating time t_2: 200-240 µs). The ratio is calculated to:

$$R_{RLI} = (RLD_1) / (RLD_2) \qquad \text{(Equation 4-1)}$$

The RLD images require that the fluorophore has a microsecond scale lifetime, EuTc-Cit is suitable for this approach. In contrast to steady-state imaging, RLD (Fig. 12 b) offers better homogeneity since the lifetime is relatively independent of the scattering and fluctuations in the intensity of the light source and advantages in terms of signal generation and of excluding artifacts including local inhomogeneities of the concentration of fluorescent probes.

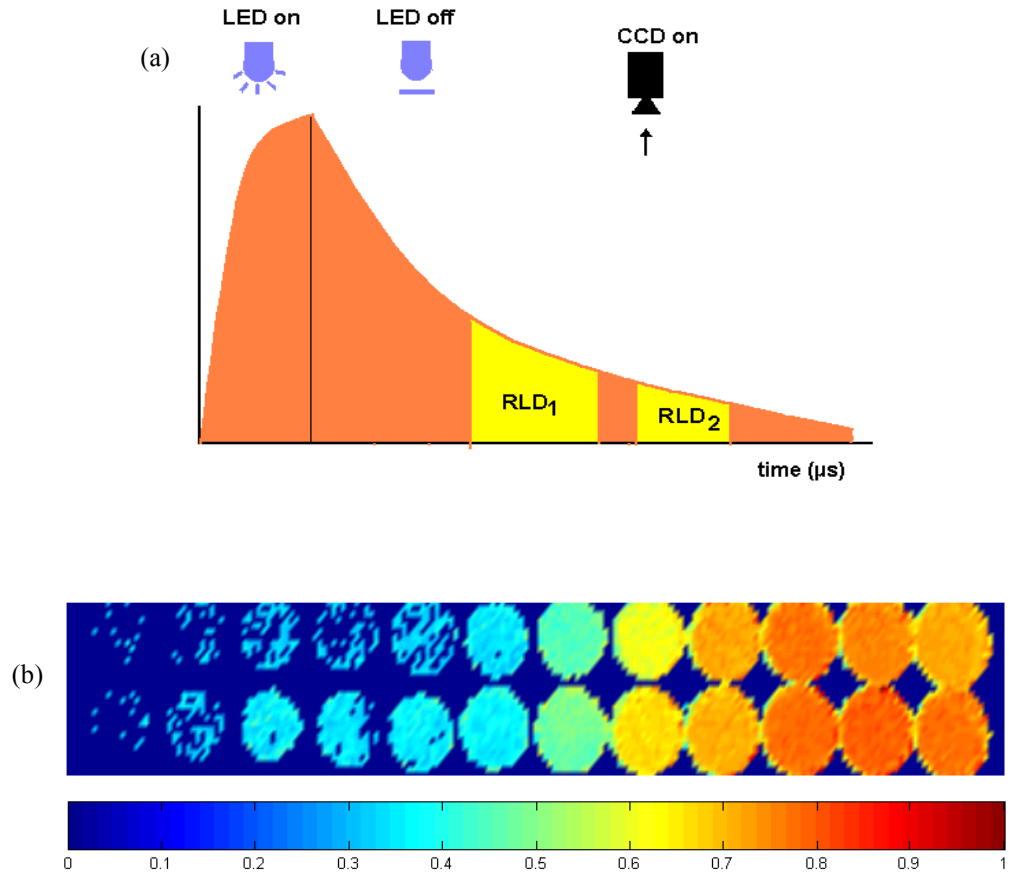

Figure 4.11.(a) Scheme of rapid lifetime detection (RLD) imaging , (b) RLD for citrate in EuTc (50 µM) two windows from 100-180 µs and from 200-240 µs. citrate concentrations (from left to right) are 0, 0.16, 0.4, 1.0, 1.6, 4.0, 10.0, 16.0, 20., 40.0, 60.0 and 80.0 µM, respectively.

4.2.4.5. Comparison with other chemical methods for citrate assay

The main methods for citrate assay are summarized in Table 4.4. These approaches focus on amperometry, colorimetry, fluorescence and chemiluminescence: (a) most of them usually need two or three reaction steps by enzymes or catalysts to yield products which have significant properties suitable for determination. These experimental processes are tedious and some side reactions occur. (b) enzyme for citrate assay via NADH as monitor, which has been commercializad, can be used in colorimetry or fluorometry. But its sensitivity is still lower than that of the EuTc-Cit method. (c) synthetic receptor is also used to recognize citrate, but its selectivity and sensitivity is not good enough. (d) EuTc-Cit method has simple reaction step and facilitation manipulation. It can be used in time-resolved fluorescence detection, which can suppress the background fluorescence, for improve selectivity and sensitivity to obtain a low the limitation of detection.

TABLE 4.4. MAIN CHEMICAL ANALYTICAL APPROACHES OF CITRATE

	methods	**principle**	**linear range**	**LOD**	**ref.**
1	enzyme (spectrophotometry)	citrate $\xrightarrow{citrate\ lyase}$ oxaloacetate + acetate oxaloacetate + NADH + H^+ $\xrightarrow{malic\ dehydrogenase}$ malate + NAD^+		0.02 µmol	48
2	enzyme-solid	same method 1. (spectrophotometry)	1-20 mg L^{-1}		49
3	amperometry	Citrate $\xrightarrow{citrate.lyase,Mg2+,Zn2+}$ acetate + oxaloacetate oxaloacetate $\xrightarrow{oxaloacetate.decarboxylase,Mg2+,Mn2+}$ pyruvate + CO_2 pyruvate + H_3PO_4 + O_2 $\xrightarrow{pyruvate.oxidase,Mg2+,Mn2+,FAD,TPP}$ acetylphosphate + CO_2 + H_2O_2	0.25-5.00 mM		50
4	amperometry (flow injection)	same method 3	0.015-0.5 mM		51
5	potentiometry	polymeric membranes + quaternary ammonium ion exchanger		$5x10^{-5}$ M	52
6	chemiluminescence	Fe(III)-citrate $\xrightarrow{hv}$ Fe^{2+} + CO_2 luminol + O_2 + $2HO^-$ $\xrightarrow{Fe2+}$ 3-aminophthalate + N_2 + $2H_2O$ + hν	$2.0x10^{-7}$-$1.0x\ 10^{-4}$ M		53
7	chemiluminescence	$Ru(bpy)_3^{2+}$ +citrate + Ce^{4+} ⟶ $[Ru(bpy)_3^{2+}]^*$ ⟶ $Ru(bpy)_3^{2+}$ + hν	0.38-38 µg mL^{-1}	0.1 µg mL^{-1}	54
8	spectrophotometry	2,4-diaminophenol + H_2O_2 $\xrightarrow{Fe(III)}$ 2,4-diaminophenol (dimer) + O_2 + H_2O citrate as inhibitor, citrate + Fe(III)→ Fe(III)-Citrate complex	0-1000 mg L^{-1}	0.96 mg L^{-1}	55
9	colorimetry	Fe(III)-citrate $\xrightarrow{hv}$ Fe(II) + CO_2 Fe(II) + 1,10-phenanthroline ⟶ $[Fe(phen)_3]^{2+}$	1-120 µg L^{-1}		56
10	colorimetry	competitive indicator for host – guest complexes		55 µM	57
11	ion chromatography	polymeric anion exchange column, trimesic acid mobile phase	1-12 µg	0.26 µg	58
12	fluorometry, imaging	europium-tetracycline-citrate (this method)	$1.6x10^{-7}$-$5.6x10^{-5}$M	$6.0\ x10^{-8}$M	

4.2.5. Different Kinds of Tetracyclines in Eu-xTc-Cit

Further studies were performed for different tetracycline derivatives as shown in Table 4.5.

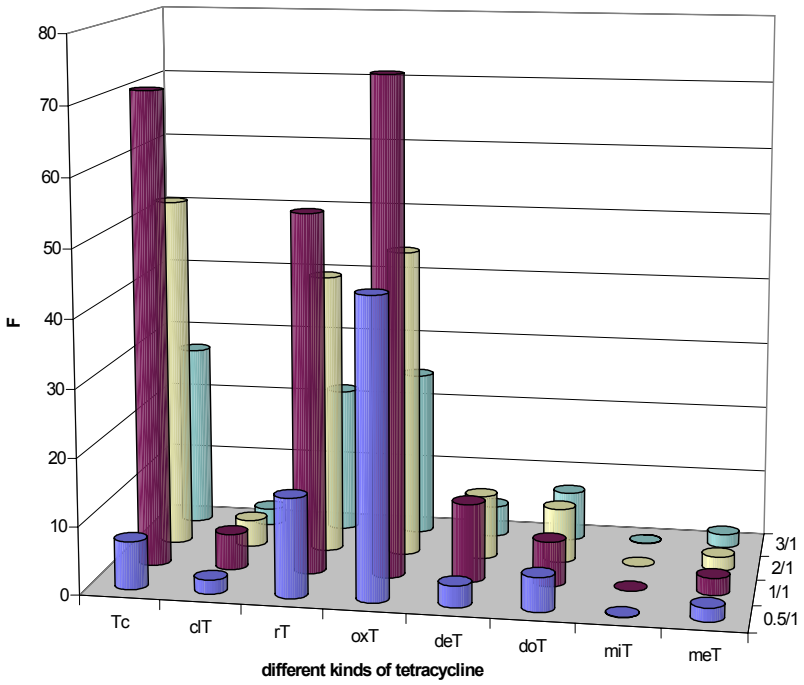

Figure 4.12. Comparison with different tetracyclines and ratio in Eu-xTc-Cit
xTc: tetracycline hydrochloride (Tc), chlortetracycline hydrochloride (clT), rolitetracycline hydrochloride (rT),oxytetracycline hydrochloride (oxT), demeclocycline hydrochloride (deT), doxycycline hydrochloride (doT), minocycline hydrochloride (miT), meclocycline sulfosalicylate salt (meT). molar ratio is Eu/xTc, concentration of citrate and xTc is 100 μM and 48 μM, respectively, concentration of Eu^{3+} is changed according to ratio.

According to Fig. 4.12, it concludes that a) among tetracycline analogs, the fluorescence intensity of oxytetracycline, tetracycline and rolitetracycline chelating europium ion with citrate are strong, that of demeclocycline, doxycycline, chlortetracycline and meclocycline sulfosalicylate are medium, and that of minocycline is very weak. These refer to their structures of molecule. Obviously, it is favorite that OH groups in R3 of tetracyclines.

TABLE 4.5. THE STRUCTURES OF FAMILY OF TETRACYCLINE

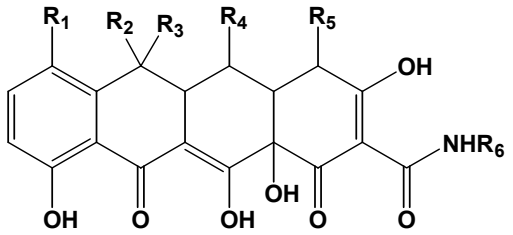

No.	Chemicals	R1	R2	R3	R4	R5	R_6
1	tetracycline	H	CH_3	OH	H	$(CH_3)_2N$-	H
2	chlortetracycline	Cl	CH_3	OH	H	$(CH_3)_2N$-	H
3	rolitetracycline	H	CH_3	OH	H	$(CH_3)_2N$-	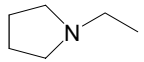
4	oxytetracycline	H	CH_3	OH	OH	$(CH_3)_2N$-	H
5	demeclocycline	Cl	H	OH	H	$(CH_3)_2N$-	H
6	doxycycline	H	CH_3	H	OH	$(CH_3)_2N$-	H
7	minocycline	$(CH_3)_2N^-$	H	H	H	(CH3)2N-	H
8	meclocycline sulfosalicylate salt	Cl	=CH2	\	OH	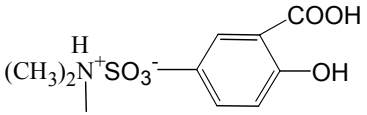	H

tetracycline hydrochloride (Tc), chlortetracycline hydrochloride (clT), rolitetracycline hydrochloride (rT),oxytetracycline hydrochloride (oxT), demeclocycline hydrochloride (deT), doxycycline hydrochloride (doT), minocycline hydrochloride (miT), meclocycline sulfosalicylate salt (meT)

However, R_1 group except H is hindrance, for example, R_1 = Cl^- in demeclocycline, and $(CH_3)_2N$- in minocycline. But R_6 = group was no influence on the coordination of Tc and Eu^{3+}, such as R_6 = 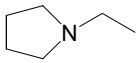 in oxytetracycline. b) the optimal molar ratio of Eu:Tc is at 1:1 regardless of any tetracycline. c) The orders of fluorescence intensity of coordination of Tc and Eu^{3+} with citrate are different. For example, at ½ (or 0.5/1) of mole ratio of Eu^{3+}:Tc, the order is oxytetracycline > rolitetracycline > tetracycline > doxycycline > demeclocycline > meclocycline sulfosalicylate > chlortetracycline > minocycline. But at 2:1 molar ratio, the order is change, tetracycline > oxytetracycline > rolitetracycline > demeclocycline > doxycycline > chlortetracycline > meclocycline > minocycline. These knowledge on structures will greatly benefit further studies, especially the optimization of Eu-xTc fluorescence probes for citrate.

4.3. Conclusion

A europium derived fluorescent probe for the measurement and visualization of citrate is first time presented. Besides a straightforward direct detection using a simple reagent and without the need for multi-enzyme assays, many lifetime and imaging techniques are utilized in this system. This probe is simple to prepare, stable both in solution and in solid , and compatible with the blue laser diodes. It will be most useful for monitoring citrate-related bioprocesses.

4.4. Experimental Section

4.4.1 Reagents

Tri-sodium citrate dihydrate and other inorganic salts were obtained in analytical purity from Merck unless otherwise stated. All solutions were prepared in 10 mM 4-(2-hydroxyethyl) piperazine-1-ethanesulfonic acid (HEPES) buffer of pH 8.0 (Sigma-Aldrich, Deisenhofen, Germany) unless otherwise specified. Europium(III) trichloride hexahydrate was from Alfa Products, tetracycline hydrochloride from Sigma.

The EuTc standard solution was obtained by dissolving Eu^{3+} chloride and tetracycline (each in 0.5 mM concentration) in 10 mM HEPES buffer of pH 8.0. This reagent is stable for at least 2 months if stored at 4 °C in the dark.

4.4.2. Apparatus

Absorption spectra were acquired on a Cary WinUV photometer. Fluorescence studies of the effect of citrate on spectra the EuTc were performed on an SLM AB2 luminescence spectrometer. Fluorescence intensity was acquired on either a Fluoroskan Ascent micro titer plate reader or on a Tecan GENios+ micro plate reader. The excitation/emission filters were set to 405/620 nm, or 405/612 nm respectively. The 96-well black, transparence, flat bottom microtiter plates for imaging were obtained from Greiner Bio-One GmbH (Frickenhausen, Germany; www.greiner-lab.com). The luminescence lifetimes of different concentration of citrate in EuTc were determined with a pulsed 392-nm laser and an H5783-P04 PMT detector with multiphoton-counting board in a multipass cuvette. Circular dichroism (CD) spectra were performed on JASCO model J – 710 spectropolarimeter (www.jasco.de). DMR fluorescence microscopy is from Leica (www.light-microscopy.com)

4.4.3. Fluorescence Microscopic Observation of Solid form EuTc-Cit

Efforts have been made to crystalize EuTc-Cit. 20 μL of EuTc (50 μM) in citrate (150 μM) forms a drop on the cover slide, which is hung over the reservior in which includes 40 % (v/v) polyethylene glycol 400. After one week, a thin solid member (instead of crystal) is observed under fluorescence microscopy. Two photos of solid EuTc-Cit were obtained on a Leica DMR fluorescence microscopy. One is in UV light with objective lens of PL FLUROTAR (cut off 470 nm) at 4.0 s exposure time and 4.1 gain; the other in white light with objective lens of N PLAN at 45.8 ms exposure time and 4.1 gain.

4.4.4. RLD Imaging

Imaging set-up was as described in section 3.4.6. Scheme of RLD with two windows of fluorescence detection at 100-180 μs and 200-240 μs are recorded. The manipulation and calculation of images, such as the rotation and crop of the images, the subtraction of the dark image (blank, without illumination) from the fluorescent image respectively, the ratio of the images and filtration of the background noise, were done by a self-developed program based on Matlab (6.1, Mathwork, Natick, MA, USA).

4.5. References

[1] Krebs, H. A. **The citric acid cycle.** Biochemical Journal, London, 1940, 34: 460-463.

[2] Berg, J. M.; Tymoczko, J. L;. Stryer, L. **Biochemistry**, 5th ed, Chapter 17 "The Citric Acid Cycle" W. H. Freeman and Company, 2001, p 465-487

[3] Bott, M. **Anaerobic citrate metabolism and its regulation in enterobacteria**. Archives of Microbiology 1997, 167(2-3), 78-88.

[4] Li, H.; Pajor, A. M. **Functional characterization of CitM, the Mg2+-citrate transporter.** Journal of Membrane Biology 2002, 185(1), 9-16.

[5] Krom, B. P.; Huttinga, H.; Warner, J. B.; Lolkema, J. S. **Impact of the Mg2+-citrate transporter CitM on heavy metal toxicity in Bacillus subtilis.** Archives of Microbiology 2002, 178(5), 370-375.

[6] Nikovskaya, G. N.; Ul'berg, Z. R.; Koval', L. A.; Nadel, L. G.; Strizhak, N. P. **Some Colloidal and Chemical Aspects of Biotransformation of Heavy Metal Citrate Complexes.** Colloid Journal (Translation of Kolloidnyi Zhurnal) 2002, 64(4), 466-471.

[7] Macey, M.; Azam, U.; McCarthy, D.; Webb, L.; Chapman, E. S.; Okrongly, D.; Zelmanovic, D.; Newland, A. **Evaluation of the anticoagulants EDTA and citrate, theophylline, adenosine, and dipyridamole (CTAD) for assessing platelet activation on the ADVIA 120 hematology system**. Clinical Chemistry 2002, 48(6, Pt. 1), 891-899.

[8] Apsner, R.; Buchmayer, H.; Lang, T.; Unver, B.; Speiser, W.; Sunder-Plassmann, G.; Horl, W. H. **Simplified citrate anticoagulation for high-flux hemodialysis**. American Journal of Kidney Diseases 2001, 38(5), 979-87.

[9] Bolan, C. D.; Greer, S. E.; Cecco, S. A.; Oblitas, J. M.; Rehak, N. N.; Leitman, S. F. **Comprehensive analysis of citrate effects during plateletpheresis in normal donors**. Transfusion 2001, 41(9), 1165-71.

[10] Renata, C.; Fabio, V.; Angela, B.; Sergio, S. **Citrate and mineral metabolism: Kidney stones and bone disease.** Frontiers in Bioscience 2003, 8 S1084-S1106.

[11] Mossetti, G.; Vuotto, P.; Rendina, D.; Numis, F. G.; Viceconti, R.; Giordano, F.; Cioffi, M.; Scopacasa, F.; Nunziata, V. **Association between vitamin D receptor gene polymorphisms and tubular citrate handling in calcium nephrolithiasis.** Journal of Internal Medicine 2003, 253(2), 194-200.

[12] Barbas, C.; Garcia, A.; Saavedra, L.; Muros, M. **Urinary analysis of nephrolithiasis markers**. Journal of Chromatography, B: Analytical Technologies in the Biomedical and Life Sciences 2002, 781(1-2), 433-455.

[13] Burdock, G. A. **Encyclopedia of food and color additives** volume I CRC Press 1997, p613-619.

[14] Europäisches Arznzeibuch 1997, p729-930.

[15] Lu, S.; Sun, X.; Shi, C.; Zhang, Y. **Determination of tricarboxylic acid cycle acids and other related substances in cultured mammalian cells by gradient ion-exchange chromatography with suppressed conductivity detection.** Journal of Chromatography, A 2003, 1012(2), 161-168.

[16] Nozal, M. J.; Bernal, J. L.; Diego, J. C.; Gomez, L. A.; Higes, M. **HPLC determination of low molecular weight organic acids in honey with series-coupled ion-exclusion columns**. Journal of Liquid Chromatography & Related Technologies 2003, 26(8), 1231-1253.

[17] Hasib, A.; Jaouad, A.; Mahrouz, M. **High-performance liquid chromatography study of citric, malic and ascorbic acid contents in various varieties of Moroccan citrus juices.** Sciences des Aliments 2002, Volume Date 2001, 21(5), 555-562.

[18]Jenke, D. R. **Quantitation of oxalate and citrate by ion chromatography with a buffered, strong acid eluent.** Journal of Chromatography 1988, 437(1), 231-7.

[19]Wang, M.; Qu, F.; Shan, X.; Lin, J. **Development and optimization of a method for the analysis of low-molecular-mass organic acids in plants by capillary electrophoresis with indirect UV detection**. Journal of Chromatography, A 2003, 989(2), 285-292.

[20] Izco, J. M.; Tormo, M.; Harris, A.; Tong, P. S.; Jimenez-Flores, R. **Optimization and validation of a rapid method to determine citrate and inorganic phosphate in milk by capillary electrophoresis**. Journal of Dairy Science 2003, 86(1), 86-95.

[21] Kanitsar, K.; Chen, Z.; Owens, G.; Naidu, R. **Influence of organic modifiers on the separation of carboxylic acids using Co-EOF capillary electrophoresis.** Journal of Liquid Chromatography & Related Technologies 2003, 26(3), 455-468.

[22] UV-method for the determination of citric acid in foodstuffs, Boehringer Mannheim, Cat.no. 139076, 1998.

[23] Hirschy, L. M.; Van Geel, T. F.; Winefordner, J. D.; Kelly, R. N.; Schulman, S. G. **Characteristics of the binding of europium(III) to tetracycline**. Analytica Chimica Acta 1984, 166 207-19.

[24] Rakicioglu, Y.; Perrin, J. H.; Schulman, S. G. **Increased luminescence of the tetracycline-europium(III) system following oxidation by hydrogen peroxide.** Journal of Pharmaceutical and Biomedical Analysis 1999, 20(1-2), 397-399.

[25] Lei, W.; Duerkop, A.; Lin, Z.; Wu, M.; Wolfbeis, O. S. **Detection of Hydrogen Peroxide in River Water via a Microplate Luminescence Assay with Time-Resolved ("Gated") Detection**. Microchimica Acta 2003, 143(4), 269-274.

[26] Schaeferling, M.; Wu, M.; Enderlein, J.; Bauer, H.; Wolfbeis, O. S. **Time–resolved luminescence imaging of hydrogen peroxide using sensor membranes in a microwell format** Applied Spectroscopy 2003, 57(11), 1386-1392.

[27] Van Houten, J.; Watts, R. J. **Effect of ligand and solvent deuteration on the excited state properties of the tris(2,2'-bipyridyl)ruthenium(II) ion in aqueous solution. Evidence for electron transfer to solvent.** Journal of the American Chemical Society 1975, 97(13), 3843-4.

[28] Glusker, J. P. **Citrate conformation and chelation: enzymic implications.** Accounts of Chemical Research 1980, 13(10), 345-52.

[29] Dickins, R. S.; Aime, S.; Batsanov, A. S.; Beeby, A.; Botta, M.; Bruce, J. I.; Howard, J. A. K.; Love, C. S.; Parker, D.; Peacock, R. D.; Puschmann, H. **Structural, Luminescence, and NMR Studies of the Reversible Binding of Acetate, Lactate, Citrate, and Selected Amino Acids to Chiral Diaqua Ytterbium, Gadolinium, and Europium Complexes.** Journal of the American Chemical Society 2002, 124(43), 12697-12705.

[30] Parker, D.; Dickins, Rachel S.; Puschmann, Horst; Crossland, Clare; Howard, Judith A. K. **Being Excited by Lanthanide Coordination Complexes: Aqua Species, Chirality, Excited-State Chemistry, and Exchange Dynamics.** Chemical Reviews, 2002, 102(6), 1977-2010.

[31] Benesi, H. A.; Hildebrand, J. H. **A spectrophotometric investigation of the interaction of iodine with aromatic hydrocarbons.** Journal of the American Chemical Society (1949), 71 2703-7.

[32] Silber, H. B.; Maraschin, V.; Sibley, S.; Richter, C.; Arif, N.; Contreras, L.; Djurovich, P.; Ratansiripong, T.; Stoddard, J. **Spectrophotometric investigations of the complexation between Ni(II) and thiocyanate in aqueous methanol.** Polyhedron 2003, 22(27), 3439-3444.

[33] Xu, M.; Lin, J.; Hu, Q.; Pu, L. **Fluorescent sensors for the enantioselective recognition of mandelic acid: Signal amplification by dendritic branching**. Journal of the American Chemical Society 2002, 124(47), 14239-14246.

[34] The Meck Index

[35] De Paula, F. C. S.; Carvalho, S.; Duarte, H. A.; Paniago, E. B.; Mangrich, A. S.; Pereira-Maia, E. C. **A physicochemical study of the tetracycline coordination to oxovanadium(IV).** Journal of Inorganic Biochemistry 1999, 76(3-4), 221-230.

[36] Martin, R. B. **In Metal Ions in Biological Systems**; Siegel, H., Ed.; Marcel Dekker: New York, 1985; Vol. 19, pp 20-52

[37] Leeson, L. J.; Krueger, J. E.; Nash, R. A. **Structural assignment of the second and third acidity constants of tetracycline antibiotics.** Tetrahedron Letters 1963, (18), 1155-60.

[38] Duarte, H. A.; Carvalho, S.; Paniago, E. B.; Simas, A. M. **Importance of Tautomers in the Chemical Behavior of Tetracyclines.** Journal of Pharmaceutical Sciences 1999, 88(1), 111-120.

[39] Hargis, L. G. **Analytical Chemistry: Principles and Techniques**, Prentice-Hall, Inc. 1988

[40] Olin, A.; Wallen, B. **Determination of citrate by potentiometric titration with copper(II) and a copper ion-selective electrode.** Analytica Chimica Acta 1983, 151(1), 65-75.

[41] http://www.chm.bris.ac.uk/motm/tetracycline/tetracycline.htm

[42] Lambs, L.; Decock-Le Reverend, B.; Kozlowski, H.; Berthon, G. **Metal ion-tetracycline interactions in biological fluids. 9. Circular dichroism spectra of calcium and magnesium complexes with tetracycline, oxytetracycline, doxycycline, and chlortetracycline and discussion of their binding modes.** Inorganic Chemistry 1988, 27(17), 3001-12.

[43] Jezowska-Bojczuk, M.; Lambs, L.; Kozlowski, H.; Berthon, G. **Metal ion-tetracycline interactions in biological fluids. 10. Structural investigations on copper(II) complexes of tetracycline, oxytetracycline, chlortetracycline, 4-(dedimethylamino)tetracycline, and 6-desoxy-6-demethyltetracycline and discussion of their binding modes.** Inorganic Chemistry 1993, 32(4), 428-37.

[44] Job, R.; Kelleher, P. J.; Stallings, W. C., Jr.; Monti, C. T.; Glusker, J. P. **Three-point attachment of citrate to a cobalt(III) tetraamine complex.** Inorganic Chemistry 1982, 21(10), 3760-4.

[45] Woods, R. J.; Scypinski, S.; Love, L. J.; Ashworth, H. A. **Transient digitizer for the determination of microsecond luminescence lifetimes.** Analytical Chemistry 1984, 56(8), 1395-400.

[46] Liebsch, G.; Klimant, I.; Frank, B.; Holst, G.; Wolfbeis, O. S. **Luminescence lifetime imaging of oxygen, pH, and carbon dioxide distribution using optical sensors.** Applied Spectroscopy 2000, 54(4), 548-559.

[47] Mayr, T.; Igel, C.; Liebsch, G.; Klimant, I.; Wolfbeis, O. S. **Cross-Reactive Metal Ion Sensor Array in a Micro Titer Plate Format**. Analytical Chemistry 2003, 75(17), 4389-4396.

[48] Moellering, H.; Gruber, W. **Determination of citrate with citrate lyase.** Analytical Biochemistry 1966, 17(3), 369-76.

[49] Planta, M.; Lazaro, F.; Puchades, R.; Maquieira, A. **Determination of citric acid and oxalacetic acid in foods by enzymic flow injection.** Analyst 1993, 118(9), 1193-7.

[50] Matsumoto, K.; Tsukatani, T. **Simultaneous quantitation of citrate and isocitrate in citrus juice by a flow-injection method based on the use of enzyme reactors**. Analytica Chimica Acta 1996, 321(2-3), 157-64.

[51] Prodromidis, M. I.; Tzouwara-Karayanni, S. M.; Karayannis, M. I.; Vadgama, P. M. **Bioelectrochemical determination of citric acid in real samples using a fully automated flow injection manifold.** Analyst 1997, 122(10), 1101-1106.

[52] Ribeiro, C. M. F.; Matos, C. D.; Sales, M. G. F.; Vaz, M. C. V. F. **Citrate selective electrodes for the flow injection analysis of soft drinks, beers and pharmaceutical products.** Analytica Chimica Acta 2002, 471(1), 41-49.

[53] Perez-Ruiz, T.; Martinez-Lozano, C.; Tomas, V.; Val, O. **Flow-injection chemiluminescence determination of citrate based on a photochemical reaction.** Analyst 1995, 120(2), 471-5.

[54] Pérez-Ruiz, T.; Martínez-Lozano, C.; Tomás, V.; Fenoll, J. **Chemiluminescence determination of citrate and pyruvate and their mixtures by the stopped-flow mixing technique** Analytica Chimica Acta 2003, 485(1), 63-72.

[55] Themelis, D. G.; Tzanavaras, P. D. **Reagent-injection spectrophotometric determination of citric acid in beverages and pharmaceutical formulations based on its inhibitory effect on the iron(III) catalytic oxidation of 2,4-diaminophenol by hydrogen peroxide**. Analytica Chimica Acta 2001, 428(1), 23-30.

[56] Luque-Perez, E.; Rios, A.; Valcarcel, M. **Flow-injection spectrophotometric determination of citric acid in beverages based on a photochemical reaction**. Analytica Chimica Acta 1998, 366(1-3), 231-240.

[57] McCleskey, S. C.; Metzger, A.; Simmons, C. S.; Anslyn, E. V. **Competitive indicator methods for the analysis of citrate using colorimetric assays.** Tetrahedron 2002, 58(4), 621-628.

[58] Chalgeri, A.; Tan, H. S. I. **Indirect photometric detection for determination of citrate in pharmaceutical matrixes by ion chromatography.** Journal of Pharmaceutical and Biomedical Analysis 1996, 14(7), 835-844.

Chapter 5. Fluorescence Imaging and Detection of Main Intermediates in the Krebs Cycle

5.1. Introduction

The Krebs cycle [1, 2] (Fig. 5.1) is a key series of metabolic reactions in aerobic cellular respiration, occurring in the mitochondria of animals and plants. It is the central metabolic hub of the cell not only for harvesting chemical energy [3, 4], but also for building the basic blocks of amino acids, nucleotide bases, porphyrins and others [5-7].

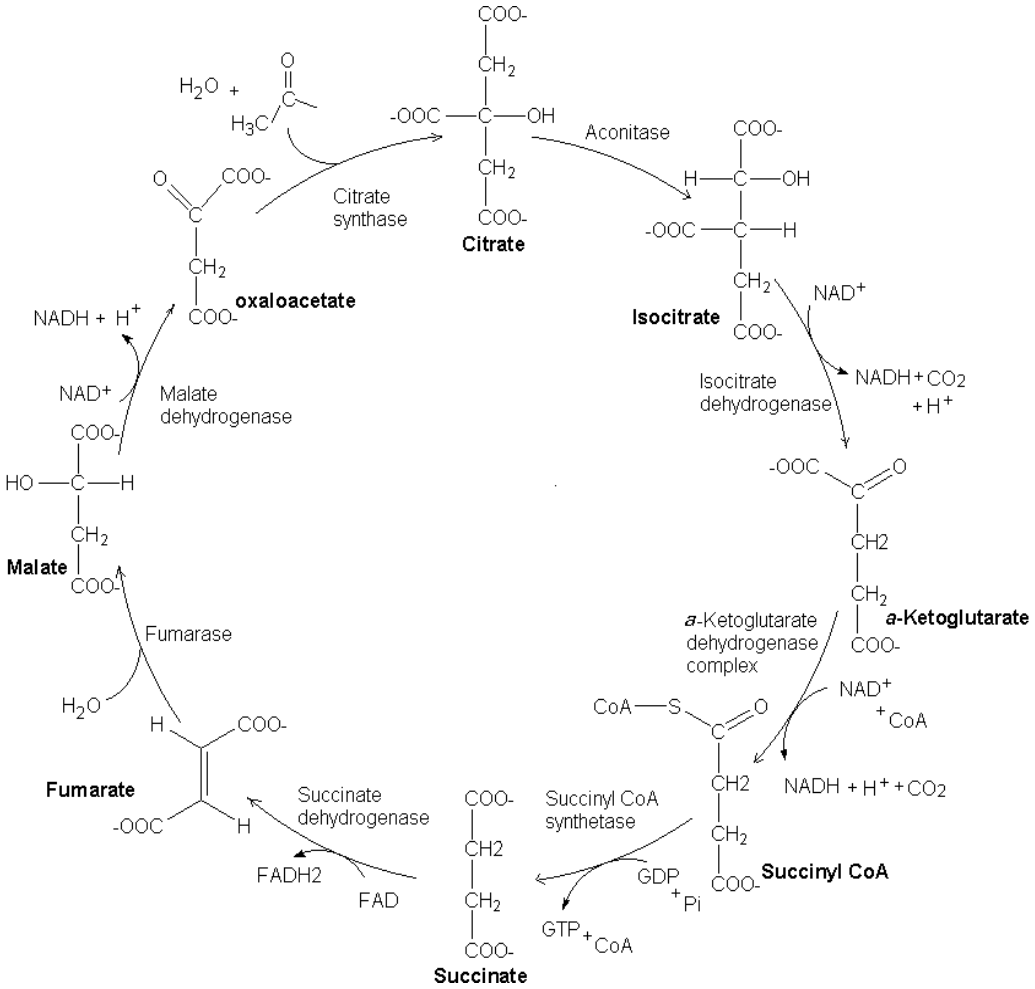

Figure 5.1. The Krebs cycle (adapted from. Berg, J. M ref.[2])

There are many intermediates in the Krebs cycle had been studied. By exploring the interactions between the Krebs cycle and other metabolism systems [8-10], intermediates are still medium. The most of studies of the Krebs cycle have been developed basically through isotropic labels [11-13] especially for the mechanism research. The main intermediates in the Krebs cycle, such as citrate, isocitrate, α-ketoglutarate (KG), succinate, fumarate, L-malate and oxaloacetate (their structures are in Fig. 5.1), are usually absent of significant physical and chemical properties suitable for direct non-radioactive determination, and therefore the Krebs cycle is difficult to visualize and to detect directly. Besides separative chromatography [14-16] and electrophoresis [17-19], enzyme or multi-enzymatic methods [20-23] are mostly employed by coupling with reactions involving NADH. These methods always depend upon the change of NADH [24-26] as a monitor to detect reactants or products. But the disadvantages of detection through NADH in biosamples are obvious: short decay times, UV excitation at 355 nm and complicated reaction processes.

Here, a europium derived fluorescent probe has been used for the detection and visualization of main intermediates. The method is based on the finding that the weakly fluorescent europium-tetracycline (EuTc) [27-29] can reversibly associate with intermediates to form differently fluorescent europium-tetracycline-ligands (EuTc-L) at neutral pH. As these complexes have the merits of lanthanide fluorescence, time-resolved fluorescence detection can be used. Fluorescence imaging is applied for the visualization of intermediates. In addition, the stepwise determination of the formation and decomposition of intermediates can be performed via the kinetic fluorescence changes.

5.2. Results and Discussion

5.2.1. Characterization of EuTc Complexes with Main Intermediates

5.2.1.1. Absorbance and fluorescence spectra

The absorption and fluorescence spectra of the EuTc-L systems are shown in Fig. 5.2. The maximal absorbances of EuTc-L are from 381 to 408 nm, similar to that of EuTc In contrast, the fluorescence intensity of the emissions of EuTc-L are stronger than that of EuTc from 615 to 619 nm. These intermediates can act as polydentate ligands and thus may be expected to form ternary complexes with EuTc. The coordination with Eu^{3+} involve oxygen atoms from carboxyl and hydroxy group, probably resulting in formation of 5-, 6-, or 7-member ring with Eu^{3+} [30-32]. Different molecule structures lead to different fluorescence intensities (Fig. 5.2), as well as in decay times and quantum yields (Table 5.1)

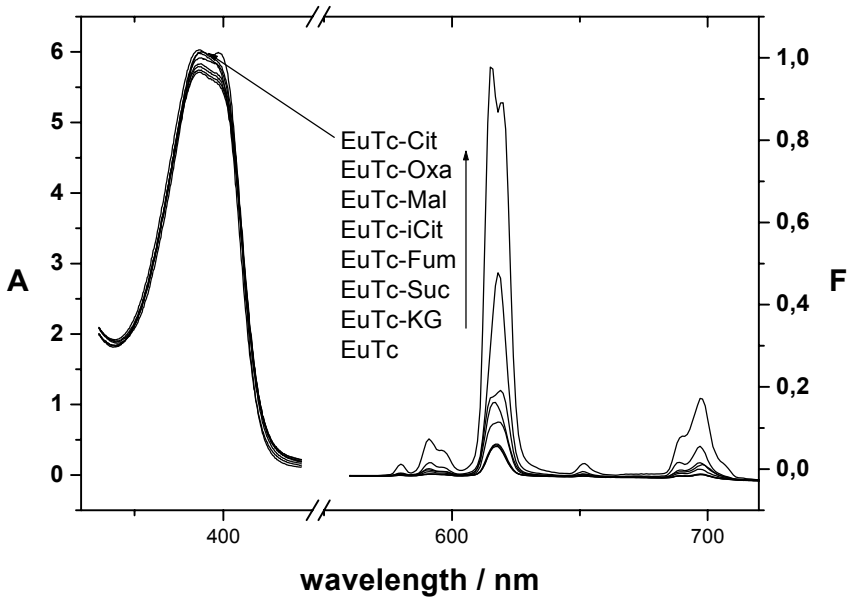

Figure 5.2. Spectra of EuTc-L complex. Eu^{3+}: 50 µM, Tc: 50 µM L:150 µM

TABLE 5.1. THE DECAY PROFILES AND QUANTUM YIELD OF EUTC-L

Samples [a]	Components [b]	Decay (μs)	Rel. Amplitude (%)	Av.(μs)	QY(%)[c]
EuTc	τ_1	8	40.7	44	0.4
	τ_2	24	55.4		
	τ_3	123	4.0		
EuTc-Cit	τ_1	15	12.5	83	3.2
	τ_2	58	32.7		
	τ_3	95	54.8		
EuTc-iCit	τ_1	16	57.4	66	0.7
	τ_2	40	27.6		
	τ_3	111	15.0		
EuTc-KG	τ_1	8	40.5	37	0.4
	τ_2	21	56.1		
	τ_3	112	3.4		
EuTc-Suc	τ_1	7	36.3	38	0.4
	τ_2	21	57.4		
	τ_3	88	6.2		
EuTc-Fum	τ_1	8	28.0	63	0.5
	τ_2	22	49.3		
	τ_3	90	22.8		
EuTc-Mal [d]	τ_1	17	53.3	77	0.8
	τ_2	61	24.2		
	τ_3	109	22.6		
EuTc-Oxa	τ_1	13	14.7	56	1.4
	τ_2	49	60.1		
	τ_3	71	25.1		

a) Eu^{3+}: 50 μM, Tc: 50 μM, for the purpose of the Krebs cycle study, only 150 μM of L (ligand) is used here.
b) Fitting function: 3-exponential decay
c) tris (2,2'-bipyridyl) dichlororuthenium(II) hexahydrate as the reference, ref [33]
d) In this case, the concentration of L-malate for EuTc is not saturated.

5.2.1.2. Fluorescence Decay times and Quantum Yields

The decay profiles of EuTc-L complexes, as obtained through TCSPC, can be fitted into a three-component model as summarized in Table 5.1. The quantum yields of EuTc-Cit and EuTc-Oxa show higher than that of other intermediates. For decay times, the average lifetime

of EuTc-Cit and EuTc-Mal are longer than others. EuTc-iCit, EuTc-Fum and EuTc-Oxa have a lifetimes longer than that of EuTc, while EuTc-Suc and EuTc-KG are almost same as EuTc. As KG and succinate cannot effectively form complexes with Eu^{3+}, no significant fluorescent intensity and lifetime enhancement are expected and indeed observed. Decay times of different components for EuTc-L are important in the time-resolved and RLD imaging. Furthermore, by choosing different lag times for "gated" detections, different intermediates can be determined in different time windows.

5.2.2. Imaging for the Krebs Cycle

Imaging [34-36] as a potential "mapping" technique has been used to show the Krebs cycle as in Fig. 5.3. From Fig. 5.3(a), the different Krebs cycle intermediates in steady-state imaging have been observed at time window from 0 – 50 μs according to their fluorescence intensity. The fluorescence of EuTc-Cit is significantly higher than others, while those of succinate and KG are almost the same as the background. The order of the rest is oxaloacetate > malate > isocitrate.

RLD imaging, which has been discussed in section 4.2.4.4, was also employed to depict the Krebs cycle. Two windows from 100 to 150 μs and from 160 to 210 μs were imaged in Fig. 5.3(b), the dramatic fluorescence changes of EuTc-L complexes were observed. Due to different decay times of EuTc-L in Table 5.1, the relative ratios (R_{RLD}) of the integrations between two windows for EuTc-L are also different. The relative ratios of L-malate and fumarate in EuTc obviously increase, however, that of oxaloacetate is significantly decreasing to a level almost as KG. RLD imaging can further explain the possibility of distinguishing intermediates by the lifetime-based fluorescence.

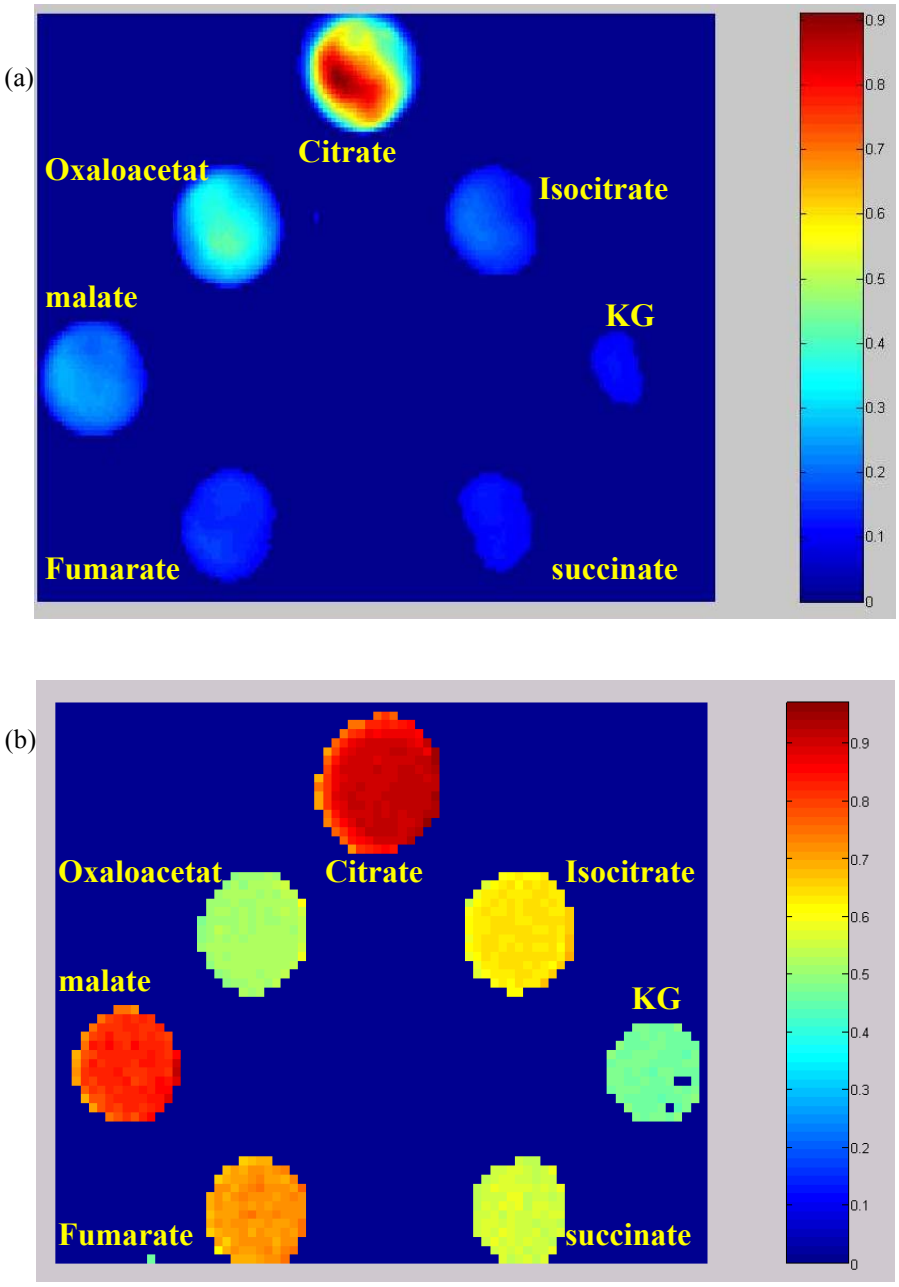

Figure 5.3. Fluorescence imaging of main intermediates in the Krebs cycle. (a) steady-state imaging, one window form 0-50 µs; (b) rapid lifetime determination (RLD) imaging, two time windows from 100-150 µs and from 160-210 µs. Intermediates (150 µM) were added in EuTc (50 µM)

5.2.3. Conversions Between Intermediates in the Krebs Cycle

5.2.3.1. Stepwise visualization of decomposition of citrate

The characteristics of the EuTc complexes with main intermediates of the Krebs cycle have made it possible for the stepwise visualization of decomposition of citrate. Oxaloacetate, L-malate and fumarate can be produced according to the following enzymatic reactions (Eq. 5-1, 5-2, 5-3),

$$\text{citrate} \xrightarrow{CL} \text{oxaloacetate} + \text{acetate} \qquad \text{(Equation 5-1)}$$

$$\text{oxaloacetate} + \text{NADH} + \text{H}^+ \underset{}{\overset{MDH}{\rightleftharpoons}} \text{L-malate} + \text{NAD}^+ \qquad \text{(Equation 5-2)}$$

$$\text{L-malate} \xrightarrow{FM} \text{fumarate} + \text{H}_2\text{O} \qquad \text{(Equation 5-3)}$$

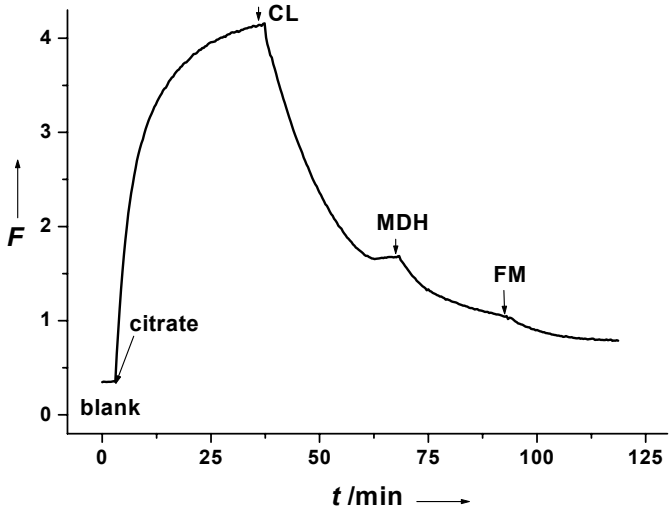

Figure 5.4. Kinetic curve of the formation and stepwise decomposition of EuTc-Cit complex. Blank solution including 200 μL of 0.5 mM EuTc and 60 μL of 4.8 mM of NADH in 1.70 mL of HEPES buffer, then 40 μL of 2 mM citrate, 70 μL of 3.4 U/mL citrate lyase (CL), 50 μL of 1588 U/mL malic dehydrogenase (MDH) and 80 μL of 618 U/mL fumarase (FM) were added, respectively.

Citrate lyase (CL), malic dehydrogenase (MDH) and fumarase (FM), respectively, were employed to catalyze these reactions. Fig. 5.4 indicates the stepwise processes via fluorescence: the fluorescence of a blank solution, composed of EuTc and NADH only, is stable over time. (In this experiment, NADH does not interfere the fluorescence of EuTc and EuTc-Cit because they have different emissions and excitations.) While adding citrate, the fluorescence increases due to the formation of the EuTc-Cit complex. After fluorescence of EuTc-Cit reached a plateau, CL, MDH and FM were added, respectively. Fluorescence decreases step by step (in three stages), thereby indicating the complete consumption of citrate and formation of EuTc-oxaloacetate, EuTc-malate and EuTc-fumarate, respectively. This experiment manifests that (a) EuTc-L acts as a reversible fluorescent probe, and the change of concentrations of the main intermediates of the Krebs cycle can be directly monitored via fluorescence, (b) Despite the fact that the reaction of Eq 5-2 can also be determined by the NADH, the dual simultaneously fluorescent measurements by EuTc-oxaloacetate and NADH have indicated the former is much more sensitive (see section 5.2.4.2). (c) The stepwise decompositions of citrate, oxaloacetate, and L-malate can be clearly visualized through their complexes with EuTc. NADH can only indicate one of the decomposition steps or the overall changes without the capability of stepwise indication of the reactions.

5.2.3.2. Formation of citrate in the Krebs cycle

The application and specificity of EuTc-L system for the Krebs cycle is further explored by the kinetic change in the intermediate steps in Eq.5-4 and Eq.5-5, which are usually considered as the last step and the first step in the Krebs cycle.

$$\text{L-malate} + NAD^+ \overset{MDH}{\rightleftharpoons} \text{oxaloacetate} + NADH + H^+ \qquad \text{(equation 5-4)}$$

$$\Delta G^{\circ\prime} = +29.7 \text{ kJ mol}^{-1}$$

$$\text{Acetyl CoA} + \text{oxaloacetate} + H_2O \xrightarrow{CS} \text{citrate} + CoA + H^+ \qquad \text{(equation 5-5)}$$

$$\Delta G^{\circ\prime} = -31.4 \text{ kJ mol}^{-1}$$

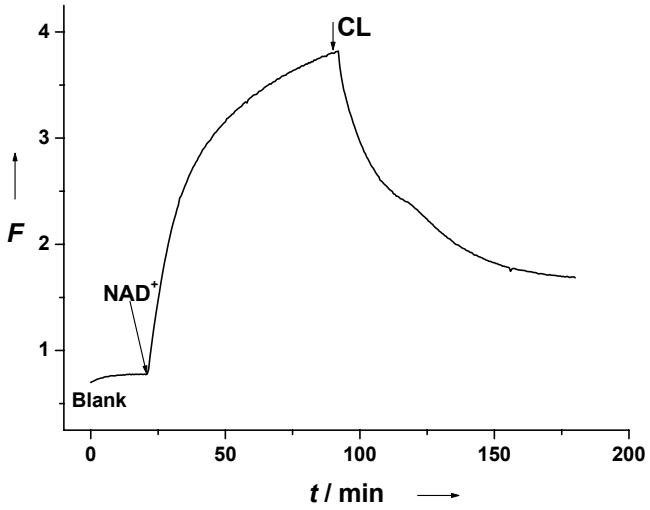

Figure 5.5. Kinetic curve of the formation and decomposition of citrate. Blank including 0.2 mL of 0.5 mM EuTc, 0.4 mL of 0.5 mM L-malate, 0.16 mL of 9.9 U/mL MDH, 0.16 mL of 1 U/mL CS, 0.16mL of 0.23 mM acetyl CoA and 0.8mL of 10 mM HEPES buffer at 8.0 pH in cuvette , plus 54 μL of 14 mM NAD^+, then add 55 μL of 4.3 U/mL CL when the maximum fluorescence was reached.

Unlike the other steps in the Krebs cycle, the standard free energy of Eq. 5-4 is significantly positive, the formation of citrate from malate is possible when coupled with Eq. 5-5, driven by the utilization of the products oxaloacetate by citrate synthase (CS) and NADH by the electron-transport chain. As shown in Fig. 5.5, the fluorescence signal of blank with L-malate, MDH, acetyl CoA, CS and EuTc is stable and low (although a litter bit higher than EuTc) over time, no reaction happened. The products in Eq. 5-4, and 5-5, NADH and CoA do

not introduce the fluorescence change. After the addition of NAD^+, the whole reaction from Eq.5-4 to Eq. 5-5 is initiated and resulted in the production of citrate, consequently the increase of the fluorescence due to the formation of the EuTc-Cit system. To further indicate the specificity of the EuTc-L system, CL is used to testify the existence of citrate in Eq. 5-6.

$$\text{citrate} \xrightarrow{CL} \text{oxaloacetate} + \text{acetate} \qquad \text{(equation 5-6)}$$

The addition of CL causes the decrease of citrate and a drop of the fluorescence. This experiment has realized (a) citrate was product by the pathway in the Krebs cycle, this process can be kinetically monitored via fluorescence. (b) Dual fluorescence determinations for EuTc-Cit and NADH can also be simultaneously monitored, they depict the reaction processes of Eq. 5-4 and Eq. 5-5, respectively.

5.2.4. Fluorescence Detection of Main Intermediates in the Krebs Cycle

5.2.4.1. Time-resolved fluorescence assays

As the different decay times of EuTc-L, the discrimination of intermediates can be performed in different time windows. In steady-state fluorescence measurement (with 0 μs lag time in Fig. 5.6), the order of the normalized intensity [defined as $(F - F_0) / F_0$] is EuTc-Cit > EuTc- Oxa > EuTc-Ma > EuTc-iCit > EuTc-Fum > EuTc-Suc ≈ EuTc-KG ≈ EuTc. Gating obviously can be used to fine tune between selectivity and sensitivity. On increasing the lag time from 0 to 100 μs, the normalized intensity of all species is increased (Fig. 5.6.) except for KG. On increasing the lag time to 250 μs, oxaloacetate is widely suppressed and citrate is reduced by 40 %, while isocitrate, fumarate and malate, remain much less affected. Obviously, L-malate and oxaloacetate can be nicely discerned. By comparing citrate with

isocitrate, it is noted that decay times of the main components of EuTc-Cit (95 μs) and EuTc-iCit (16 μs) are quite different (Table 5.1).

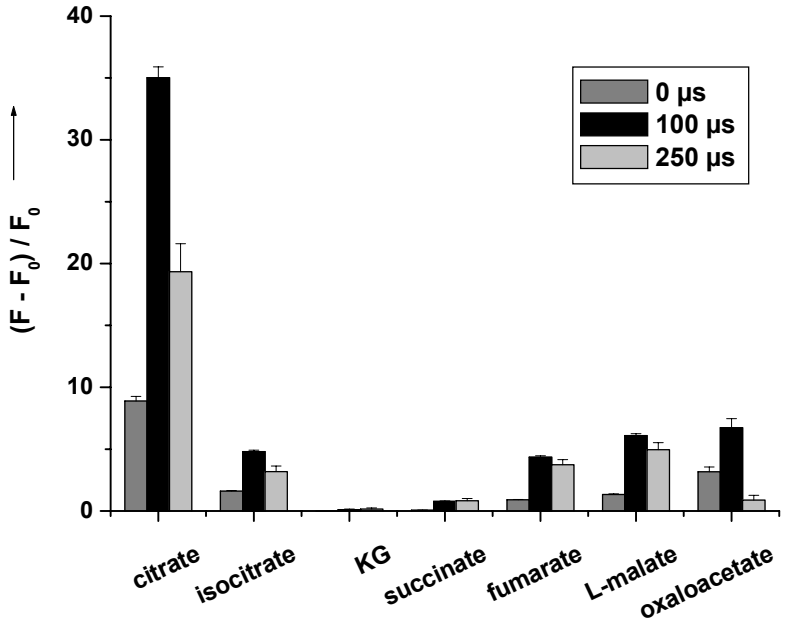

Figure 5.6. The relative fluorescence intensities of EuTc-L complexes at different lag times. Concentration of EuTc is 50 μM, L: citrate, isocitrate, ketoglutarate, succinate, fumarate, L-malate and oxaloacetate is 150 μM. F_0 and F are fluorescence intensities of EuTc and EuTc-L complex.

It should be emphasized that the main intermediates can be sensed and imaged directly through their complexes with EuTc, and that no enzymes or multi-enzyme systems are needed. However, assays for other intermediates have to exclude any interference by citrate.

5.2.4.2. Dual fluorescence detection the decomposition process of oxaloacetate

Dual fluorescence measurement here refers to detection of two fluorophores which have different excitation wavelengths and emissions. This method not only offers multi-parameters for analytes, but also benefits for monitor of the kinetic processes of reaction. In the decomposition of oxaloacetate (Eq. 5-2), the fluorescence intensities of EuTc-Oxa and NADH were detected, the excitation and emission of EuTc-Oxa are at 405 and 620 nm, the respective

data for NADH are at 355 and 460 nm. The fluorescence kinetic changes of EuTc-Oxa and NADH express the oxaloacetate consumed by MHD catalytically. The time trace of EuTc-Oxa is Y = 7.73 + 0.38 X (R = 0.97), that of NADH is Y = 162 + 0.14 X (R = 0.96), Y and X denote corrected fluorescence intensity and time. But the former method is more sensitive because of steeper slope.

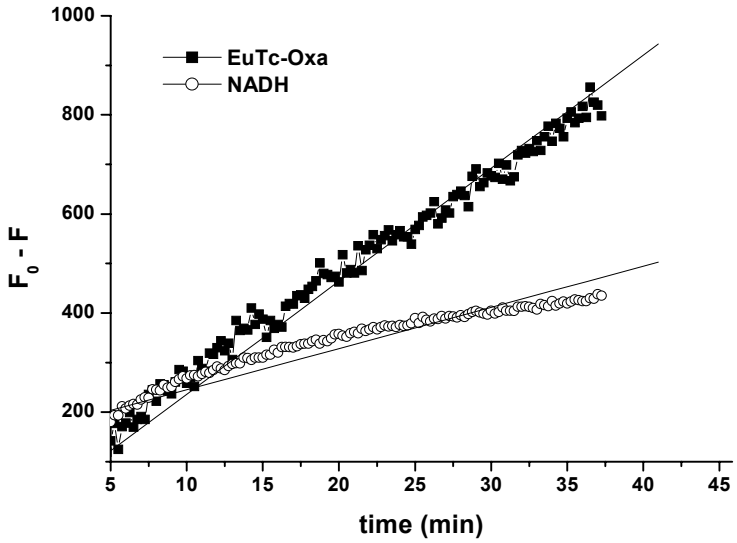

Figure 5.7. Dual fluorescence determination of the decomposition of oxaloacetate via the fluorescence changes of EuTc-Oxa (exc: 400 nm, em: 620 nm) and NADH (exc: 355 nm, em: 460 nm). Concentration of EuTc, oxaloacetate and NADH are 48, 96 and 185 μM, respectively. The activity of MDH is 7 U/mL. F and F_0 are the fluorescence intensity of EuTc-Oxa and NADH at t and 0 min

5.3. Conclusion

The time-resolved fluorescence detection and imaging of main intermediates of the Krebs cycle has been made possible for the first time. Some lifetime and imaging techniques are utilized in this system as the discrimination of their characteristics of fluorescence. The process of the stepwise decompositions of intermediates, such as citrate, isocitrate, oxaloacetate and L-malate can be also directly visualized. This probe will be widely used in other bioassays.

5.4. Experimental Section

5.4.1. Reagents

Citrate lyase (EC: 4.1.3.6, from *Enterobacter aerogenes*), citrate synthase (EC: 4.1.3.7, from porcine heart), mitochondrial malic dehydrogenase (EC: 1.1.1.37, from porcine heart), and fumarase (EC: 4.2.1.2 from porcine heart) were from Sigma and used without further purification.

Tri-sodium citrate dihydrate, α-ketoglutaric acid (α-oxoglutaric acid), fumaric acid, *di*-sodium succinate and other inorganic salts were obtained in analytical purity from Merck unless otherwise stated. Ds-isocitric acid, oxaloactic acid, L-sodium malate were in analytical purity from Sigma-Aldrich. All solutions were prepared in 10 mM 4-(2-hydroxyethyl) piperazine-1-ethanesulfonic acid (HEPES) buffer of pH 8.0 unless otherwise specified. Europium(III) trichloride hexahydrate was from Alfa Products, and tetracycline hydrochloride from Sigma.

The EuTc standard solution was obtained by dissolving Eu^{3+} chloride and tetracycline (each in 0.5 mM concentration) in 10 mM HEPES buffer of pH 8.0. This reagent is stable for at least 2 months if stored at 4 °C in the dark.

5.4.2. Apparatus

Absorption spectra were acquired on a Cary WinUV photometer. Fluorescence studies of the effect of intermediates (L) in the Krebs cycle on the EuTc spectra were performed on an SLM AB2 luminescence spectrometer. Fluorescence intensity (steady-state and time-gated) were acquired on a Tecan GENios+ micro plate reader. The excitation/emission filters were set to 405/612 nm respectively. The 96-well black, transparence, flat bottom microtiter plates

for imaging were obtained from Greiner Bio-One GmbH. The decay times of EuTc-L were detected with a pulsed 392-nm laser and an H5783-P04 PMT detector with multiphoton-counting board in a multipass cuvette. Data were processed with the FluoFit. Dual fluorescence detection, EuTc-Oxa (excitation is at 405 nm, emission is at 620 nm) and NADH (excitation is at 355 nm, emission is at 460 nm) were simultaneously were performed in FLUOstar OPTIMA (BMG LABTECH, Offenburg, Germany, www.bmglabtech.com). Imaging data were evaluated by a self-developed program based on Matlab (6.1, Mathwork, Natick, MA, USA)

5.5. References

[1] Krebs, H. A. **The citric acid cycle.** Biochemical Journal, London, 1940, 34: 460-463.

[2] Berg, J. M. J.; Tymoczko, L.; Stryer, L. **Biochemistry**, 5th ed, Chapter 17 "The Citric Acid Cycle" W. H. Freeman and Company, 2001, p 465-487.

[3] Xie, L.; Wang, D. I. C. **Energy metabolism and ATP balance in animal cell cultivation using a stoichiometrically based reaction network**. Biotechnology and Bioengineering 1996, 52(5), 591-601.

[4] Gottlieb, D. **Carbohydrate catabolism by fungi.** Pure and Applied Chemistry 1963, 7(4), 603-9.

[5] Peng, L.; Hertz, L.; Huang, R.; Sonnewald, U.; Petersen, S. B.; Westergaard, N.; Larsson, O.; Schousboe, A. **Utilization of glutamine and of TCA cycle constituents as precursors for transmitter glutamate and GABA**. Developmental Neuroscience 1993, 15(3-5), 367-77.

[6] Attwood, P. V. **The structure and the mechanism of action of pyruvate carboxylase**. International Journal of Biochemistry and Cell Biology 1995, 27(3), 231-49.

[7] Miller, A. L. **The tricarboxylic acid cycle [in the developing brain].** Developmental Neuroscience. 1985, 127-59.

[8] Rennie, M. J.; Bowtell, J. L.; Bruce, M.; Khogali, S. E. O. **Interaction between glutamine availability and metabolism of glycogen, tricarboxylic acid cycle intermediates and glutathione**. Journal of Nutrition 2001, 131(9S), 2488S-2490S.

[9] Lane, M. D.; Mooney, R. A. **Tricarboxylic acid cycle intermediates and the control of fatty acid synthesis and ketogenesis.** Current Topics in Cellular Regulation 1981, 18 221-42.

[10] Biasioli, S.; Feriani, M.; Bigi, L.; Dell'Aquila, R.; Bragantini, L.; Chiaramonte, S.; Fabris, A.; Brendolan, A.; Ronco, C.; Pradella, M. **Tricarboxylic acid cycle intermediates in chronic renal failure**. Nephrology, Dialysis, Transplantation 1987, 2(5), 313-5.

[11] Comte, B.; Vincent, G.; Bouchard, B.; Des Rosiers, C. **Probing the origin of acetyl-CoA and oxaloacetate entering the citric acid cycle from the 13C labeling of citrate released by perfused rat hearts.** Journal of Biological Chemistry 1997, 272(42), 26117-26124.

[12] Vogt, J. A.; Yarmush, D. M.; Yu, Y.; Zupke, C.; Fischman, A. J.; Tompkins, R. G.; Burke, J. F. **TCA cycle flux estimates from NMR- and GC-MS-determined [13C]glutamate isotopomers in liver.** American Journal of Physiology 1997, 272, C2049-C2062.

[13] Chatham, J. C.; Bouchard, B.; Des Rosiers, C. **A comparison between NMR and GCMS 13C-isotopomer analysis in cardiac metabolism.** Molecular and Cellular Biochemistry 2003, 249(1&2), 105-112.

[14] Lu, S.; Sun, X.; Shi, C.; Zhang, Y. **Determination of tricarboxylic acid cycle acids and other related substances in cultured mammalian cells by gradient ion-exchange chromatography with suppressed conductivity detection.** Journal of Chromatography, A 2003, 1012(2), 161-168.

[15] Krivankova, L.; Pantuckova, P.; Gebauer, P.; Bocek, P.; Caslavska, J.; Thormann, W. **Chloride present in biological samples as a tool for enhancement of sensitivity in capillary zone electrophoretic analysis of anionic trace analytes.** Electrophoresis 2003, 24(3), 505-517.

[16] Fu, X.; Kimura, M.; Iga, M.; Yamaguchi, S. **Gas chromatographic-mass spectrometric screening for organic acidemias using dried urine filter paper: determination of α-ketoacids**. Journal of Chromatography, B: Biomedical Sciences and Applications 2001, 758(1), 87-94.

[17] Markuszewski, M. J.; Otsuka, K.; Terabe, S.; Matsuda, K.; Nishioka, T. **Analysis of carboxylic acid metabolites from the tricarboxylic acid cycle in Bacillus subtilis cell extract by capillary electrophoresis using an indirect photometric detection method**. Journal of Chromatography, A 2003, 1010(1), 113-121.

[18] Rosello, S.; Galiana-Balaguer, L.; Herrero-Martinez, J. M.; Maquieira, A.; Nuez, F. **Simultaneous quantification of the main organic acids and carbohydrates involved in tomato flavour using capillary zone electrophoresis**. Journal of the Science of Food and Agriculture 2002, 82(10), 1101-1106.

[19] Fujima, J. M.; Danielson, N. D. **Enzymatic amplification by substrate recycling for α-ketoglutarate in conjunction with capillary electrophoresis.** Journal of Capillary Electrophoresis and Microchip Technology 2002, 7(1 & 2), 19-22.

[20] Moellering, H.; Gruber, W. **Determination of citrate with citrate lyase.** Analytical Biochemistry 1966, 17(3), 369-76.

[21] UV-method for the determination of citric acid in foodstuffs, Boehringer Mannheim, Cat.no. 139076, 1998.

[22] Planta, M.; Lazaro, F.; Puchades, R.; Maquieira, A. **Determination of citric acid and oxalacetic acid in foods by enzymic flow injection.** Analyst 1993, 118(9), 1193-7.

[23] Matsumoto, K. Tsukatani, T. **Simultaneous quantitation of citrate and isocitrate in citrus juice by a flow-injection method based on the use of enzyme reactors**, Anal. Chim. Acta 1996, 321, 157-164

[24] Ince, C.; Coremans, J. M. C. C.; Bruining, H. A**. In vivo NADH fluorescence**. Advances in Experimental Medicine and Biology 1992, 317 277-96.

[25] Luong, J. H. T.; Mulchandani, A. **Applications of NADH-dependent fluorescence sensors for monitoring and controlling bioprocesses**. Bioprocess Technology (1990), 6, 75-94.

[26] Atlante, A.; Gagliardi, S.; Marra, E.; Calissano, P.; Passarella, S. **Glutamate neurotoxicity in rat cerebellar granule cells involves cytochrome c release from mitochondria and mitochondrial shuttle impairment.** Journal of Neurochemistry 1999, 73(1), 237-246.

[27] Hirschy, L. M.; Van Geel, T. F.; Winefordner, J. D.; Kelly, R. N.; Schulman, S. G. **Characteristics of the binding of europium(III) to tetracycline.** Analytical Chimical Acta 1984, 166 207-19.

[28] Rakicioglu, Y.; Perrin, J. H.; Schulman, S. G. **Increased luminescence of the tetracycline-europium(III) system following oxidation by hydrogen peroxide.** Journal of Pharmaceutical and Biomedical Analysis 1999, 20(1-2), 397-399.

[29] Wolfbeis, O. S.; Duerkop, A.; Wu, M.; Lin, Z. **A Europium-ion-based luminescent sensing probe for hydrogen peroxide.** Angewandte Chemie, International Edition 2002, 41(23), 4495-4498.

[30] Bruce, J. I.; Dickins, R. S.; Govenlock, L. J.; Gunnlaugsson, T.; Lopinski, S.; Lowe, M. P.; Parker, D.; Peacock, R. D.; Perry, J. J. B.; Aime, S.; Botta, M. **The Selectivity of Reversible Oxy-Anion Binding in Aqueous Solution at a Chiral Europium and Terbium Center: Signaling of Carbonate Chelation by Changes in the Form and Circular Polarization of Luminescence Emission.** Journal of the American Chemical Society 2000, 122(40), 9674-9684.

[31] Dickins, R. S.; Aime, S.; Batsanov, A. S.; Beeby, A.; Botta, M.; Bruce, J. I.; Howard, J. A. K.; Love, C. S.; Parker, D.; Peacock, R. D.; Puschmann, H. **Structural, Luminescence, and NMR Studies of the Reversible Binding of Acetate, Lactate, Citrate, and Selected Amino Acids to Chiral Diaqua Ytterbium, Gadolinium, and Europium Complexes.** Journal of the American Chemical Society 2002, 124(43), 12697-12705.

[32] Parker, D.; Dickins, R. S.; Puschmann, H.; Crossland, C.; Howard, J. A. K. **Being Excited by Lanthanide Coordination Complexes: Aqua Species, Chirality, Excited-State Chemistry, and Exchange Dynamics.** Chemical Reviews 2002, 102(6), 1977-2010.

[33] Van Houten, J.; Watts, R. J. **Effect of ligand and solvent deuteration on the excited state properties of the tris(2,2'-bipyridyl)ruthenium(II) ion in aqueous solution. Evidence for electron transfer to solvent.** Journal of the American Chemical Society 1975, 97(13), 3843-4.

[34] Woods, R. J.; Scypinski, S.; Love, L. J.; Ashworth, H. A. **Transient digitizer for the determination of microsecond luminescence lifetimes.** Analytical Chemistry 1984, 56(8), 1395-400.

[35] Liebsch, G.; Klimant, I.; Frank, B.; Holst, G.; Wolfbeis, O. S. **Luminescence lifetime imaging of oxygen, pH, and carbon dioxide distribution using optical sensors.** Applied Spectroscopy 2000, 54(4), 548-559.

[36] Schaeferling, M.; Wu, M.; Enderlein, J.; Bauer, H.; Wolfbeis, O. S. **Time–resolved luminescence imaging of hydrogen peroxide using sensor membranes in a microwell format** Applied Spectroscopy 2003, 57(11), 1386-1392.

Chapter 6. Chiral Fluorescence Discrimination of L-/D-Malate

6.1. Introduction

Chiral discrimination is of central importance in the field of molecular chirality. It is a key technology in the molecular elucidation of the processes of chemical biology [1], in the characterization and optimization of new therapeutic drugs [2, 3], as well as in the development of sensory agents for chiral biological molecules.

Fluorescence for chiral recognition [4-8] is known for over 20 years, especially as an interesting topic in supramolecular chemistry. However, most of them so far has been confined to synthetic receptors in organic solvents or water-organic solvent mixtures. Lanthanide complexes [9, 10] have been widely utilized in chiral discrimination based on chiroptical scheme (such as circular dichroism [11-13] and circular polarized luminescence [14-16]), nuclear magnetic resonance [17-19] and in mass spectroscopy [20-22]. But none research based on lanthanide fluorescence intensity and lifetime is reported now.

Malates are optically active α–hydroxy acids that exist abundantly in nature [23] and serve as convenient starting materials for the synthesis of homochiral compounds [24]. Chiral

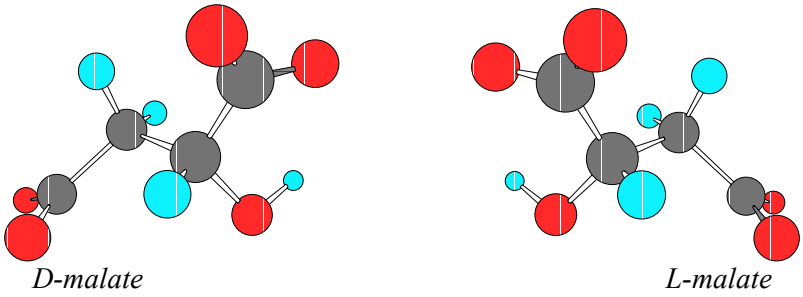

Figure 6.1. Sterochemistry of L-/ D-malate. H atom (cyan), carbon atom (grey), and oxygen atom (red). The specific optical rotation of malate : $[\alpha]_D$ *-2.3°*

discrimination and resolution of malates and other hydroxy acids are mostly achieved through HPLC [25-28] or electrophoresis [29-31]. Only a few fluorescent methods have been reported based on the use of synthetic receptors in organic solvents, such as the bisbinaphthyls for differentiating enantiomeric mandelic acids [32].

Here a novel fluorescent molecular chirality sensor based on the finding that both the fluorescence intensity and the fluorescence decay time are quite different for ternary complexes formed between the europium-tetracycline complex (EuTc) [33-35] and the enantiomeric malates in aqueous solution at neutral pH. As a result, one can discriminate chiral malates by either intensity-based or decay-based fluorescence.

6.2. Results and Discussion

6.2.1. Fluorescent Spectra of Enantiomeric Malate in EuTc

The different spectral characteristics of EuTc complexes with enantiomeric malates are shown in Fig. 6.2. The absorbances of the ternary EuTc-L-malate and EuTc-D-malate complexes peak both at 381 nm, with shoulders at around 405 nm. The maximal emissions of EuTc-L-malate and EuTc-D-malate are also similar at 619 nm and at 618 nm as the europium emission. Side bands are formed at 580, 591, 651, and 697 nm. The different mainband splittings of the two complexes result from different effects of the enantiomers on the crystal field [36]. The maximal capability of discrimination $[(F_L-F_0)/(F_D-F_0)]$ for chiral malates is found to be 5.9 at 619 nm, where F_0, F_L, and F_D denote the fluorescence intensities of EuTc, EuTc-L-malate and EuTc-D-malate, respectively. The quantum yields (QY) [37] of energy transfer from Tc to Eu^{3+} increase from 0.4% in case of EuTc to 1.7 % of EuTc-L-malate and 0.7 % EuTc-D-malate.

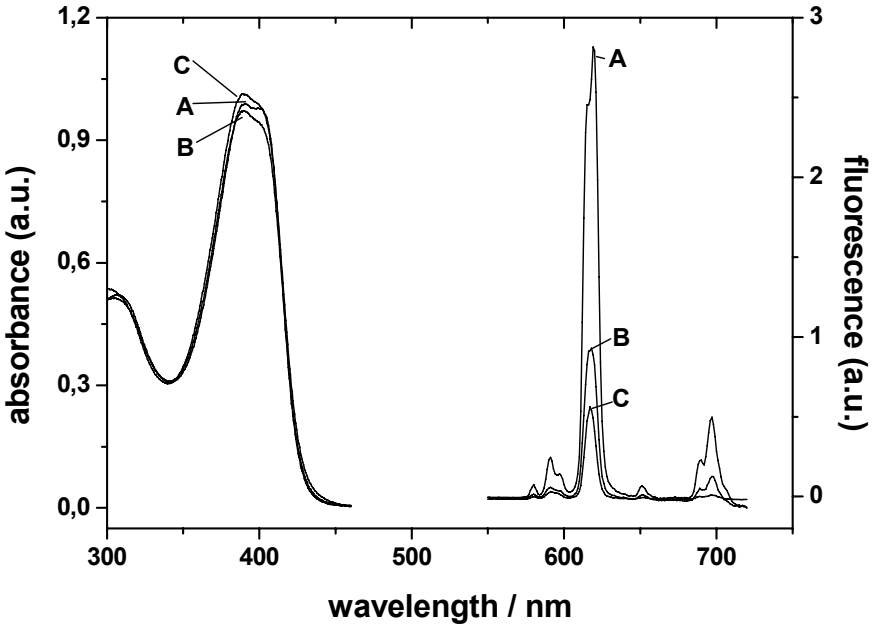

Figure 6.2. Absorption and emission spectra of the europium-tetracycline complex (50 μM) in HEPES buffer of pH 8.0 (C) in the presence of 2 mM of L- malate (A) or D-malate (B).

6.2.2. Optimal Experimental Conditions

The fluorescence of the EuTc-malate system is stable between pH 7.7 and 8.7 for EuTc-L-malate and from 7.2 to 8.7 for EuTc-D-malate in Fig. 6.3. The acid dissociation constants [38] of malic acid are $pKa_1 = 3.4$ and $pKa_2 = 5.1$. In above-mentioned pH range, both protons of malic acid are dissociated, and malate dianion can readily chelate with Eu^{3+}. On the other hand, tetracycline [39] (section 4.2.2) may also lose two protons in this case. A 10 mM HEPES buffer solution at 8.0 pH was used throughout this work. It is important to note that phosphate buffer may not be used since phosphate forms a complex with EuTc.

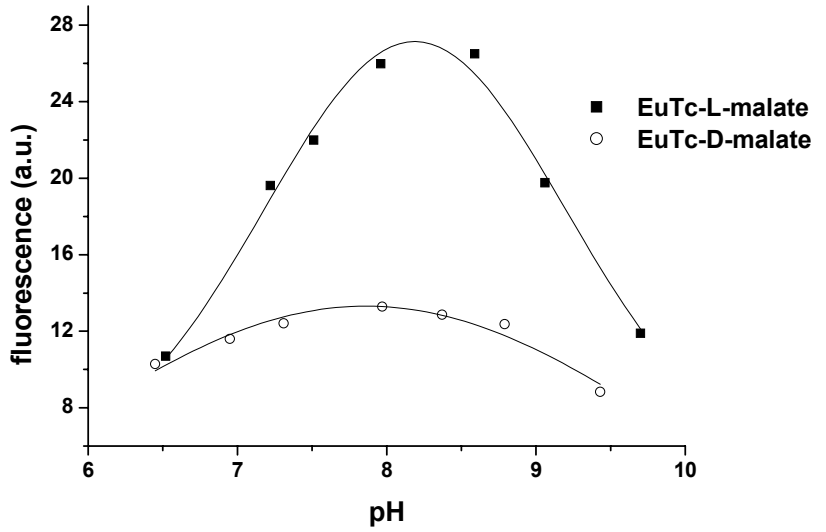

Figure 6.3. The effect of pH on fluorescence intensities of EuTc (50 μM) in D-malate (160 μM) or L-Malate (160 μM).

The time traces of chelation of enantiomeric malates with EuTc are shown in Fig. 6.4. Their fluorescent intensities reach a plateau, usually forming the stable fluorescence in 10 min when malate (either L-malate or D-malate).

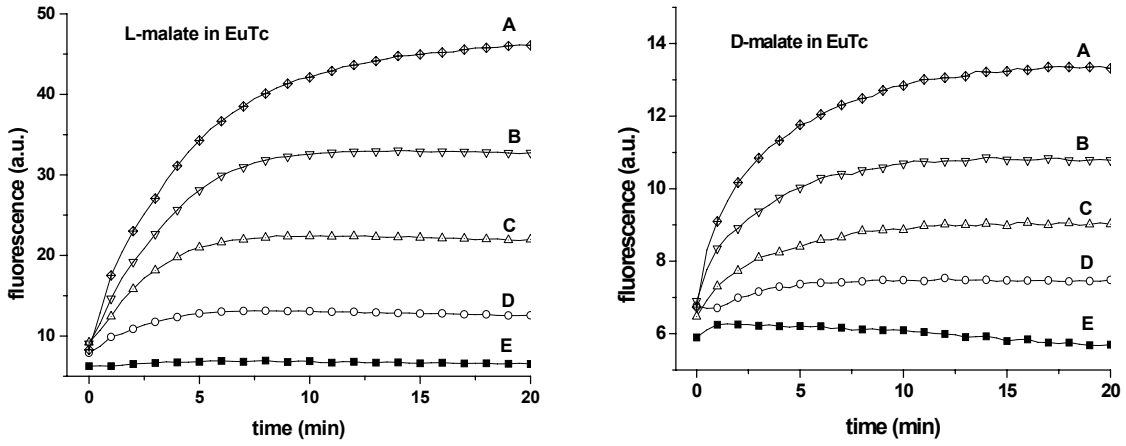

Figure 6.4. Time trace of the chelation of enantiomeric malate in EuTc (50 μm).
E: Blank, EuTc, A, B, C, and D with malate are 1.6, 0.4, 0.16 and 0.04 mM, respectively.

6.2.3. Fluorescence Decay Times of EuTc-L-malate and EuTc-D-malate

The decay profiles of the emissions of EuTc-L-malate and EuTc-D-malate are also different as detected by TCSPC (Fig. 6.5 a). It reveals a complex decay pattern from which three components can be extracted for either complex. EuTc-L-malate has components of 16 μs (with a relative amplitude of 28 %), 78 μs (48 %) and 104 μs (24 %). The respective data for EuTc-D-malate are 16 μs (62%), 49 μs (35 %) and 123 μs (3 %). Obviously, the average lifetimes of EuTc-L-malate and EuTc-D-malate are largely different (84 and 48 μs, respectively). The distributions of their decay times (Fig. 6.5b) are the basis for their

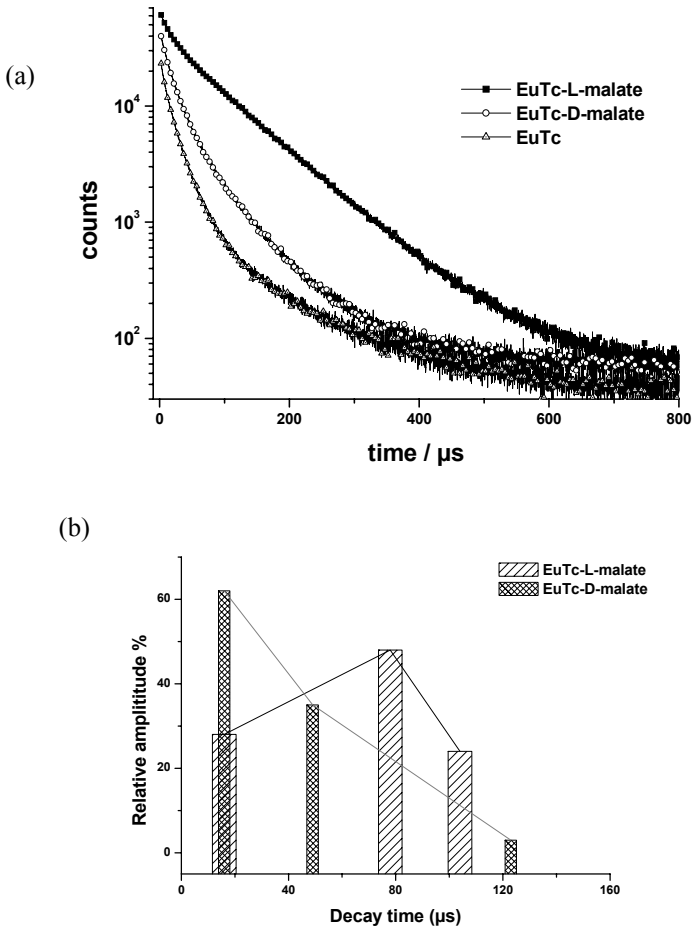

Figure 6.5. The decay profiles of EuTc-L-malate and EuTc-D-malate (a) decay time; (b) distribution of decay time. Eu^{3+}: 50 μM; Tc: 50 μM; L-malate: 2 mM; D-malate: 2 mM

discrimination by time-resolved fluorescence. Consequently, chiral discrimination may also be achieved by TCSPC, despite the presentation of six decay times in a mixed solution and the complication of instrumentation.

6.2.4. Optimal Lag Time for Discrimination of Chiral Malates

As TCSPC is complex, alternatively, time-resolved ("gated") fluorescence, which is experimentally easier, can be applied to chiral differentiation by measuring fluorescence intensity after a certain delay time, since the effect is much more pronounced for the longer decaying EuTc-L-malate. It is based on the selection of time-delay (lag time) before detection of the selected window (gate) after excitation. The difference of lifetimes of EuTc-L-malate and Eu-Tc-D-malate result in the different intensities in the detection windows. The effect of different lag times on F / F_0 of the EuTc with enantiomeric malates are displayed in Fig. 6.6. For L-malate, the value of F/F_0 increases on going from 0 μs to a 100 μs lag time with a 80 μs integration time, and decreases after 150 μs; for D-malate, the value of F / F_0 has only a minimal increase up to 300 μs lag time. The changes of fluorescence intensity in different lag

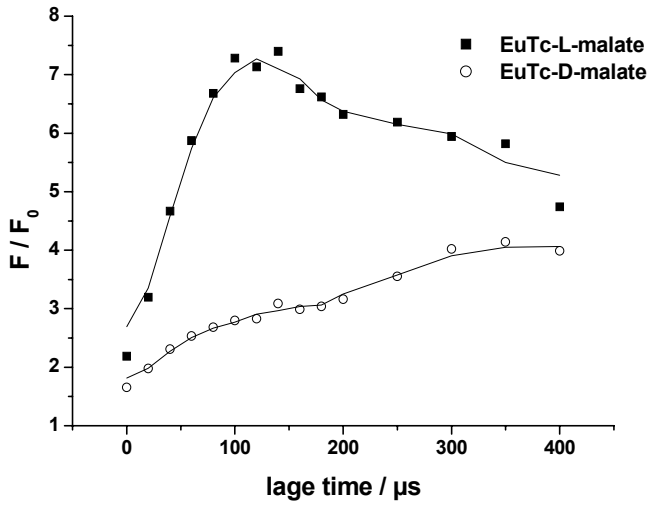

Figure 6.6. The change of F / F_0 versus lag time. F_0 is the fluorescence of EuTc. F is the fluorescence of enantiomer malate (150 μM)in EuTc (50 μM)

time can be explained by the distribution of decay time in Fig. 6.5 b. The most efficient fluorescent discrimination of enantiomeric malates is at 120 μs decay time.

6.2.5. Fluorometric Determination of Enantiomeric Excess of Chiral Malate

The applicability of EuTc as a fluorescent probe for chiral discrimination of malate is best presented in the quantitative determination of their optical purity. Steady-state fluorescence can be used to determine the enantiomeric excess (*ee*, defined as in Eq. 6-1) of a system in Fig. 6.7. The *ee* of malates is indicated by normalized fluorescence intensity according to $(F–F_0)/F_0$ when EuTc was added to a solution of a mixture of L- and D-malate. A linear relationship exists between normalized fluorescence intensity and *ee*.

$$ee\% = \left[\frac{\left(mole\ of\ one\ enantiomer - mole\ of\ other\ enantiomer \right)}{total\ moles\ of\ both\ enantiomers} \right] \times 100\% \quad \text{(equation 6-1)}$$

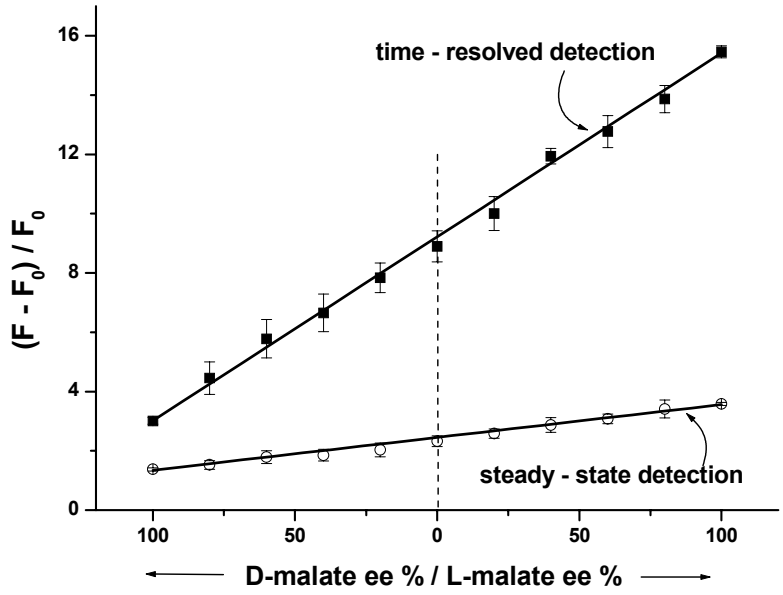

Figure 6.7. Relationships between ee % of malate and fluorescence. F and F_0 are the fluorescence intensities of EuTc (50 μM)in presence and absence of a mixture of ([L-malate]+[D-malate]=500 μM) .

The time-resolved fluorescence is also applied to chiral differentiation. Therefore, a 120 μs delay time and a 80 μs integration time were chosen in order to suppress the contribution of D-malate to a substantial extent. Fig. 6.7 shows the resulting plot of gated fluorescence intensity versus *ee*. It is obvious that gated discrimination is more sensitive than the steady-state fluorescence determination for *ee*. The linear correlation coefficients are 0.99 for both graphs when the total concentration is kept constant. Thus, this relationship can be employed and detect the optical purity of malate.

6.2.6. Fluorescence Imaging of Enantiomeric Malates

Fluorescent imaging is a viable tool for two-dimensional presentation ("mapping") of analytes [40-43]. Here for the first time, chiral discrimination can also be accomplished through time-resolved fluorescence imaging. As shown in Fig. 6.8, both the steady-state and the time-resolved fluorescence imaging can be utilized to visualize the ee of malates. Fig. 6.8

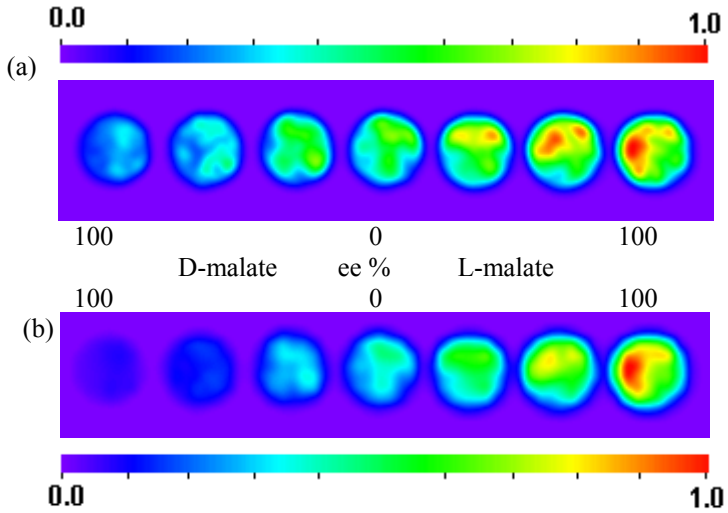

Figure 6.8. Imaging (2D) of enantiomer malates([L-malate]+[D-malate] = 500 μM) in EuTc (50 μM). (a) steady-state fluorescence imaging, window from 0-50 μs; (b) time-gated fluorescence imaging, window from 140-220 μs.

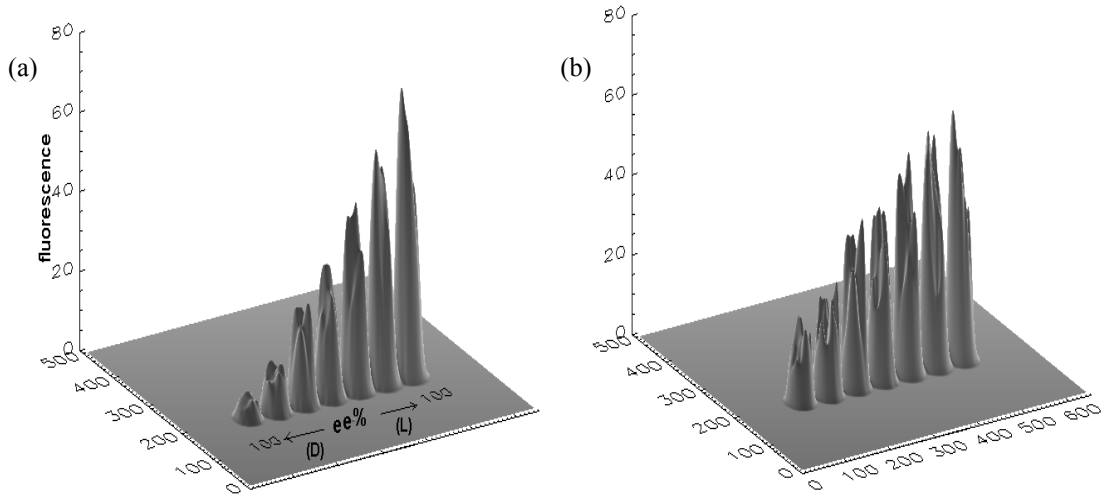

Figure 6.9. Imaging (3D) of enantiomer malates([L-malate]+[D-malate] = 500 μM) in EuTc (50 μM). (a) time-resolved imaging, one time window from 160-240 μs; (b) steady-state imaging, one time window from 0-50 μs; Composition of ee (%), in (b) is the same as in (a).

(top) gives the data as a conventional fluorescence two - dimensional graph (false color), and Fig. 6.8 (bottom) as a time-resolved (gated) fluorescence imaging. The latter has large discrimination capability for enantiomeric malates. These data can also be shown as three-dimensional graphs as in Fig. 6.9. Contrast to Fig. 6.8, the conventional and time-gated fluorescence imaging in Fig. 6.9 have more direct and clear expression of the relationship of ee % and imaging.

This probe shows the potential to map the chiral-specific spatial arrangement of ligands on the surface. In addition to, the several promising features of the time-resolved fluorescence imaging of chiral lanthanide complex have been expressed, such as large chiral selectivity (which facilitates quantitative analysis) and the capability of chiral recognition independent of the relative concentrations of analytes and the chirality probe.

6.2.7. Calibration Curves for L-/D-malates

Both steady-state (Fig. 6.10 a) and time-resolved (Fig. 6.10 b) fluorometries were used in the determination of L-/D-malate. In the steady-state method, linear ranges of L-malate and

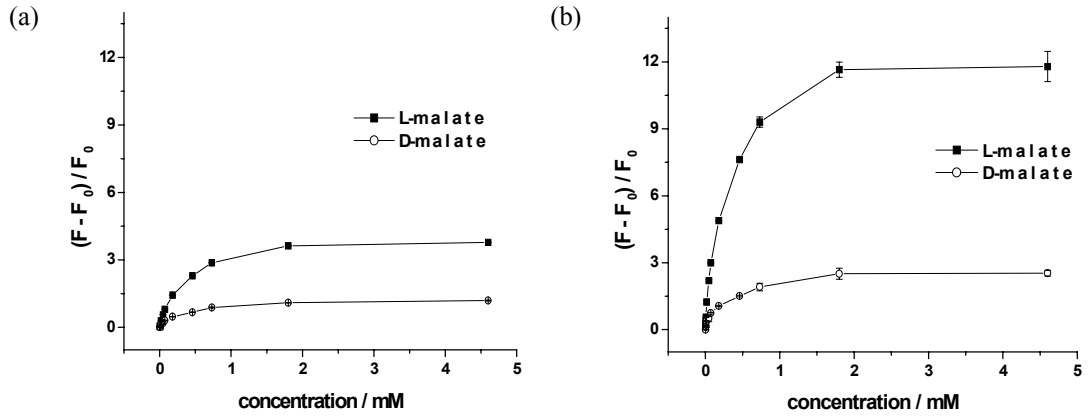

Figure 6.10. Calibration curve of L-/D-malate .
(a) steady-state fluorescence detection, (b) time-laged fluorescence detection at 120 μs. Different concentration of enantiomer malates in EuTc (50 μM) probe-

D-malate are $4.6x10^{-6}$ - $1.8x10^{-4}$ M and $4.6x10^{-6}$ – $7.3x10^{-5}$ M, with the limits of detection (S/N = 3) of $1.8x10^{-6}$ M and $4.6x10^{-6}$ M, respectively. In the time-gated mode, linear ranges are from 7.3 x 10^{-7} to 7.3 x 10^{-5} M and from 4.6 x 10^{-6} to 7.2 x10^{-5} M, with the limits of detection of 4.4 x 10^{-7} M and 4.6 x 10^{-6} M for L-malate and D-malate, respectively. Obviously, measurement of L-malate with EuTc probe by time-resolved fluorescence, contrast to steady-state fluorescence, can improve sensitivity and limit of detection.

6.2.8. Origin of the Enantioselectivity

6.2.8.1. Characteristics of chirality of EuTc-L-malate and EuTc-D-malate

Unlike some coordinatively saturated binary europium complex [44-45], such as that of cryptands, calixarene ligands, EuTc itself is not coordinatively saturated and therefore is prone to form fairly stable ternary complexes to replace the water molecules in the inner coordination field, which is a quencher of the lanthanide fluorescence. As in the case of EuTc-malates, the chirality of EuTc creates a chiral environment for the binding of enantiomeric malates, which would result in different fluorescence. For the characterization of the

asymmetric coordination, the circular dichroism can offer more information about ligands or the relationship between lanthanide and ligands.

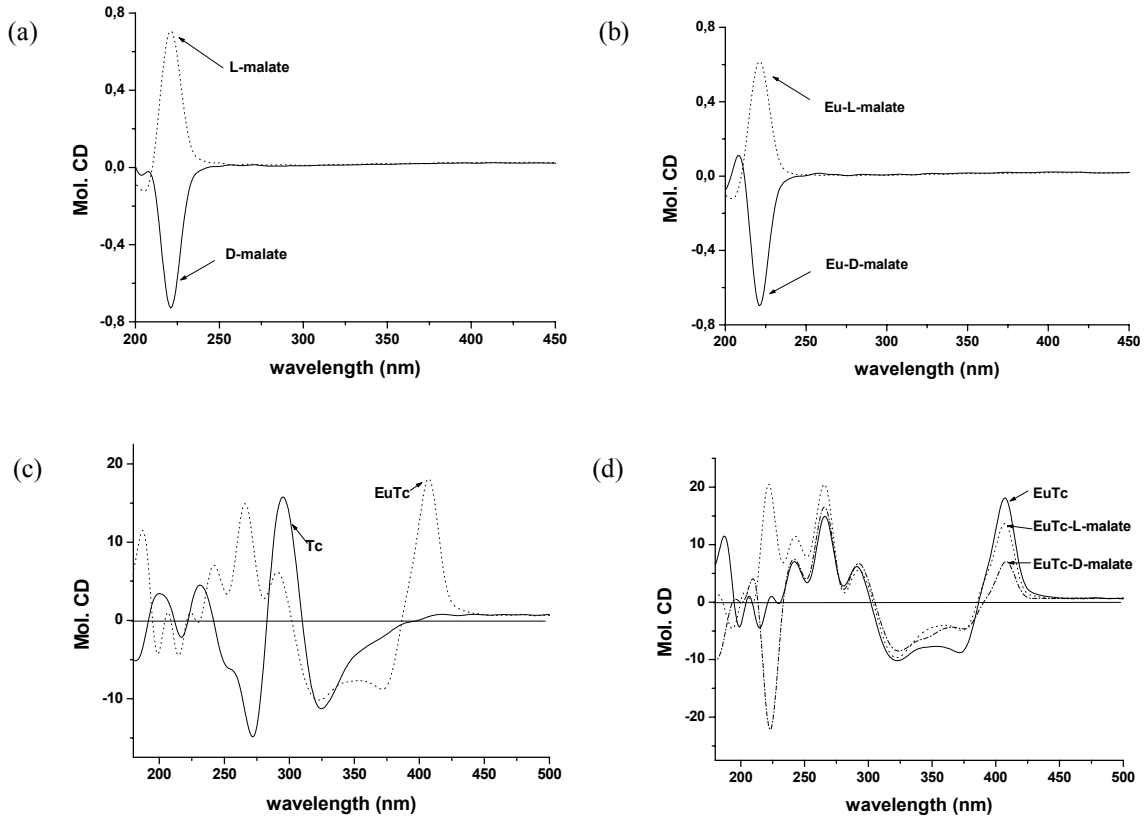

Figure 6.11. CD spectra. (a) L-malate and D-malate; (b) Eu-L-malate and Eu-D-malate; (c)Tc and EuTc; (d) EuTc, EuTc-L-malate and EuTc-D-malate. Concentrations of Eu^{3+}, Tc, L-malate and D-malate are 50 μM, 50 μM, 2 mM and 2 mM, respectively. In (a) and (b), concentration of malate was used to calculate the value of Mol. CD; in (c) and (d), concentration of Tc was used to caluculate the value of Mol. CD.

In Fig. 6.11 a, each enantiomeric malate has a corresponding CD peak which have opposite signs. Enantiomeric malates binding Eu^{3+} still keep the character of chiral in Fig.6.11b. As the chirality of Tc, this leads to the asymmetric EuTc in Fig. 6.11 c (see Section 4.2.1.4). In Fig. 6.11 d, the values of molar CD in the positive Cotton effects of EuTc, EuTc-L-malate and EuTc-D-malate at 242, 266 and 408 nm have a little different, other Cotton effects (positive and negative) are almost same except that at 222 nm, which is the opposite signals of CD peak from enantiomeric malates (compare with Fig. 6.11b). They can be

discriminated if the value of molar CD is calculated by the concentration of Tc. Nevertheless, if calculated by the concentration of malate, the CD spectra of enantiomeric malates will be not quite different since that can be overshadowed by the strong spectra of EuTc or Tc. It means that the CD spectra of EuTc or Tc can overlap that of enantiomeric malate and make them difficult to distinguish between L-malate and D-malate. On the other hand, it shows that the influences of L-/D-malate in EuTc in the ground state (S_1) are not significant, the different fluorescence intensity may be due to their excited state, because they coordinate differently and the spatial orientation with the tetracycline ligand is different.

6.2.8.2. Composition of EuTc-malate

Job´s method has been employed for determination of the molar ratio of Eu^{3+}:Tc :malate. In Fig. 6. 12 a, the maximum fluorescence intensity is reached at 1:1 molar ratio of Eu^{3+}: Tc in excess malate, regardless of L-malate or D-malate. In Fig. 6. 12b, the concentration of Eu^{3+} is excess, the molar ratio of Tc:malate is approximately at 1:2. In combination of Fig. 12 a and b, the molar ratio of Eu:Tc:malate is 1:1:2, or (EuTc):Tc is 1:2.

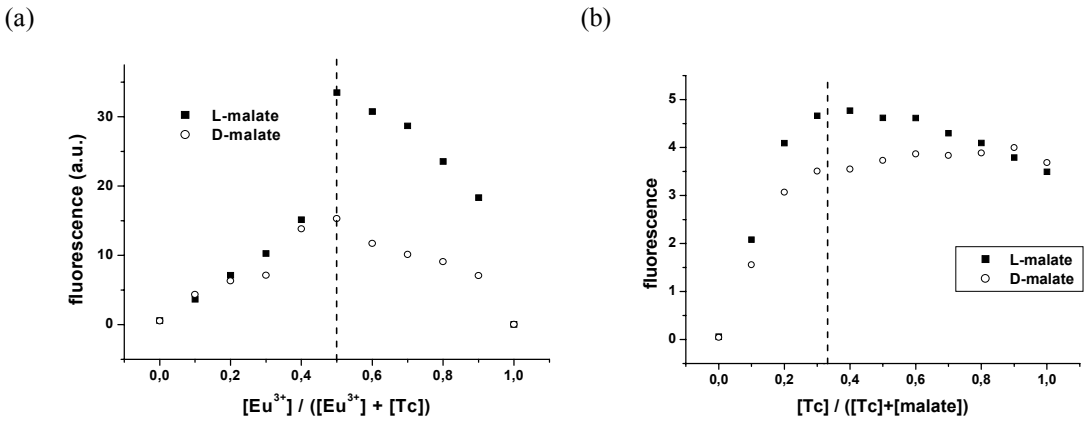

Figure 6.12. Job´s plot for molar rationof EuTc-malate.
(a) ratio of Eu^{3+} to Tc, concentrations of malate and($[Eu^{3+}]$+[Tc]) are 333 and 83 µM; (b) ratio of Tc to malate, concentrations of Eu^{3+} and ([Tc])+[malate] are 130 and 50 µM

Rough estimations of the disassociation constants of EuTc-malates (EuTc:malate = 1:2) are calculated by the following Benesi-Hidebrand type equation [32, 46, 47] for a two binding site saturation.

$$\frac{F - F_0}{F} = \frac{B_{\max}[M]}{K_{d1} + [M]} + \frac{B_{\max 2}[M]}{K_{d2} + [M]} \qquad \text{(equation 6-2)}$$

where F_0 and F are the fluorescence intensities of EuTc in the absence and present of malate, [M] is the concentration of malate, B_{max1} and B_{max2} are constants. the dissociation constants are K_{d1} of 4 x 10^{-4} M, K_{d2} of 3 x 10^{-5} M for EuTc-L-malate and K_{d1} of 6 x 10^{-4} M, K_{d2} of 7x 10^{-5} M for EuTc-D-malate.

6.2.9. Other α–Hydroxy Acids and Amino Acids

The α-hydroxy acids lactate and tartrate were also studied. Lactate does not undergo significant changes in fluorescence on addition of EuTc. The enantiomeric tartrates, in contrast, cause an increase in fluorescence intensity of EuTc. The fluorescence intensities of the EuTc complex with enantiomeric tartrates at different lag time are shown in Fig. 6.13a, EuTc-R-tartrate and EuTc-S-tartrate have a maximum discrimination at 60 μs lag time.

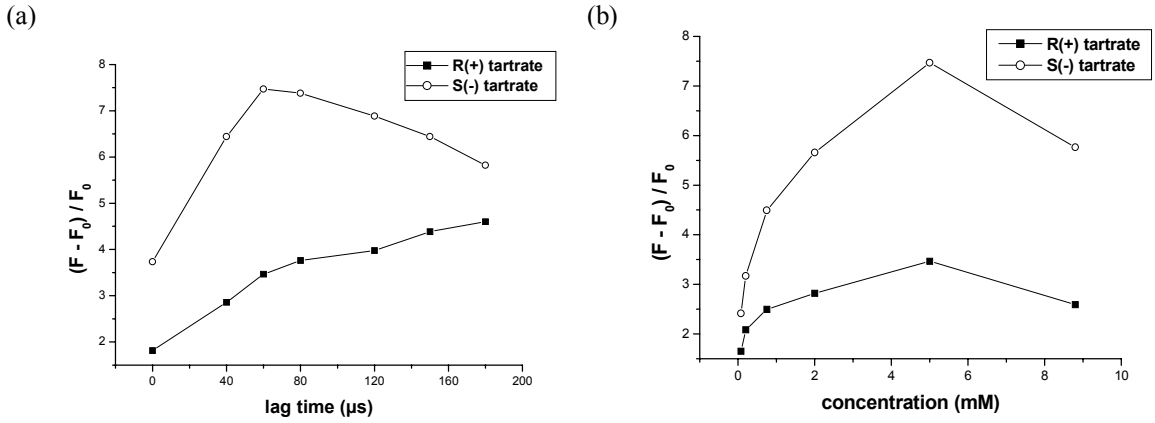

Figure 6.13. (a) The fluorescence intensities at different lag time for enantiomeric tartrates(5mM) in EuTc; (b) the calibration curves for enantiomeric tartrates in EuTc, with 60 μs lag time. Concentration of Eu^{3+} and Tc are 50 and 50 μM.

The calibration curves by time-resolved fluorescence determination are depicted in Fig. 6.14b, but their discriminative ability [$(F_R–F_0)/(Fs–F_0)$] is only 30 % of that of enantiomeric malate in EuTc.

Amino acids, such as L-histidine, phenylalanine, arginine, lysine, glutamine, cysteine, asparagine, aspartic acid, threonine, proline, isoleucine, glutamine acid, tryptophan, serine, methionine, valine, leucine and tyrosine, were investigated in EuTc, but no (or only insignificant) fluorescence enhancements were observed.

6.3. Conclusion

The probe EuTc represents a novel lanthanide-based sensing probe for chiral discrimination using time-resolved fluorescence, and for direct imaging of enantiomeric hydroxy acids in aqueous solution of near-neutral pH. Chiroselective imaging is of great potential with respect to mapping the spatial arrangement of (chiral) ligands on solid surfaces, i.e. in biosensor arrays and in high-throughput screening.

6.4. Experimental Section

6.4.1. Reagents

L-sodium malate, D-malic acid were obtained in analytical purity from Sigma-Aldrich. (2R, 3R)-(+) tartaric acid, (2S, 3S)-(-) tartaric acid, and other inorganic salts were obtained in analytical purity from Merck unless otherwise stated. All solutions were prepared in 10 mM 4-(2-hydroxyethyl) piperazine-1-ethanesulfonic acid (HEPES) buffer of pH 8.0 unless otherwise specified. Europium(III) trichloride hexahydrate was from Alfa Products, and tetracycline hydrochloride from Sigma.

The EuTc standard solution was obtained by dissolving Eu^{3+} chloride and tetracycline (each in 0.5 mM concentration) in 10 mM HEPES buffer of pH 8.0. This reagent is stable for at least 2 month if stored at 4 °C in the dark.

6.4.2. Apparatus

Absorption spectra were acquired on a Cary WinUV photometer. Fluorescence studies were performed on an SLM AB2 luminescence spectrometer. Fluorescence intensity (steady-state and time-resolved) were acquired on a Tecan GENios+ micro plate reader. The excitation/emission filters were set to 405/612 nm respectively. The decay times of EuTc-malate were detected with a pulsed 392-nm laser and an H5783-P04 PMT detector with multiphoton-counting board in a multipass cuvette. Data were processed wither by FluoFit (PicoQuant). Circular dichroism (CD) spectra were acquired on JASCO model J – 710 spectropolarimeter (www.jasco.de). The 96-well black, transparence, flat bottom microtiter plates for imaging were obtained from Greiner Bio-One GmbH. Imaging data were evaluated by the IDL software module.

6.5. References

[1] MacDermott, A. J. **The origin of biomolecular chirality.** Chirality in Natural and Applied Science 2002, 23-52.

[2] Challener, C. A. **Chiral drugs** 2001

[3] Testa, B.; Mayer, J. M. **Chiral recognition in biochemical pharmacology: an overview.** Handbook of Experimental Pharmacology 2003, 153(Stereochemical Aspects of Drug Action and Disposition), 143-159.

[4] James, T. D.; Sandanayake, K. R. A. Samankumara; Shinkai, S. **Chiral discrimination of monosaccharides using a fluorescent molecular sensor.** Nature 1995, 374(6520), 345-7.

[5] Pu, Lin. **Synthesis and study of binaphthyl-based chiral dendrimers**. Journal of Photochemistry and Photobiology, A: Chemistry 2003, 155(1-3), 47-55.

[6] Prasanna de Silva, A. **Bright spies for chiral molecules**. Nature 1995, 374(6520), 310-11.

[7] Beer, G.; Rurack, K.; Daub, J. **Chiral discrimination with a fluorescent boron-dipyrromethene dye**. Chemical Communications 2001, (12), 1138-1139.

[8] Yan, Y.; Myrick, M. L. **Simultaneous Enantiomeric Determination of Dansyl-D,L-Phenylalanine by Fluorescence Spectroscopy in the Presence of a-Acid Glycoprotein**. Analytical Chemistry 1999, 71(10), 1958-1962.

[9] Aspinall, H. C. **Chiral Lanthanide Complexes: Coordination Chemistry and Applications**. Chemical Reviews 2002, 102(6), 1807-1850.

[10] Tsukube, Hi.; Shinoda, S. **Lanthanide Complexes in Molecular Recognition and Chirality Sensing of Biological Substrates.** Chemical Reviews 2002, 102(6), 2389-2403.

[11] Tsukube, H.; Hosokubo, M.; Wada, M.; Shinoda, S.; Tamiaki, H. **Specific Recognition of Chiral Amino Alcohols via Lanthanide Coordination Chemistry: Structural Optimization of Lanthanide Tris(b-diketonates) toward Effective Circular Dichroism/Fluorescence Probing**. Inorganic Chemistry 2001, 40(4), 740-745.

[12] Parac-Vogt, T. N.; Binnemans, K.; Gorller-Walrand, C. **Absolute configuration assignment of D3-symmetric lanthanide complexes based on circular dichroism induced by interaction with a chiral probe.** ChemPhysChem 2001, 2(12), 767-769.

[13] Parker, D.; Dickins, R. S.; Puschmann, H.; Crossland, C.; Howard, J. A. K. **Being Excited by Lanthanide Coordination Complexes: Aqua Species, Chirality, Excited-State Chemistry, and Exchange Dynamics.** Chemical Reviews 2002, 102(6), 1977-2010.

[14] Metcalf, D. H.; Snyder, S. W.; Wu, S.; Hilmes, G. L.; Riehl, J. P.; D., J. N.; Richardson, F. S. **Excited-state chiral discrimination observed by time-resolved circularly polarized luminescence measurements**. Journal of the American Chemical Society 1989, 111(8), 3082-3.

[15] Carter, R. C.; Miller, C. E.; Palmer, R. A.; May, P. S.; Metcalf, D. H.; Richardson, F. S. **Circularly polarized luminescence (CPL) spectra of samarium(III) in trigonal trisodium [tris(oxydiacetato) samarate] bis(sodium perchlorate) hexahydrate (Na3[Sm(oxydiacetate)3]. 2NaClO46H2O).** Chemical Physics Letters 1986, 131(1-2), 37-43.

[16] Meskers, S. C. J.; Dekkers, H. P. J. M. **Enantioselective quenching of luminescence: Molecular recognition of chiral lanthanide complexes by biomolecules in solution**. Journal of Physical Chemistry A 2001, 105(19), 4589-4599.

[17] Rothchild, R. **NMR methods for determination of enantiomeric excess**. Enantiomer 2000, 5(5), 457-471.

[18] Parker, D. **NMR determination of enantiomeric purity**. Chemical Reviews 1991, 91(7), 1441-57.

[19] Wenzel, T. J. **Lanthanide-chiral solvating agent couples as chiral NMR shift reagents**. Trends in Organic Chemistry 2000, 8 51-64.

[20] Tao, W. A.; Wu, L.; Cooks, R. G. **Rapid enantiomeric determination of a-hydroxy acids by electrospray ionization tandem mass spectrometry.** Chemical Communications 2000, (20), 2023-2024.

[21] Filippi, A.; Giardini, A.; Piccirillo, S.; Speranza, M. **Gas-phase enantioselectivity**. International Journal of Mass Spectrometry 2000, 198(3), 137-163.

[22] Mazurek, J.; Lisowski, J. **Chiral macrocyclic lanthanide complexes derived from (1R,2R)-1,2-diphenylethylenediamine and 2,6-diformylpyridine**. Polyhedron 2003, 22(21), 2877-2883.

[23] Berg, J. M.; Tymoczko, J. L.; Stryer, L. **Biochemistry**, 5th ed, Chapter 17 "The Citric Acid Cycle" W.H.Freeman and Company, 2001, p 465-487

[24] Cppola, G. M.; Schuster, H. F. **α-hydroxy Acids in Enantioselective Synthesis**, Wiley-VCH, Weinheim, 1997.

[25] Doner, L. W.; Cavender, P. J. **Chiral liquid chromatography for resolving malic acid enantiomers in adulterated apple juice.** Journal of Food Science 1988, 53(6), 1898-9.

[26] Oi, N.; Kitahara, H.; Kira, R. **Direct separation of enantiomers by high-performance liquid chromatography on a new chiral ligand-exchange phase**. Journal of Chromatography 1992, 592(1-2), 291-6.

[27] Fransson, B.; Ragnarsson, U. **Separation of enantiomers of α-hydroxy acids by reversed-phase liquid chromatography after derivatization with 1-(9-fluorenyl)ethyl chloroformate**. Journal of Chromatography, A 1998, 827(1), 31-36 .

[28] Brightwell, M.; Pawlowska, M.; Zukowski, J. **HPLC resolution of hydroxy carboxylic acid enantiomers using 2-quinoxaloyl chloride as a new precolumn derivatizing agent**. Journal of Liquid Chromatography 1995, 18(14), 2765-81.

[29] Schmid, M. G.; Grobuschek, N.; Lecnik, O.; Gubitz, G.; Vegvari, A.; Hjerten, S. **Enantioseparation of hydroxy acids on easy-to-prepare continuous beds for capillary electrochromatography.** Electrophoresis 2001, 22(12), 2616-2619.

[30] Kodama, S.; Yamamoto, A.; Matsunaga, A.; Soga, T.; Hayakawa, K. **Direct chiral resolution of malic acid in apple juice by ligand-exchange capillary electrophoresis using copper(II)-L-tartaric acid as a chiral selector.** Electrophoresis 2001, 22(15), 3286-3290.

[31] Belder, D.; Deege, A.; Maass, M.; Ludwig, M. **Design and performance of a microchip electrophoresis instrument with sensitive variable-wavelength fluorescence detection**. Electrophoresis 2002, 23(14), 2355-2361.

[32] Xu, M.; Lin, J.; Hu, Q.; Pu, L. **Fluorescent sensors for the enantioselective recognition of mandelic acid: Signal amplification by dendritic branching.** Journal of the American Chemical Society 2002, 124(47), 14239-14246

[33] Hirschy, L. M.; Van Geel, T. F.; Winefordner, J. D.; Kelly, R. N.; Schulman, S. G. **Characteristics of the binding of europium(III) to tetracycline**. Analytica Chimica Acta 1984, 166, 207-19.

[34] Rakicioglu, Y.; Perrin, J. H.; Schulman, S. G. **Increased luminescence of the tetracycline-europium(III) system following oxidation by hydrogen peroxide.** Journal of Pharmaceutical and Biomedical Analysis 1999, 20(1-2), 397-399.

[35] Wolfbeis, O. S.; Duerkop, A.; Wu, M.; Lin, Z. **A Europium-ion-based luminescent sensing probe for hydrogen peroxide.** Angewandte Chemie, International Edition 2002, 41(23), 4495-4498.

[36] Richardson, F. S. **Terbium(III) and europium(III) ions as luminescent probes and stains for biomolecular systems,** Chemistry Review 1982, 82, 541-552.

[37] Van Houten, J.; Watts, R. J. **Effect of ligand and solvent deuteration on the excited state properties of the tris(2,2'-bipyridyl)ruthenium(II) ion in aqueous solution. Evidence for electron transfer to solvent.** Journal of the American Chemical Society 1975, 97(13), 3843-4.

[38] Hargis, L. G. **Analytical Chemistry: Principles and Techniques**, Prentice-Hall, Inc. 1988

[39] Duarte, H. A.; Carvalho, S.; Paniago, E. B.; Simas, A. M. **Importance of Tautomers in the Chemical Behavior of Tetracyclines.** Journal of Pharmaceutical Sciences 1999, 88(1), 111-120.

[40] Cubeddu, R.; Comelli, D.; D'Andrea, C.; Taroni, P.; Valentini, G. **Time-resolved fluorescence imaging in biology and medicine.** Journal of Physics D: Applied Physics 2002, 35(9), R61-R76.

[41] Sharman, K. K.; Periasamy, A.; Ashworth, H.; Demas, J. N.; Snow, N. H. **Error Analysis of the Rapid Lifetime Determination Method for Double-Exponential Decays and New Windowing Schemes.** Analytical Chemistry 1999, 71(5), 947-952.

[42] Schneider, P. C.; Clegg, R. M. **Rapid acquisition, analysis, and display of fluorescence lifetime-resolved images for real-time applications**. Review of Scientific Instruments 1997, 68(11), 4107-4119.

[43] Herman, P.; Lin, H.; Lakowicz, J. R. **Lifetime-based imaging**. Tuan Vo-Dinh (Editor-in-chief) Biomedical Photonics Handbook , CRC Press, 2003, 9/1-9/30

[44] Arnaud-Neu, F. **Solution chemistry of lanthanide macrocyclic complexes.** Chemical Society Reviews 1994, 23(4), 235-41.

[45] Atwood, J. L.; Barbour, L. J.; Hardie, M. J.; Raston, C. L. **Metal sulfonatocalix[4,5]arene complexes: bi-layers, capsules, spheres, tubular arrays and beyond.** Coordination Chemistry Reviews 2001, 222 3-32.

[46] Benesi, H. A.; Hildebrand, J. H. **A spectrophotometric investigation of the interaction of iodine with aromatic hydrocarbons.** Journal of the American Chemical Society 1949^^^^^^^^^^, 71 2703-7.

[47] Silber, H. B.; Maraschin, V.; Sibley, S.; Richter, C.; Arif, N.; Contreras, L.; Djurovich, P.; Ratansiripong, T.; Stoddard, J. **Spectrophotometric investigations of the complexation between Ni(II) and thiocyanate in aqueous methanol.** Polyhedron (2003), 22(27), 3439-3444.

7. Summary

The dissertation describes the development of europium-derived fluorescence probes for biological substances in aqueous solution. A scheme is shown in Fig. 7.1. Europium-tetracycline-hydrogen peroxide and europium-tetracycline-hydroxy acid probes have the merits of large Stokes´ shift, line-like emission and long lifetime.

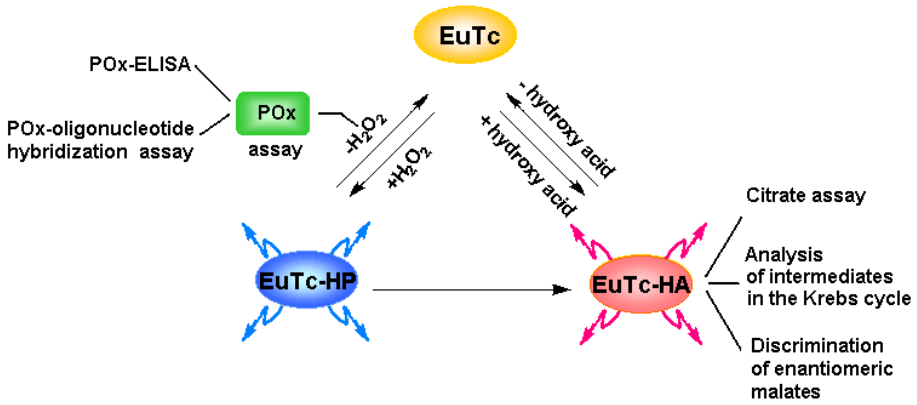

Figure 7.1. Scheme of research.
HP: hydrogen peroxide; EuTc: europium-tetracycline complex; HA: hydroxy acid.

In chapter 1 the mechanism of lanthanide complex luminescence is introduced. The three main approaches for time-resolved fluorescence in heterogeneous phase, namely direct lanthanide chelate label-based luminescence assay (DLCLLA), dissociation enhanced lanthanide fluoroimmunoassay (DELFIA) and enzyme-amplified lanthanide luminescence (EALL) are reviewed.

The time-resolved assay of the activity of peroxidase (POx) by the fluorescent probe europium-tetracycline-hydrogen peroxide (EuTc-HP) is presented in chapter 2. At first, the catalytic mechanism of POx, as a widely studied enzyme across a range of scientific disciplines, is discussed. Quantification is based on the finding that the strongly fluorescent complex EuTc-HP (which is in equilibrium with unbound H_2O_2) is indirectly decomposed by

POx to give the weakly fluorescent EuTc following the consumption of H_2O_2 in MOPS buffer at neutral pH. The rate of consumption of the EuTc-HP as monitored via the decrease in fluorescence intensity (or change in decay time) is a direct parameter for the activity of the POx. The time-resolved assay can detect as little as 1.0×10^{-5} Units/ mL of POx, with a dynamic range from 4.0×10^{-5} to 5.9×10^{-3} Units/mL. The effects of cyanide, hydroxylamine, and azide (all known to inhibit POx) are also studied.

When POx is exploited as a label and EuTc-HP as a probe, ELISA and oligonucleotide hybridization assays can be developed as shown in chapter 3. The time-resolved fluorescent assays for biological specimens have advantages over the conventional steady-state assays. Two schemes for POx-ELISA, sandwich and direct, have been investigated. The linear range is from 0.1 to 8.0 ng/ml for IgG in POx-sandwich ELISA, with 0.1 ng/ml of the limit of detection in time-gated method. EuTc-HP also can be used as a reversible molecular sensor for the imaging of POx-ELISA. The competitive oligonucleotide hybridization assay by the POx label is discussed as well.

The direct fluorescence detection and imaging of citrate are demonstrated in chapter 4. The method is based on the fact that the weakly fluorescent europium-tetracycline (EuTc) complex reversibly associates with citrate to form the strongly fluorescent europium-tetracycline-citrate (EuTc-Cit) complex in HEPES buffer at pH 8.0. Average fluorescence lifetime is also increased from 44 μs (for EuTc) to 88 μs (for EuTc-Cit). Steady-state fluorometry, TCSPC, time-resolved fluorometry and RLD imaging have been used in citrate determination. The time-resolved assay has a dynamic response between 1.6×10^{-7} and 5.6×10^{-5} M, with a detection limit of 6.0×10^{-8} M for citrate. Compared with other main analytical methods for citrate, it is the most sensitive and simplest scheme available up to now. Different

tetracycline derivatives are also studied. In addition, this probe is simple to prepare, stable both in solution and in solid , and compatible with the blue laser diodes.

The Krebs cycle, a key series of metabolic reactions in aerobic cellular respiration, is occurring in the mitochondria of animals and plants. Fluorescence imaging of main intermediates in the Krebs cycle and the some bioprocesses of the intermediates are depicted for the first time in chapter 5. Intermediates, i.e. oxaloacetate, citrate, isocitrate, α-ketoglutarate (KG), succinate, fumarate and L-malate, can reversibly associate with EuTc to form EuTc-L complexes having different fluorescent intensities and lifetimes in neutral pH. The steady-state fluorescence intensity and rapid lifetime determination imaging have been employed in the visualization of the Krebs cycle. The stepwise detection of the formation and decomposition of intermediates can be performed via kinetic fluorescence changes. In addition, dual fluorescence method, monitoring both NADH and EuTc-L, is exploited.

Fluorescence chirality sensing is presented in chapter 6. EuTc as a lanthanide chelate is employed for the fluorescence discrimination of enantiomeric malates in aqueous solution. The fluorescence discriminating ability $(F_L - F_0) / (F_D - F_0)$ is 5.9 at 619 nm, which is more sensitive than any other chiral fluorometry for α-hydroxy acids reported so far. The average lifetimes and quantum yields of EuTc-L-malate and EuTc-D-malate are 84 and 48 μs, 1.7 % and 0.7 %, respectively. It is important that this probe can be also applied for the time-resolved fluorescent determination of the optical purity (ee %) of malate with 120 μs lag time. Chiral malates can also be achieved by time-resolved imaging. Other chiral α-hydroxy acids, lactate and tartrate are also discussed. It is the first report on using lanthanide ternary complexes as a “turn-on” fluorescence chiral molecular sensor.

8. Zusammenfassung

Die vorliegende Dissertation zeigt die Entwicklung und praktische Erprobung von Europium-Komplexen als Fluoreszenzsonden für biologisch aktive Substanzen in wässriger Lösung. Abbildung 7.1 fasst die resultierenden Anwendungsmöglichkeiten zusammen. Europium-Tetracyclin geht Komplexverbindungen mit Wasserstoffperoxid oder Hydroxysäuren ein, die sich in ihren optischen Eigenschaften durch eine große Stokesssche Verschiebung, eine scharfe Emissionslinie und lange Fluoreszenzabklingzeiten auszeichnen

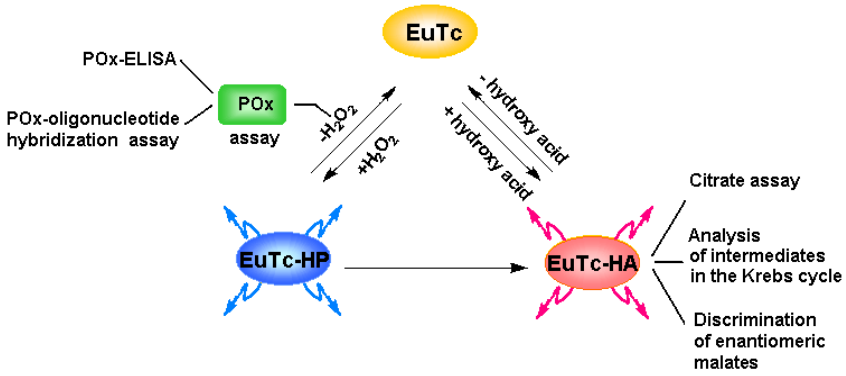

Abbildung 7.1. Schematische Zusammenfassung der Forschungsarbeit. HP: Wasserstoff-peroxid; EuTc: Europium(III)-tetracyclin; HA: Hydroxysäure.

Im ersten Teil der Arbeit werden die grundlegenden Eigenschaften und Mechanismen der Lumineszenz von Lanthanid-Komplexen erläutert. Im Mittelpunkt stehen dabei die drei wichtigsten Methoden zeitaufgelöster Fluoreszenzmessungen in heterogenen Systemen, zum einen der „direct lanthanide chelate label-based luminenescence assay“ (DLCLLA) , zum anderen der „dissociation enhanced lanthanide fluoroimmunoassay“ (DELFIA), und schließlich die „enzyme-amplified lanthanide luminescence“ (EALL).

In Kapitel 2 wird ein neuer zeitaufgelöster Fluoreszenztest zur Bestimmung der Aktivität von Peroxidase (POx) eingeführt, der auf dem System Europium-Tetracyclin-

Wasserstoffperoxid (EuTc-HP) als molekulare Sonde basiert. Zunächst wird der Katalysemechanismus von POx beschrieben, einem Enzym, das in der wissenschaftlichen Forschung bereits eingehend untersucht wurde. Die Quantifizierung der Enzymaktivität erfolgt über den indirekten Abbau des stark fluoreszierenden EuTc-HP-Komplexes. Dieser steht im Gleichgewicht mit ungebundenen H_2O_2 in der gepufferten Lösung, das durch den enzymatischen Einfluss von POx umgewandelt wird. Die Umsatzrate von EuTc-HP kann als direkter Parameter für die Enzymaktivität durch die Abnahme der Fluoreszenzintensität oder Veränderungen in der Fluoreszenzabklingzeit detektiert werden. Der zeitlich aufgelöste Fluoreszenztest hat eine Nachweisgrenze von 1 x 10^{-5} U/mL POx mit einem dynamischen Messbereich von 4.0 x 10^{-5} bis 5,9 x 10^{-3} U/mL. Der Einfluss von Inhibitoren wie Cyanid, Hydroxylamin und Azid auf die Aktivität von POx wurde ebenfalls untersucht.

Wird POx als Biomarker und EuTc-HP als molekulare Sonde eingesetzt, können ELISAs und DNA-Hybridisierungsassays detektiert werden. Kapitel 3 verdeutlicht, dass zeitaufgelöste Fluoreszenztests für Biomoleküle den gebräuchlichen Intensitätsmessungen überlegen sind. Ein Sandwich- und ein direkter POx-ELISA wurden im Rahmen dieses Projekts untersucht. Dabei wurde ein linearer Messbereich für IgG von 0,1 bis 8.0 ng/ml mit einer Nachweisgrenze von 0,1 ng/ml erhalten. EuTc-HP kann auch als reversibler molekularer Sensor für das Imaging von POx-ELISAs verwendet werden. Ein kompetitiver Hybridisierungstest für Oligonukleotide mit Hilfe von POx-Markern wird ebenfalls diskutiert.

Ein direkter Fluoreszenznachweis auf Citrat, einem in der Natur allgegenwärtigen Stoff, mittels bildgebender Verfahren wird in Kapitel 4 entwickelt. Die Methode basiert auf der Fähigkeit des schwach fluoreszierenden Europium-Tetracyclins reversibel Citrat zu binden und dabei einen stark fluoreszierenden Europium-Tetracyclin-Citrat-Komplex (EuTc-Cit) zu bilden. Die mittlere Fluoreszenzlebensdauer wird in Folge ebenfalls von 44 µs (EuTc) auf 88

μs (EuTc-Cit) erhöht. Stationäre Fluorometrie, TCSPC, zeitaufgelöste Fluorometrie und RLD Imaging können so zur Bestimmung von Citrat herangezogen werden. Der zeitauf-gelöste Fluoreszenztest ergibt einen dynamischen Messbereich von 1,6 x 10^{-7} bis 5,6 x 10^{-5} M bei einer Nachweisgrenze von 6.0 x 10^{-8} M Citrat. Verglichen mit anderen Bestimmungs-methoden für Citrat ist dies momentan das empfindlichste und einfachste verfügbare analytische Verfahren. Darüber hinaus ist dieser molekulare Sensor einfach zu synthetisieren, stabil sowohl in gelöster als auch in fester Form und kompatibel zur Anregungswellenlänge eines blauen Diodenlasers. Die Eigenschaften anderer Tetracyclin-Derivate wurden ebenfalls untersucht.

Der Citrat (Krebs)-Zyklus ist ein essentieller Bestandteil des aeroben Zellstoffwech-sels und findet in den Mitochondrien von tierischen und pflanzlichen Zellen statt. Das Fluo-reszenz-Imaging der wichtigsten Zwischenprodukte des Citrat-Zyklus steht im Mittelpunkt von Kapitel 5. Diese Zwischenprodukte wie Oxalacetat, Citrat, Isocitrat, α–Ketoglutarat, Succinat, Fumarat und L-Malat können reversibel an EuTc als weiterer Ligand (L) gebunden werden. Die resultierenden EuTc-L-Komplexe weisen unterschiedliche Fluoreszenzintensitä-ten und Abklingzeiten auf. Die Aufnahme der stationären Fluoreszenzintensität einerseits und RLD Imaging andererseits wurden zur Visualisierung dieser Verbindungen eingesetzt. Die Bildung und der Verbrauch der verschiedenen Zwischenstufen kann mit Hilfe kinetischer Fluoreszenzmessungen schrittweise detektiert werden. Zusätzlich kann mit einer dualen Fluoreszenzmethode die Änderung des Gehalts von NADH und EuTc-L gleichzeitig über-wacht werden.

Schließlich werden in Kapitel 6 chirale Fluoreszenzsensoren beschrieben. EuTc kann zur Unterscheidung der beiden enantiomeren Formen von Malat in wässriger Lösung benutzt werden. Der Unterschied in der Fluoreszenzintensität nach der Koordination beider Isomerer

$(F_L-F_0) / (F_D-F_0)$ beträgt 5,9 bei einer Emissionswellenlänge von 619 nm. Das ist ein höherer Faktor als bei allen anderen bekannten chiralen fluorimetrischen Verfahren für α-Hydroxysäuren. Die mittleren Fluoreszenzabklingzeiten von EuTc-L-Malat und EuTc-D-Malat betragen 84 bzw. 48 µs, die Quantenausbeuten 1,7 % bzw. 0,7 %. Die enantiomeren Formen von Malat können auch mittels zeitaufgelöstem Fluoreszenzimaging angezeigt werden. Weitere chirale α-Hydroxysäuren, sowie Laktat und Tartrat werden ebenso diskutiert. Somit ist diese die erste Arbeit, bei der ternäre Lanthanid-Komplexe als „einschaltbare" molekulare chirale Fluoreszenzsensoren eingesetzt werden.

* Please notice that the German summary is just for your information. For the details, please check the English version.

9 Recent Publications and Patent

9.1. Publications

1. Wolfbeis, Otto. S.; Duerkop, Axel; Wu, Meng; ***Lin, Zhihong.*** A Europium-ion-based luminescent sensing probe for hydrogen peroxide. *Angew. Chem., Intl. Ed. (2002), 41, 4495-4498.*

2. ***Lin****,* ***Zhihong;*** *WU, Meng; Schäferling, Michael; Wolfbeis. Otto S.* Fluorescent Sensing and Imaging of Citrate and Other Intermediates of the Krebs Cycle. *Angew. Chem. Intl Ed. accepted (2003).*

3. Wolfbeis, O. S.; Boehmer, M.; Duerkop, A.; Enderlein, J.; Gruber, M.; Klimant, I.; Krause, C.; Kuerner, J.; Liebsch, G.; ***Lin, Zhihong****.; Oswald, B.; Wu, Meng.* Advanced luminescent labels, probes and beads, and their application to luminescence bioassay and imaging. Springer Series on Fluorescence. *(2002), 2 (Ed. R. Kraayenhof, Fluorescence Spectroscopy, Imaging and Probes), 3-42.*

4. Wu, Meng; ***Lin, Zhihong****; Wolfbeis, Otto. S.* Determination of the Activity of Catalase Using a Europium(III)-tetracycline Derived Fluorescent Substrate. *Anal. Biochem. (2003), 320, 129–135.*

5. Wu Lei, Axel Dürkop, ***Zhihong Lin****, Meng Wu, and Otto S. Wolfbeis.* Detection of Hydrogen Peroxide in River Water via a Microplate Luminescence Assay with Time-Resolved ("Gated") Detection. *Microchim. Acta. 2003,143, 269-274*

6. ***Lin****,* ***Zhihong;*** *WU, Meng; Wolfbeis. Otto S.* A time-resolved fluorescence-based chirality sensor for malate in aqueous solution. *J. Am. Chem. Soc. submitted (2003).*

7. Wu, Meng; ***Lin, Zhihong****; Dürkop, Axel; Wolfbeis, Otto. S.,* Direct and Time-Resolved Enzymatic Determination of Glucose Using a Fluorescent Europium Probe for Hydrogen Peroxide*, Anal. Bioanal. Chem. submitted (2003).*

8. ***Zhihong Lin****, Meng Wu, and Otto S. Wolfbeis.* A Europium-Derived Fluorescent Probe for Time-Resolved ("Gated") Determination of the Activity of Peroxidases. *in preparation.*

9. Michael Schäferling, ***Zhihong Lin****, Otto S. Wolfbeis.* Time-Resolved Imaging of Enzyme-linked Immunosorbent Assays. *in preparation.*

9.2. Patent

German patent: Ger. Offen. DE 10155160 Determination of catalases and peroxidases, their conjugates, substrates, activators and inhibitors using europium (III) complexes with ligands and hydrogen peroxide. 2003, May 22.

US patent in application

10. Acknowledgements

Although this dissertation is an individual research work, it is obviously not possible without the guidance, helps, supports and efforts of numerous people. Firstly, I would especially like to thank my supervisor, Professor Otto S. Wolfbeis. He has given me exceptional academic guidance and his unflagging support throughout my Ph.D education, not to mention spending his weekends for discussing experiments and reviewing manuscripts.

I wish to express my gratitude to Bernhard Weidgans, who shares the same lab with me, for his assistances and his good-natured supports, especially “Bitte helfen Sie mir, Deutsch zu erlernen” and introducing the history, the culture and foods of Germany. My thanks also extend to Dr. Michael Schäferling for our cooperation on the imaging of POx-ELISA, and for his help with translation of German summary. I am grateful to Dr. Christian Krause for his helps, especially when I was first in Regensburg and worked in the same lab. He has generously given his time and expertise. I also thank Dr. Axel Dürkop, for his initial EuTc-HP fluorescence probe experience. Thank to PD. Dr. Vladmir Mirsky for his patience to solve my questions of electrochemistry.

I would also like to acknowledge to Claudia Schröder for helps with imaging devices and programs, Sarina Arain for helps with FluoroSkan Ascent reader, Athanasios Apostolidis for helps with the Hamilton dispensing robot, Thomas Hirsch for helps with fluorescence microscopy. I want to thank our secretary Edeltraud Schmid for her organizational supports.

Thanks to Dr. Jörg Enderlein of Institute for Biological Information Processing, Research Center Jülich, Dr. Thomas Gensch of the same center, and Mr. Henrik Bauer of PicoQuant GmbH, Berlin, for the helps and assistance in the determination of decay times.

I also like to express my gratitude to Bianca Wetzl, Alexander Karasyov, Torsten Mayr, Michael Meier, Qingli Hao, Stafan Nagl, Valentin Kulikov as well many other friends, colleagues, and technicans who assisted, advised, and supported my research.

Chromeon GmbH and University of Regensburg are gratefully acknowledged for the provision of financial support. Appreciation also to Dr. Petra Bastian and Dr. Michaela Gruber of Chromeon for their hospitality and kindly helps.11

Finally, affectionate appreciation to my husband. Sincere gratitude also goes to my parents, my son and other family members for their love, support, and patience over the last few years.